

ABSTRACT

Title of Thesis: SYSTEM PERFORMANCE
ENHANCEMENT OF MOBILE COOLING
SYSTEM WITH THERMAL BATTERY AND
THERMOSIPHON RECHARGE

Darren Key, Master of Science, 2018

Thesis Directed By: Research Professor, Yunho Hwang, Department
of Mechanical Engineering

A personalized mobile cooling device was modified and tested with different components to deliver better system performance. The device uses a miniaturized vapor compression cycle (VCC) to deliver approximately 165 W of cooling to an individual. The device stores the waste heat from the VCC condenser in a phase change material (PCM) carried on-board the device. The PCM is then recharged by rejecting heat stored in the PCM with a thermosiphon recharge cycle. The PCM was enhanced with copper and graphite matrices. The system was tested with the goal of increasing the coefficient of performance (COP) of the VCC and decreasing the PCM recharge time. This study found that a copper enhancement provided the highest COP at 4.43, an improvement over the baseline COP of 2.41.

SYSTEM PERFORMANCE ENHANCEMENT OF MOBILE COOLING
SYSTEM WITH THERMAL BATTERY AND THERMOSIPHON RECHARGE

by

Darren Key

Thesis submitted to the Faculty of the Graduate School of the
University of Maryland, College Park, in partial fulfillment
of the requirements for the degree of
Master of Science

2018

Advisory Committee:

Research Professor Yunho Hwang, Chair

Professor Bao Yang

Professor Amir Riaz

© Copyright by

Darren Key

2018

Acknowledgements

Thank you to the University of Maryland and the Center for Environmental Energy Engineering for the support and resources necessary for this project. My goal in getting my Masters degree was to engage in rigorous engineering design work while advancing my hands-on skills. CEEE and the RoCo project afforded me that opportunity.

Thank you to my advisor, Dr. Hwang for his guidance throughout the thesis writing process. I achieved more than I thought possible. Thank you to Dr. Radermacher for his inspiring leadership, support and for providing so many wonderful opportunities. Thank you to Vikrant Aute for insight and knowledge, as well as pushing the need for creating such a device as RoCo. Thank you to Kristen Hines for piquing my interest in thermodynamics during my undergraduate studies.

Thank you to Yilin Du for paving the way for the RoCo project. Thank you to Yiyuan Qiao for being my research partner and dedicating hours to data collection and analysis, building RoCo prototypes and for taking over for me when I'm gone. Thank you to Ye Tao for your words of support and for letting me have the good desk.

Thank you to Mary Baugher and Tanya Pringle for keeping everything running. Thank you to Kerri Poppler James for being my first point of contact at UMD and making sure I graduated. Thank you to Terry Island for helping me navigate coursework and helping me graduate on my timeline.

Finally, a most sincere thank you to Jan Muehlbauer. Your enthusiasm, knowledge and technical ability inspire me daily.

Dedication

To Alisa

Table of Contents

Acknowledgements.....	ii
Dedication.....	iii
Table of Contents.....	iv
List of Tables.....	vii
List of Figures.....	viii
Chapter 1: Introduction.....	1
1.1 Background.....	1
1.2 Objectives.....	5
Chapter 2: Test Facility and Experimental Setup.....	7
2.1 System Schematic.....	7
2.2 Test Facility.....	9
2.2.1 Environmental Chamber.....	9
2.3 Breadboard Description.....	9
2.3.1 Compressor.....	10
2.3.1.1 Oil Charge.....	11
2.3.2 Expansion Valve (TXV).....	12
2.3.3 Actuated Ball Valves.....	14
2.3.4 Receiver.....	15
2.3.5 Evaporator Heat Exchanger.....	16
2.3.6 PCM-side Heat Exchanger.....	21
2.3.6.1 Phase Change Material.....	21

2.3.6.2 Non-enhanced PCMHX.....	24
2.3.6.3 Copper Enhanced PCMHX.....	25
2.3.6.3.1 Four-tube PCMHX.....	29
2.3.6.3.2 Eight-tube PCMHX.....	30
2.3.6.4 Graphite-enhanced PCMHX.....	31
2.3.6.4.1 2-hour graphite-enhanced PCMXH	32
2.3.6.4.2 4-hour graphite-enhanced PCMXH	34
Chapter 3: Instrumentation	36
3.1 Mass-flow Meter	36
3.2 Temperature	37
3.2.1 Refrigerant Temperature	37
3.2.2 PCMHX Temperature	39
3.2.3 Air Temperature	42
3.3 Pressure Transducers.....	43
3.4 Power/Current	45
3.5 DAQ.....	46
3.6 Safety Systems	47
3.7 Uncertainty Analysis	47
Chapter 4: Testing Procedures	50
Chapter 5: Test Results	52
5.1 Single Cycle Tests at Room Temperature.....	52
5.1.1 8.6 kg Baseline Non-enhanced PCM Test.....	52
5.1.2 8.6 kg Copper-enhanced PCM Test.....	58

5.1.3 5.4 kg Graphite-enhanced PCM Test	63
5.2 15.1 kg Copper-enhanced PCM Cycle Tests	70
5.2.1 Cycle Test: 26.3 °C	71
5.2.2 Cycle Test: 30.0 °C	76
5.2.3 Cycle Test: 35.0 °C	80
5.3 12.7 kg Graphite-enhanced PCM Cycle Test.....	82
Chapter 6: Data Analysis	89
Chapter 7: Results and Discussion.....	94
7.1 Setpoint Thermocouple Placement.....	95
7.2 System Performance.....	99
7.2.1 COP	99
7.2.2 Overall Heat Transfer Coefficient	102
Chapter 8: Conclusion and Future Work	106
Bibliography	108

List of Tables

Table 1: Oil Charge for Aspen Q Compressor	12
Table 2: Evaporator Heat Exchanger Options	17
Table 3: Coil Designer Input Parameters	18
Table 4: Coil Designer Simulation Results	19
Table 5: PureTemp 37 Material Properties	22
Table 6: Effective Thermal Conductivity Calculation of Copper Matrix Enhancement	29
Table 7: Sensor Placement for Capacity of VCC Component	39
Table 8: Instrument Specification and Systematic Uncertainty	48
Table 9: Uncertainty Analysis Sample Calculations	49
Table 10: Ambient Air Test Conditions	51
Table 11: Cooling and Recharge Times with Different PCM Enhancement	90
Table 12: COP Results with Different PCM Enhancements	92
Table 13: Additional Heat Loss Between Condenser Outlet and Evaporator Inlet	93
Table 14: PCM Heat Exchanger Performance and Characteristics	102
Table 15: UA Calculations	104

List of Figures

Figure 1: Typical phase change of PT37 when used in RoCo condenser.....	7
Figure 2: Schematic diagram of RoCo breadboard.....	9
Figure 3: Aspen Q-series 1.4 cc rotary compressor.....	11
Figure 4: Danfoss TUA expansion valve.....	13
Figure 5: TXV placement	14
Figure 6: Belimo CMB24 actuator	14
Figure 7: 300 cc receiver.....	16
Figure 8: Evaporator heat exchanger options	17
Figure 9: Thermatron 2-Row 720 AHX.....	19
Figure 10: Thermatron 1-Row 720 AHX.....	20
Figure 11: Sanhua Microchannel AHX	20
Figure 12: PureTemp 37 DSC analysis.....	23
Figure 13: PCMHX Version 1: Non-enhanced PCMHX	24
Figure 14: Single copper mesh enhancement	26
Figure 15: Influence of ligament shape on k_e in metal foams [31]	27
Figure 16: Influence of pore density on k_e in metal foams [31].....	27
Figure 17: 4-coil copper-enhanced PCMHX	30
Figure 18: Eight-tube PCMHX.....	31
Figure 19: Graphite-enhanced PCMHX	32
Figure 20: Post-processed graphite block, a) gap around tube, b) full cross-section	33
Figure 21: Graphite-enhanced PCMHX with PCM.....	34

Figure 22: 4-hour graphite-enhanced PCMHX.....	35
Figure 23: Micro Motion coriolis flow-meter and transmitter.....	37
Figure 24: RTD sensor.....	38
Figure 25: System schematic with sensor locations	38
Figure 26: Typical thermocouple placement in PCMHX.....	40
Figure 27: 2-hour non-enhanced PCMHX thermocouple placement	40
Figure 28: 2-hour GrPCMHX thermocouple placement	41
Figure 29: 4-hour CuPCMHX thermocouple placement	41
Figure 30: 4-hour GrPCMHX thermocouple placement	42
Figure 31: Air temperature of AHX.....	42
Figure 32: VCC pressure-enthalpy diagram	43
Figure 33: Setra pressure transducer.....	44
Figure 34: Pressure calibrator	44
Figure 35: Current and voltage transducers	45
Figure 36: National Instruments DAQ modules	46
Figure 37: 8.6 kg baseline non-enhanced PCMHX PCM temperature.....	53
Figure 38: 8.6 kg baseline non-enhanced PCMHX tube temperature	54
Figure 39: 8.6 kg baseline non-enhanced COP.....	55
Figure 40: 8.6 kg baseline non-enhanced pressure	55
Figure 41: 8.6 kg baseline average air temperature in and out of AHX	56
Figure 42: 8.6 kg baseline capacity of evaporator and condenser	57
Figure 43: 8.6 kg baseline refrigerant mass-flow rate	57
Figure 44: 8.6 kg copper-enhanced PCMHX PCM temperature.....	59

Figure 45: 8.6 kg copper-enhanced COP	60
Figure 46: 8.6 kg copper-enhanced pressure	60
Figure 47: 8.6 kg copper-enhanced air temperature of AHX	61
Figure 48: 8.6 kg copper-enhanced capacity of evaporator and condenser	62
Figure 49: 8.6 kg copper-enhanced refrigerant mass-flow rate	62
Figure 50: 2-hour GrPCMHX heat map at 2.7 hours into the cooling cycle	63
Figure 51: 5.4 kg graphite-enhanced PCMHX PCM temperature.....	64
Figure 52: 5.4 kg graphite-enhanced PCMHX tube temperature	65
Figure 53: Warpage in the graphite blocks after post-processing.....	65
Figure 54: 5.4 kg graphite-enhanced COP.....	66
Figure 55: 5.4 kg graphite-enhanced pressure	67
Figure 56: 5.4 kg graphite-enhanced air temperature of AHX	68
Figure 57: 5.4 kg graphite-enhanced capacity of evaporator and condenser.....	69
Figure 58: 5.4 kg graphite-enhanced refrigerant mass-flow rate	69
Figure 59: 2-hour graphite-enhanced PCMHX container crack	70
Figure 60: 15.1 kg copper-enhanced PCMHX PCM temperature cycle test.....	71
Figure 61: 15.1 kg copper-enhanced PCMHX tube temperature cycle test	72
Figure 62: 15.1 kg copper-enhanced COP cycle test.....	72
Figure 63: 15.1 kg copper-enhanced pressure cycle test	73
Figure 64: 15.1 kg copper-enhanced air temperatures of AHX for cycle test	74
Figure 65: 15.1 kg copper-enhanced capacity of evaporator and condenser for cycle test	75
Figure 66: 15.1 kg copper-enhanced mass-flow for cycle test	76

Figure 67: Copper-enhanced PCMHX PCM temperature cycle test with ambient air at 30.0 °C	77
Figure 68: Copper-enhanced PCMHX tube temperature cycle test with ambient air at 30.0 °C	78
Figure 69: Copper-enhanced COP cycle test with ambient air at 30.0 °C	79
Figure 70: Copper-enhanced pressure cycle test with ambient air at 30.0 °C	79
Figure 71: Copper-enhanced PCMHX PCM temperature, ambient air at 35.0 °C	80
Figure 72: Copper-enhanced PCMHX tube temperature with ambient air at 35.0 °C	81
Figure 73: Copper-enhanced COP with ambient air at 35.0 °C	81
Figure 74: Copper-enhanced pressure with ambient air at 35.0 °C	82
Figure 75: 12.7 kg graphite-enhanced PCMHX PCM temperature cycle	83
Figure 76: 12.7 kg graphite-enhanced cycle COP	84
Figure 77: 12.7 kg graphite-enhanced cycle pressure.....	85
Figure 78: 12.7 kg graphite-enhanced air temperature of AHX for cycle test	86
Figure 79: 12.7 kg graphite-enhanced capacity of evaporator and condenser for cycle test	87
Figure 80: 12.7 kg graphite-enhanced mass-flow for cycle test	87
Figure 81: Graphite disk swelling after PCM backfill and cycle test	88
Figure 82: Different level of insulation on the graphite-enhanced PCMHX (left) and the copper-enhanced PCMHX (right)	96
Figure 83: Copper-enhanced PCMHX thermocouple placement	97
Figure 84: Copper-enhanced PCMHX cooling and recharge heat map	97
Figure 85: Graphite-enhanced PCMHX cooling and recharge heat map	99

Figure 86: COP by weight of PCM and enhancement type.....	100
Figure 87: Thermal resistance analysis of PCM condenser	103

Chapter 1: Introduction

1.1 Background

Thermal comfort is a vital component to the indoor build environment. Worldwide urban areas could add another 2.5 billion people by 2050 [1]. As populations migrate to urban areas and demand for improved thermal comfort increases, associated energy use also increases [2]. People in developed countries spend most of their time inside, with Americans spending on average 90% of their time indoors [3]. Buildings account for 20-40% of final worldwide energy consumption [4], and half of that is used for HVAC systems [5]. Climate change is also likely to contribute to increased energy use in buildings, especially for cooling purposes during the summer months [6 – 7]. A proven technique for reducing energy use is by using temperature setbacks [6]. A temperature setback involves raising the thermostat temperature during the summer months and lowering the thermostat temperature during the winter months. Summer thermostat setbacks of 1 °C was associated with 6% of HVAC energy use reduction [7]. Additional field tests, experiments and computer simulations indicate that temperature setbacks can deliver up to 30% total energy savings for heating systems and 23% energy savings for space cooling systems [8]. Another study found that increasing the cooling setpoint from 22.2 to 25.0 °C resulted in an average of 29% of cooling energy [9]. Additionally, conventional space cooling systems do an inadequate job of providing personalized thermal comfort [10]. The comfort zone established in ASHRAE Std. 55 corresponds to thermal conditions which will be acceptable to 80% of the occupants in a conditioned space when using the Predicted Mean Vote method [11]. By this metric, up to 20% of the occupants of an indoor space are dissatisfied with the thermal conditions at any given. Although there is an association

between thermal comfort and worker productivity [14 – 17], increasingly narrow temperature ranges do not result in increased levels of thermal comfort [12]. Comfort with indoor spaces is influenced by thermal comfort, as well as cognitive and behavioral processes [13]. To achieve better thermal comfort, it has been shown that individualized control results in better thermal comfort [20 – 22]. These findings support the increasingly popular adaptive thermal comfort theory which states that humans will tolerate a larger range of thermal conditions when they have control over their immediate environment [14]. New space cooling and heating approaches are required to realize the energy savings potential from thermostat setbacks and to achieve better overall satisfaction with thermal comfort conditions. For example, localized cooling directed at the torso or face can have significant impacts on thermal sensation, especially for cooling [24 – 25]. In other words: personalized thermal comfort is needed. The Advanced Research Projects Agency-Energy's (ARPA-E) DELTA program aims to address this very need. The program's purpose is "to reduce the costs for heating and cooling buildings by developing Localized Thermal Management Systems (LTMS)" [15]. RoCo one of eleven total projects that were awarded funding under this program. The projects range from thermoregulatory textiles that reduce their level of insulation when warm and increase the insulation when cold, to smart vent registers (Stony Brook University) [15]. Only one other project, by Syracuse University, proposed to provide cooling by using a miniaturized VCC system and phase change material (PCM) heat storage for condenser waste heat. The promising Syracuse device is intended to be placed under a desk, and provide cooling to an individual only while they are sitting at their desk. As of this writing, RoCo is currently the only truly mobile air conditioning device in existence today.

The Roving Comforter (RoCo) is such a device that provides personalized thermal comfort for individuals in inadequately heated or cooled environments. RoCo allows for liberal use of temperature setbacks while maintaining or improving thermal comfort satisfaction levels when compared with traditional space cooling technologies. RoCo directs cool air towards the torso or face of a single person, thus maximizing the cooling effect experienced by the individual [24 – 25]. The RoCo device in its current form consists of a mobile robotic platform with a small, battery powered air-conditioning unit. There is currently no heating mode for RoCo. The conditioned air is discharged from the unit towards a single person through an adjustable nozzle. In a typical air conditioning unit, the waste heat must be kept out of the conditioned space. This can be achieved by placing the condenser outside of the conditioned space, or by venting the hot exhaust air out of the room via ventilation ducts. The novel concept with RoCo is that the waste heat is stored in a PCM on-board the device during the cooling operation, eliminating the need for a separate outdoor unit or ventilation ducts. Phase change materials have been researched extensively as a method to improve cooling in buildings [27 – 32]. The stored waste heat can then be rejected by using a highly efficient thermosiphon operation in a different time and place, taking advantage of the benefits of load shifting. The RoCo device is also fitted with rechargeable batteries, charged overnight. The fact that RoCo is fully mobile allows it to be used as a supplement to traditional cooling systems, as well as providing cooling in spaces where none currently exists.

High energy efficiency is obtained because of the small temperature lift and relatively high evaporating temperature: the inlet air for the evaporator is at room temperature. Additional energy savings can be realized by relaxing the thermostat for space cooling systems. The

device can also be configured to deliver air at temperature and velocity as specified by the user, thus giving the individual superior control over their own thermal comfort and improving satisfaction with thermal comfort levels. Research suggests that air flow should be between 0.3 m/s and 1.5 m/s, as desired by the user [16].

The keys to a successful personal thermal comfort device such as RoCo is that it must be portable, it must blow cool air at the user, and it must have a sufficiently long operating time. An informative potential use-case for RoCo is in mid-rise apartment buildings during the main cooling season summer [17]. Indoor spaces in buildings typically reach their peak temperature in the mid-afternoon [18], which also coincides with the highest daily cost of energy [19]. RoCo can also be used to shift the peak load of the building [20]. Although load shifting does not reduce energy usage, it does have a significant impact on energy cost [21]. By recharging RoCo's battery at night when energy costs are lower, electricity cost reduction is realized. RoCo can also be particularly useful during heatwaves when the peak load on the power grid is highest [22]. Based on this use-case, RoCo's continuous cooling time should coincide with higher afternoon indoor temperatures, typically about 4 hours [40 – 41]. The cooling time of the device is dependent on the capacity of the electrical battery, the capacity of the thermal storage container, and the overall efficiency of the system. The overall capacity of the thermal storage device is a function of the latent heat and mass of the phase change material used. The efficiency of the system includes two main factors: (1) the coefficient of performance (COP) of the VCC cooling cycling and (2) the amount of time it takes for the PCM to re-solidify after the cooling cycle. By increasing the cooling cycle COP and decreasing the PCM recharge time, the device is more useful to

the end user. Both factors can be improved by increasing the thermal conductivity of the PCM.

1.2 Objectives

The objective of this thesis is to evaluate system performance improvements for RoCo. The concept and initial tests of this device are reported in detail in the Master's Thesis of Yilin Du, 2016, University of Maryland [23]. This document builds off the work done in Du's thesis, and makes extensive use of the work presented therein. As describe in Du's thesis, RoCo is intended to be used for personal cooling needs in an indoor environment in which the ambient air temperature is 26.0 °C (78.8 °F). This temperature corresponds with a typical temperature setback in a commercial office space or residential setting. Du's device has already been developed and tested, and is capable of delivering 165.6 W of cooling with a system COP of 2.85 for a duration of 2 hours [23]. In the original configuration, the PCM was fully solidified and thus thermally recharged and ready for another cooling cycle in nearly 8 hours of thermosiphon mode operation. In this thesis, system enhancements which can improve the COP of the system in cooling mode and decrease the amount of time needed to recharge the thermal battery will be evaluated. Phase change materials have the advantage of being able to store relatively large amounts of heat, but are limited by low thermal conductivity and thus have low heat charging and discharging rates [24]. Improving the thermal conductivity of the PCM can help transfer the condenser waste heat throughout the container, thus improving the performance of the cooling system reducing the re-solidification recharge time. Like the original system, all configurations evaluated in this thesis used a vapor compression cycle to provide cooling while storing the waste heat on-board the device in a phase change material. The device

provided a delta T of -3 K from the inlet to the outlet of the evaporator. This change in temperature is consistent with findings in literature, which state that for a room air temperature of 23-26 °C, delivered air should be 3-4 K below the ambient air temperature [16]. The device recharged the thermal battery with a thermosiphon cycle. A test facility was set up to measure all system characteristics including refrigerant temperature, pressure and mass-flow as well as system inlet and outlet air temperature. Tests were run at a baseline ambient air temperature of 26.0 ± 0.5 °C and then again at ambient temperatures of 30.0 °C and 35 °C. These temperatures were selected based on ASHRAE Std. 116 [25]. The system performance will be evaluated against the baseline system built in the previous thesis by Yilin Du.

Chapter 2: Test Facility and Experimental Setup

2.1 System Schematic

The schematic diagram of the breadboard system is shown in Figure 2. The system runs in two modes: cooling mode and thermosiphon recharge mode, shown in Figure 1(a) and 1(b), respectively. In cooling mode, the system operates as a traditional vapor compression cycle (VCC) and the refrigerant flows in a counter-clockwise direction. Waste heat is rejected into the PCM condenser by taking advantage of the latent heat of the PCM. The PCM slowly melts for the duration of a single cooling cycle. The cooling cycle is complete when the PCM has completed phase change and is fully liquified. The instantaneous capacity of the thermal battery is determined by monitoring the temperature of the PCM and refrigerant in the system. The temperature of the PCM increases slowly during the phase change process, and then has a pronounced rate of increase once fully melted. This inflection point indicates the completion of phase change as shown in Figure 1: Typical phase change of PT37 when used in RoCo condenser

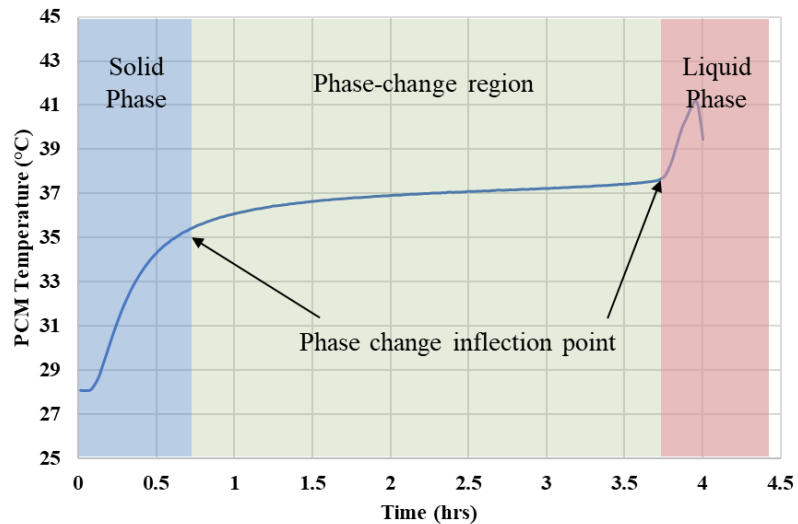
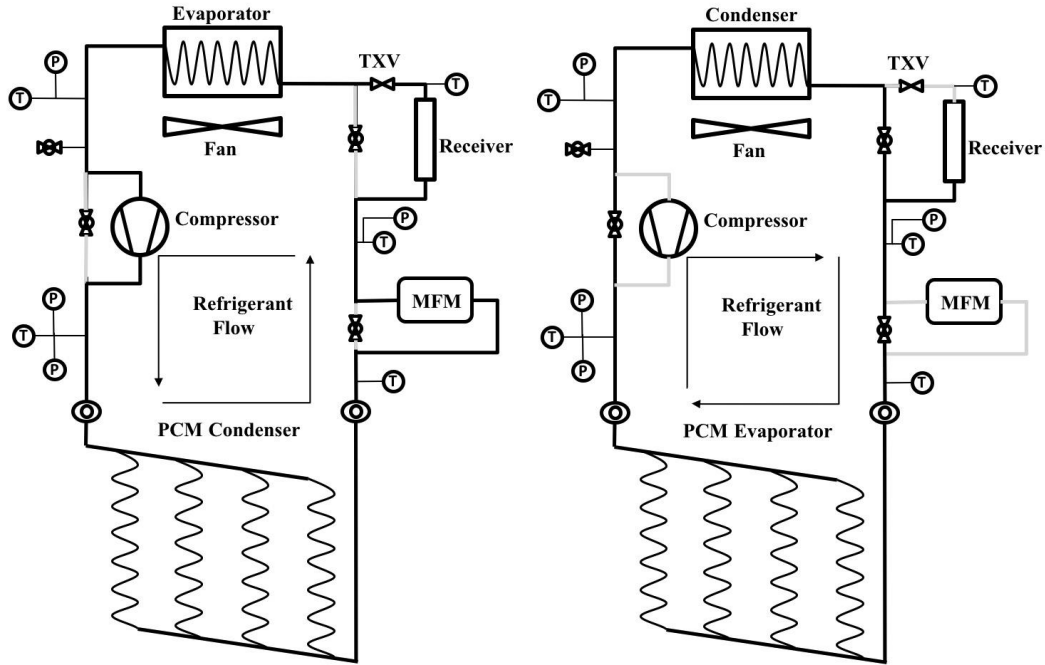


Figure 1: Typical phase change of PT37 when used in RoCo condenser

Once all the PCM is melted, the system automatically switches to a clockwise thermosiphon mode by turning off the compressor and automatically opening all three ball valves. In the gravity assisted thermosiphon mode, the liquid refrigerant drains down and collects at the bottom of the system. The refrigerant absorbs heat from the melted and superheated PCM and becomes a vapor. It then rises up the left side of the system. The compressor is bypassed, and the system rejects heat as the refrigerant passes through the top heat exchanger which has now become the condenser. Because the evaporator and condenser switch their functions depending on the mode of the cycle, the upper heat exchanger will be referred to as the Air-Side Heat Exchanger (AHX) and the lower heat exchanger will be referred to as the Phase Change Material Heat Exchanger (PCMHX). The refrigerant used in the system was R134a. No additional refrigerants were used during testing. Internal pressures and temperatures of the system were monitored using sensor as indicated by P and T in the schematics. Additional information on the instrumentation is included in Chapter 3:



(a) Cooling mode (VCC)

(b) Recharge mode (thermosiphon)

Figure 2: Schematic diagram of RoCo breadboard

2.2 Test Facility

2.2.1 Environmental Chamber

All of the experiments were run in the same environmental chamber at the University of Maryland, College Park. The test chamber was 2.7 m wide by 4.6 m deep by 2.1 m tall. The chamber has three windows and a door. It maintains an ambient steady-state temperature within ± 0.2 °C of the setpoint with a maximum air velocity of 2.0 ± 0.1 m/s. The door remained closed during all tests.

2.3 Breadboard Description

The breadboard used in this experiment was a modified version of the system used by Du. The original system was manually operated. This includes the ball valves, the compressor, and the expansion valve. The ball valves were manually actuated and were opened or

closed depending on the desired cycle: cooling or recharge. The compressor was turned on and off by the data acquisition system, but had to be done manually by the user each time. The expansion valve was a manually adjusted unit and required the operator to actively adjust the knob for the duration of the cooling cycle. All three of these systems were replaced by automated versions for this set of tests. The specifications are listed below. Du's original breadboard system will be referred to as Breadboard Version 1 (BV1) and the updated breadboard system used in this series of test will be referred to as Breadboard Version 2 (BV2).

2.3.1 Compressor

The compressor used in all tests was the Aspen Q-series rotary compressor, shown in Figure 3. The unit body is 67.1 mm in diameter and 83.3 mm tall. The Aspen Q has a 1.4 cc displacement volume and has a variable speed range from 2100 – 6500 RPM. The variable speed range was used to achieve a 1.1 g/s refrigerant mass-flow while operating in cooling mode. Once the targeted mass-flow was achieved by varying a 5 V control signal using a potentiometer, the compressor speed was not changed again for the duration of all the tests. The compressor was run near the lower end of this RPM range because the only partial capacity was needed. A smaller capacity compressor was not commercially available, but ideally the system would be run with a smaller compressor. Future work on utilizing the variable speed of the compressor is recommended to study variable delivered cooling capacity. The compressor is powered by 24 VDC.



Figure 3: Aspen Q-series 1.4 cc rotary compressor

2.3.1.1 Oil Charge

The breadboard system was filled with compressor oil as per the compressor manufacturer's recommendation. The oil used with the Aspen compressor was the factory recommended Emkarate POE RL 68H oil. The Aspen Q compressor is shipped factory charged with 23 g of the Emkarate oil. The recommended amount of compressor oil in the system was 25% - 30% of the refrigerant charge volume. To determine the amount of oil needed, the following assumptions were made: in cooling mode, the refrigerant is assumed to have a quality of 0 in the entire receiver and 25% of the condenser, due to subcooling. The amount of oil needed is calculated by summing 25% of the condenser volume and the entire receiver volume and then multiplying the sum by 25%. A 1.2 safety factor was added to ensure sufficient oil volume. A sample calculation for the oil charge is shown in Table 1. The oil was measured by extracting the oil from the container with a small syringe, and then weighing the additional weight of the oil in the syringe. The oil has a density of 0.977 g/ml at 20 °C.

Table 1: Oil Charge for Aspen Q Compressor

25% of Condenser Volume (cc)	Receiver Volume (cc)	Estimated Refrigerant Charge	Safety Factor	Oil Needed* (g)
53	212	265	1.2	56.5

*note: Aspen Q compressor comes factory charged with 23 cc of oil

The tubing volume calculations were made using dimensions provided by industry standards. All tubing used was ACR copper tubing and inner diameters were based on dimensions in Copper Tube Handbook as provided by The Copper Development Association, Inc [26]. The oil keeps the compressor fully lubricated and working smoothly. During normal operation, the oil is carried along with the circulating refrigerant and is distributed throughout the system. When the condenser is changed, as it frequently was during the tests described in this thesis, an unknown amount of oil remains in the removed condenser. No reliable method for determining the amount of oil removed each time the condenser was changed was found. Each time a new condenser was added, it was assumed that all the oil from the previous test had drained into the condenser and a new batch of oil was added, as described above. Future work is suggested for optimized oil charge as a function of system volume and determining how much oil is removed when the condenser is changed.

2.3.2 Expansion Valve (TXV)

In the original breadboard system, a manually adjusted expansion valve was used. It was initially assumed that the system would operate under steady-state conditions for the entirety of the cooling cycle: a constant condensing temperature of 37.0 °C and a constant evaporation temperature of 26. 0°C. The phase change material has a nominal phase-

change temperature of 37.0 °C, but the actual phase change takes place over a range of 36.0 – 38.0 °C. The system must also be able to operate efficiently when the PCM is subcooled to room temperature, such as when the device has been sitting unused overnight. Therefore, the actual operating band of the cooling cycle is much greater than just the 37.0 °C original assumption. In the initial test, the operator manually adjusted the expansion valve for the entire duration of the cooling cycle to maintain a constant compressor inlet pressure of about 400 kPa. Manual operation was not a viable option for the cycle testing planned for the PCM enhancement testing.

In BV2, the manually adjusted expansion valve was replaced with a Danfoss TUA expansion valve (Figure 4), part number 068U2212 with a #0 orifice.



Figure 4: Danfoss TUA expansion valve

The valve was placed directly upstream of the evaporator (Figure 5, left) and the bulb was placed horizontally at the 2 o'clock position, directly downstream of the evaporator (Figure 5, right).

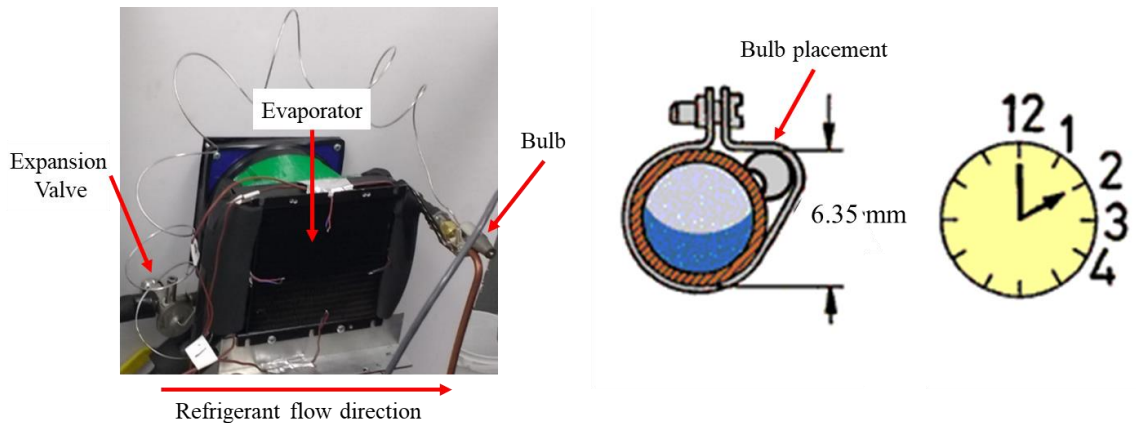


Figure 5: TXV placement

2.3.3 Actuated Ball Valves

Another part of the system that had to be modified to allow automatic cycling was the ball valves. The ball valves used in the original system were manual Swagelok 6.35 mm (1/4") full-port 1/4-turn brass ball valves. Each of these three valves were retrofitted with Belimo CMB24 actuator. The Belimo actuators have a power consumption of 1 W and operate on 24 VDC. They turn 90° in 35 seconds and have a torque of 2 Nm. These actuators are designed to actuate ventilation duct dampers. The actuators were controlled with the data acquisition system and were set to open or close based on a temperature measurement taken in the PCM.



Figure 6: Belimo CMB24 actuator

A refrigeration-specific valve and actuator combination was researched extensively, but nothing appropriate was found. The limiting factor for these valves is that they must be full-port valves. The breadboard system uses a thermosiphon operation to recharge the

PCM, and a thermosiphon will not run if there is a choke-point in the cycle. The performance of the thermosiphon circuit is significantly improved when the minimum hydraulic diameter is at least 5 mm (0.197 in) [27]. Conventional refrigeration valves do not maintain this minimum opening size and will not work on the breadboard system.

2.3.4 Receiver

The receiver, shown in Figure 7, is included for improved operation during thermosiphon mode. During recharge mode (Figure 2(b)), the entire PCMHX should be filled with liquid refrigerant. A receiver must be included to store the extra refrigerant during cooling mode. The receiver is sized to have the same internal volume as the PCMHX. The receiver must be mounted upstream of the TXV in cooling mode and above the PCMHX to accommodate the gravity feed of the thermosiphon. The receiver must also drain from the lowest point of the receiver to allow all the refrigerant to fully drain out of it while in recharge mode. Previous versions of the receiver were constructed by hand and did not drain fully, leading to issues with thermosiphon operation.



Figure 7: 300 cc receiver

2.3.5 Evaporator Heat Exchanger

The design requirement for the evaporator heat exchanger (AHX) is that it must deliver 150 W of cooling. Based on calculations done by Du [23], the Thermatron 720 2-row AHX was used, as shown on the left of Figure 8. The Thermatron heat exchanger has copper tubes and aluminum fins and uses copper tubing with a 6.35 mm OD ($1/4$ " ACR) throughout. A critical design feature of this heat exchanger is that all the circuitry must be able to drain completely during recharge mode. From top to bottom, each tube drains down into the tube below it and refrigerant traps are avoided. Any future AHX must share this feature to be compatible with thermosiphon operation. Additionally, any AHX must have a minimum hydraulic diameter of 5 mm (0.197 in) to promote refrigerant flow during thermosiphon mode.

In addition to the Thermatron 2-Row 720 AHX, calculations were done to explore the possibility of using a Thermatron 1-Row 720 AHX as well as a Sanhua Microchannel AHX. All three heat exchangers are shown side-by-side in Figure 8. The physical dimensions of each heat exchanger and their weights are given in Table 2.

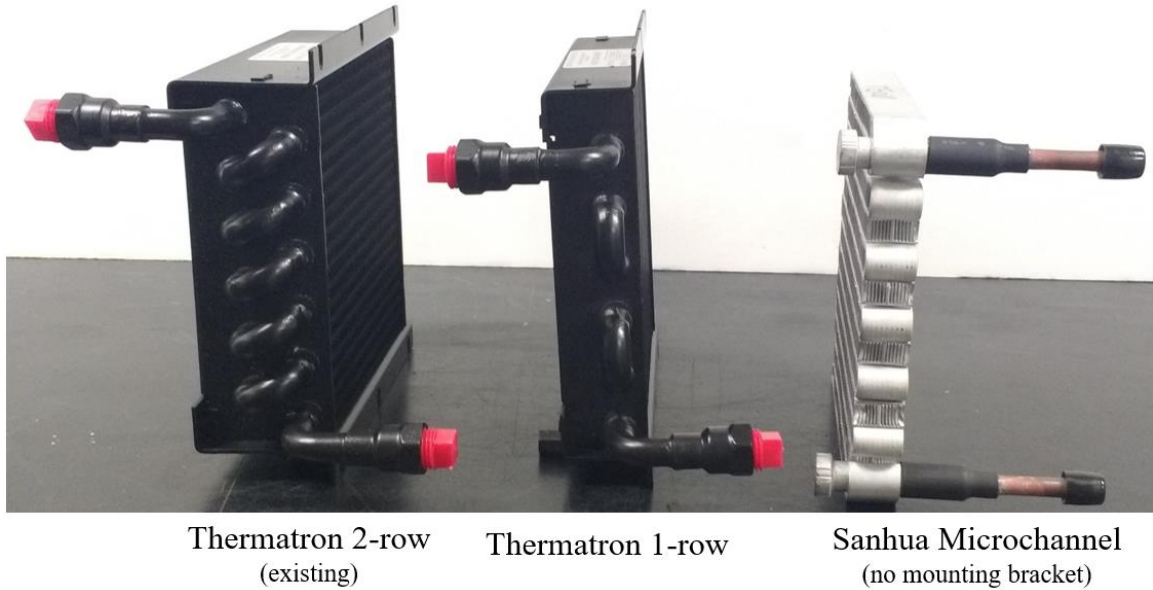


Figure 8: Evaporator heat exchanger options

Table 2: Evaporator Heat Exchanger Options

AHX	Length (mm)	Width (mm)	Thickness (mm)	Weight (g)	% Weight Change
Thermatron 2-row	177	125	44	998	-
Thermatron 1-row	177	125	28	561	-43.8%
Sanhua Microchannel	140	127	16	146	-85.4%

Based on calculations done in Coil Designer, the Thermatron 1-Row 720 AHX cannot deliver enough cooling capacity, but the Sanhua Microchannel AHX can. The parameters listed in Table 3 were used for all Coil Designer simulations. Pressure and refrigerant mass flow rate are typical measured values from BV1 and quality is calculated using TXV enthalpy-in and evaporating pressure. Relative humidity and air flow are also measured values

Table 3: Coil Designer Input Parameters

Pressure (kPa)	Refrigerant mass flow (kg/s)	Quality	Air Temp. (°C)	Air R.H. %	Air Flow m³/s
525.0	0.0011	0.1	26.0	40	0.0472

The results from the Coil Designer simulations are shown in Table 4. The heat loads of each AHX are shown Figures Figure 9 - Figure 11. Initially, it was thought that the Thermatron 1-row evaporator would be able to deliver sufficient cooling, but the Coil Designer simulation shows otherwise. The Thermatron 1-row is therefore not a good candidate for us with RoCo. Both the Thermatron 2-row and Sanhua Microchannel can deliver the required amount of cooling, but the Sanhua model offers significant weight and refrigerant charge savings, as shown in Table 2. Although the Sanhua Microchannel heat exchanger is the smallest and the lightest, the size of the microchannels prevent the circulation of the refrigerant in thermosiphon mode and is therefore not a good candidate for the final product. If a future design is implemented in which the PCM re-solidification is driven by a compressor, then it is recommended to test the Sanhua Microchannel heat exchanger. A compressor driven re-solidification cycle would have the added benefit of

removing the receiver from the system, thus further reducing the amount of refrigerant charge.

Table 4: Coil Designer Simulation Results

Evaporator	2-phase correlation	Air ΔT (K)	Heat Load (W)
Thermatron 2-row	Shah, 2016 Unified TF	2.95	174.5
Thermatron 1-row	Shah, 2016 Unified TF	1.94	115.9
Sanhua Microchannel	Shah, 2016 Unified MC	3.24	193.3

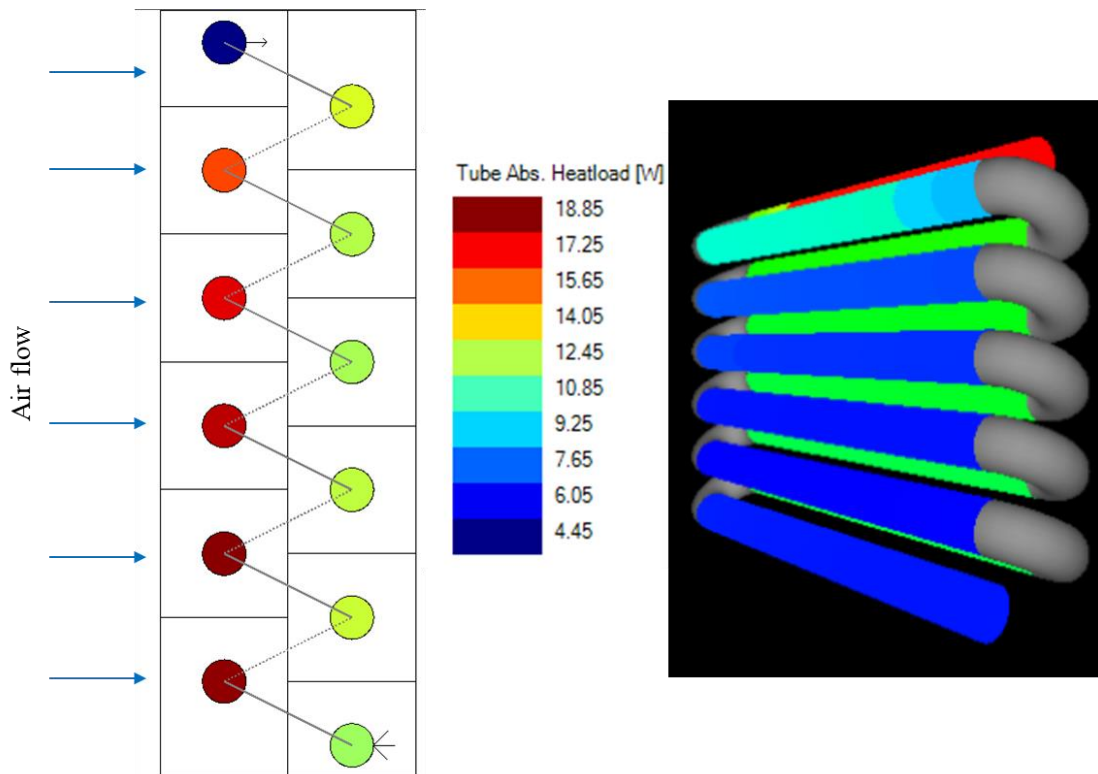


Figure 9: Thermatron 2-Row 720 AHX

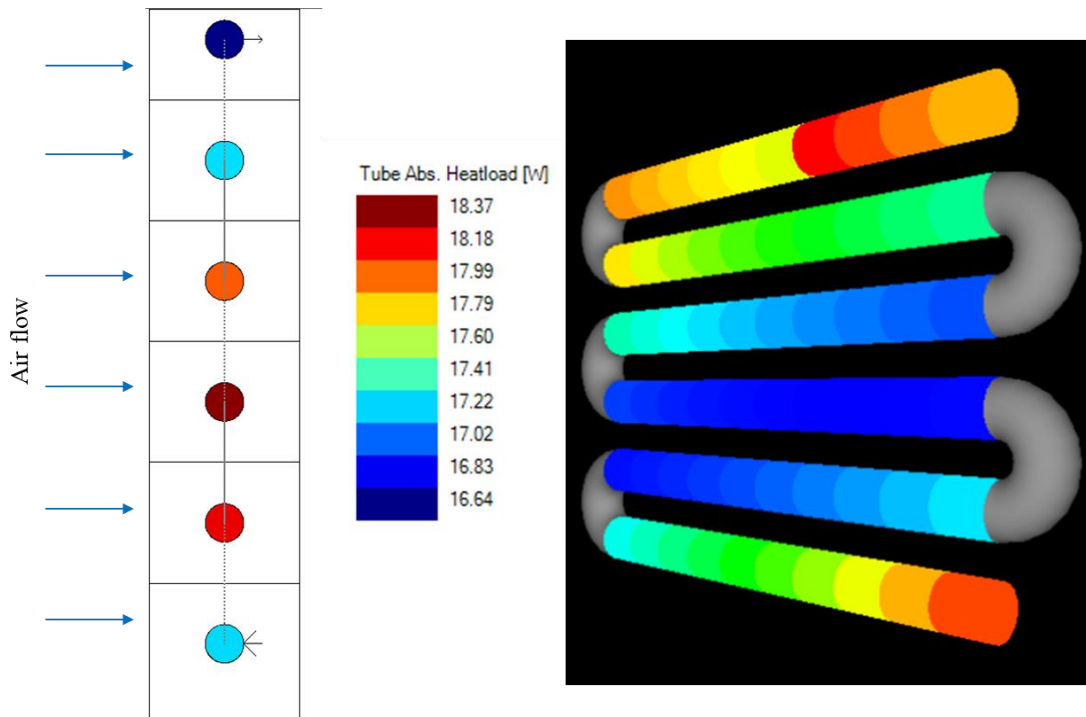


Figure 10: Thermatron 1-Row 720 AHX

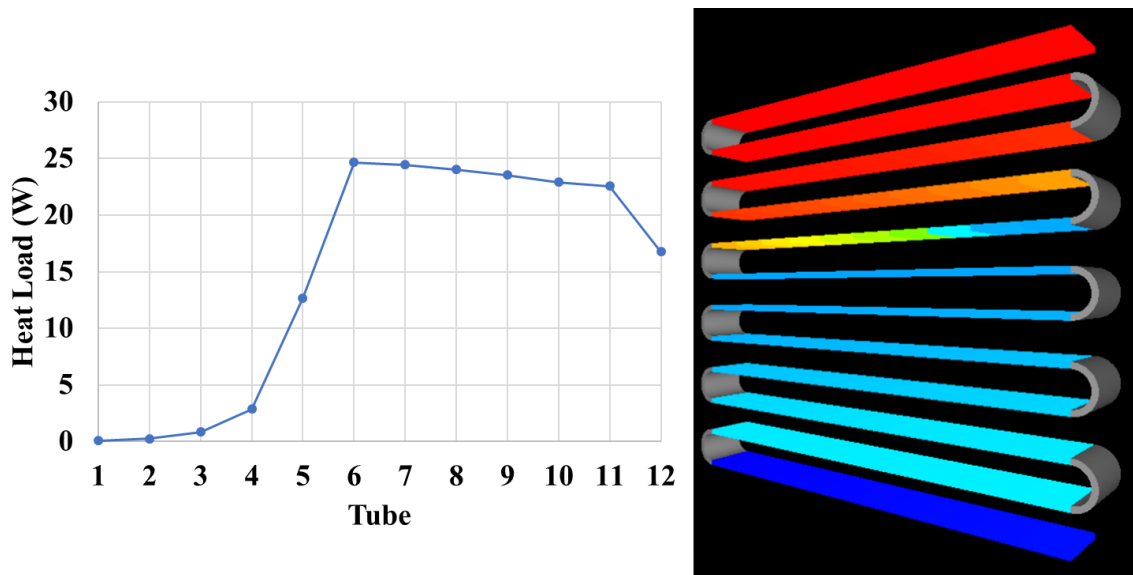


Figure 11: Sanhua Microchannel AHX

2.3.6 PCM-side Heat Exchanger

Most of the testing for this project was done on the PCM-side Heat Exchangers (PCMHX). The thermal conductivity of the PCM is the weak link in the heat transfer process and has significant impact on cooling cycle COP as well as total recharge time during thermosiphon mode [28]. The PCMHX acts as the condenser in the compressor-driven cooling mode and is the evaporator when the cycle is in thermosiphon mode. To accommodate the thermosiphon cycle, the heat exchanger is designed to promote the refrigerant to flow in a clockwise direction during thermosiphon mode. This is done by tilting the bottom header to the lower right corner of the container and tilting the outlet to the upper left corner of the PCMHX, as shown in Figure 2(b). If this design is not implemented correctly, the vapor will get trapped in the PCMHX and the refrigerant will not flow. The interaction between the tubes and PCM in the PCMHX is critical for the device. Therefore, different tube configurations, PCM container sizes, and enhancement types were designed and tested.

2.3.6.1 Phase Change Material

The core innovation of the RoCo device is that it does not reject waste heat into its local environment, and therefore requires no ventilation during the cooling operation. This is made possible with a PCM in which the waste heat is stored. The PCM used for this project was PureTemp 37 (PT37). The material is a paraffin wax based material, specially formulated so that the bulk of the material changes phase from a solid to a liquid at 37 °C. The properties of the material as reported by PureTemp are listed in Table 5.

Table 5: PureTemp 37 Material Properties

Property	Value
Melting point	37 °C
Heat storage capacity	210 kJ/kg
Thermal conductivity (liquid)	0.15 W/m·K
Thermal conductivity (solid)	0.25 W/m·K
Density (liquid)	840 kg/m ³
Density (solid)	920 kg/m ³
Specific heat (liquid)	2.63 kJ/kg·K
Specific heat (solid)	2.21 kJ/kg·K

Although the material used is called PureTemp 37, the entire phase change does not happen exactly at this temperature. The Differential Scanning Calorimetry (DSC) analysis presented by PureTemp is only for melting and does not include solidification. The solidification characteristics of the PCM is important for heat rejection and condenser design. An independent analysis of The PT37 was done by Ahmet et al. [29]. The resulting DSC curve is shown in Figure 12. The bulk of the PT37 material should be melted around 38 °C and fully solidified 35 °C. This is supported by experimental data, presented in Chapter 5:

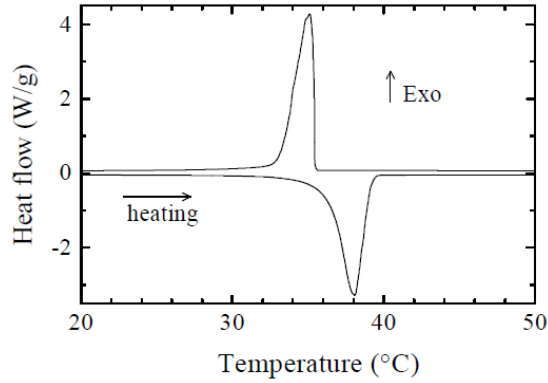


Figure 12: PureTemp 37 DSC analysis

The amount of PCM used in each in each PCMHX is calculated by weight. From experimental data gathered from BV1, the PCMHX absorbs 185 W during the cooling cycle operation. The amount of PCM needed was calculated using the properties listed in Table 5. The system was originally designed for an operating time of 2 hours by using Equation 1.

$$m = \frac{J}{l} \quad \text{Equation 1}$$

$$J = 185 \text{ W} * 2 \text{ hr} * 3600 \text{ s/hr} = 1.33 \text{ MJ} \quad (\text{energy stored})$$

$$l = 210 \text{ kJ/kg} \quad (\text{latent heat of fusion})$$

$$m = 6.34 \text{ kg} \quad (\text{mass of PCM})$$

With a factor of safety of 1.4 to ensure a full 2 hours of operation, the total amount of PCM needed is 8.6 kg. The internal volume of the container must be calculated using the liquid density of the PCM, which is 840 kg/m³. 8.6 kg / 840 kg/m³ = 0.0102 m³. The same process was used to calculate the weight of PCM needed and the volume of each container for the non-enhanced PCMHX, the two copper-enhanced PCMHX, and the two graphite-enhanced PCMHX.

2.3.6.2 Non-enhanced PCMHX

In Du's work, a baseline PCMHX performance was established. The weight of PCM used was calculated as shown above in section 2.3.6.1 The original PCMHX is shown in Figure 13.



Figure 13: PCMHX Version 1: Non-enhanced PCMHX

The non-enhanced PCMHX has four 6.35 mm OD copper tubes ($1/4$ " ACR copper tubing) embedded in the PCM, each 1.2 m long. This length was determined using Coil Designer by Du [23]. The headers are each 9.53 mm OD copper tubes ($3/8$ " ACR copper tubing). 6.35 mm holes were drilled into the headers and the tubes were brazed into place. Removable spacers were placed in the headers to set the spacing between the back of the sidewall of the headers and the inserted tubes. Nitrogen was used during brazing to promote a clean connection and prevent soot in the system. The R134a refrigerant runs through the

copper tubes in a clockwise direction during cooling mode and a counter clockwise direction in thermosiphon recharge mode (Figure 2). The copper PCMHX was built in the CEEE Heat Pump Lab and then inserted into the clear PVC pipe PCMHX container before the PCM was added. The PCM was then melted and poured into the PCMHX container. The amount of PCM added was measured by weight. A total of 8.6 kg of PCM was added to the container. During normal operation, the PCM is in contact with the copper tubes at all times.

With the non-enhanced PCMHX design, the thermal conductivity of the bulk material is 0.15 W/m·K, which is the thermal conductivity of PT37 in the liquified state. The reason the liquid thermal conductivity is used is because as soon as the cooling operation starts, the material directly next to the copper tube goes through a phase change and melts, creating a liquid barrier at all the tubes. The goal of introducing an enhancement to the PCM is to increase the bulk thermal conductivity of the PCM.

2.3.6.3 Copper Enhanced PCMHX

To increase the thermal conductivity of the PCM, a copper matrix was added to the PCMHX to create a copper enhanced PCMHX. The use of metal matrices to enhance thermal conductivity has become popular in recent decades. In a 2016 study done by Wu et al., a copper mesh was used to successfully improve thermal conductivity within a PCM plate for battery thermal management [30]. The copper enhancement used in this study was a pure-copper scouring pad, shown in Figure 14.



Figure 14: Single copper mesh

A specific type of metal matrix known as metal foams are already used widely in existing thermal energy storage units [50 – 51]. Their light weight and high thermal conductivity make them ideal candidates for PCM enhancements. In 2014, Yao et al. developed a prediction model for the effective thermal conductivity (k_e) of high porosity open cell metal foams [31]. Metal foams are made up of interconnected tetrakaidecahedrons (14-sided polyhedron) and are characterized by two main parameters: (1) relative density and (2) pore size. The relative density is defined as foam density divided by the density of the parent material. The pore size is a function of pore density, which is defined as the number of pores per inch in a sample. Figure 15 shows the various possible cross-sectional ligament (web) shapes and the negligible effect of the cross that section on k_e . Figure 16 shows the negligible effect of pore density on k_e in metal foams.

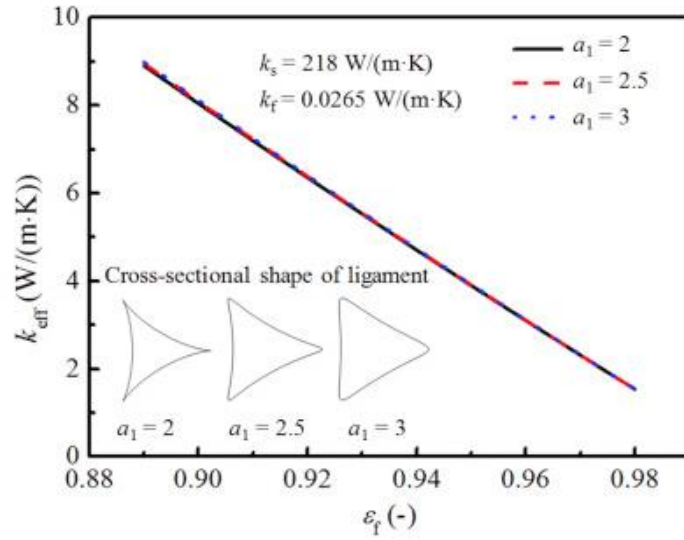


Figure 15: Influence of ligament shape on k_e in metal foams [31]

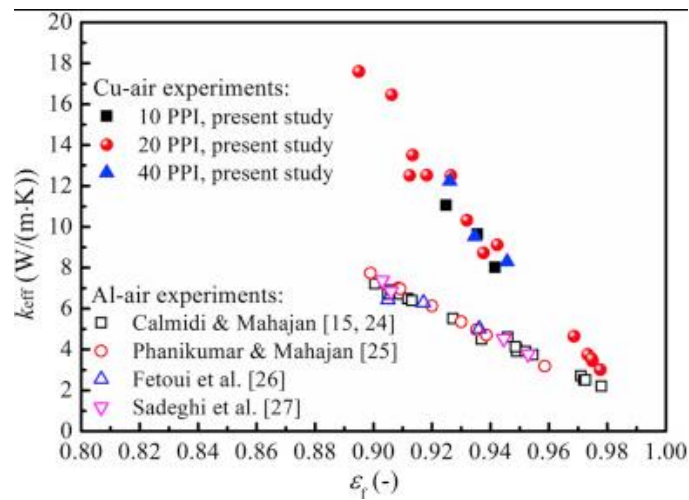


Figure 16: Influence of pore density on k_e in metal foams [31]

The k_e of metal foams therefore depends mostly on the foam porosity (ϵ_f). Ligament shape and pore density have negligible effect on k_e and therefore this model can be used to calculate k_e of the copper matrix used in this thesis even though the ligament shape copper scouring pad used in this study was different. Equation 2 is used to calculate the foam porosity (ϵ_f), where m_e is the mass of the enhancement, ρ is the density of the enhancement metal, and V is the total volume of the PCM and enhancement. The total volume is

calculated from the weight of the PCM: m_{pcm}/ρ_{pcm} where ρ_{pcm} is taken in the liquid state. Then, ε_f is used to iteratively solve for λ in Equation 3. The a_1 parameter used in equations 3 – 6 defines the ligament shape, which is not a sensitive parameter in this model. Therefore, a constant value of $a_1 = 2.1$ is acceptable. Equations 4 – 6 are used to calculate k_A , k_B and k_C . Finally, Equation 7 is used to calculate k_e .

$$\varepsilon_f = 1 - \frac{m_e}{\rho V} \quad \text{Equation 2}$$

$$\varepsilon_f = 1 - \frac{\sqrt{2}}{2} \pi \lambda (3 - 5\lambda) \frac{1+a_1^2}{a_1^2} \quad \text{Equation 3}$$

$$k_A = \frac{\sqrt{2}}{6} \pi \lambda (3 - 4\lambda) \frac{1+a_1^2}{a_1^2} k_{cu} + \left[1 - \frac{\sqrt{2}}{6} \pi \lambda (3 - 4\lambda) \frac{1+a_1^2}{a_1^2} \right] k_{pcm} \quad \text{Equation 4}$$

$$k_B = \frac{\sqrt{2}}{2} \pi \lambda^2 \frac{1+a_1^2}{a_1^2} k_{cu} + \left[1 - \sqrt{2} \pi \lambda^2 \frac{1+a_1^2}{a_1^2} \right] k_{pcm} \quad \text{Equation 5}$$

$$k_C = \frac{\sqrt{2}}{6} \pi \lambda^2 \frac{1+a_1^2}{a_1^2} k_{cu} + \left[1 - \frac{\sqrt{2}}{6} \pi \lambda^2 \frac{1+a_1^2}{a_1^2} \right] k_{pcm} \quad \text{Equation 6}$$

$$k_e = \frac{1}{\frac{\lambda}{k_A} + \frac{1-2\lambda}{k_B} + \frac{\lambda}{k_C}} \quad \text{Equation 7}$$

The amount of copper mesh used in each copper enhanced PCMHX was 5.5% by weight of the total PCM for a total copper weight of 0.473 kg for the four-tube PCMHX. The calculated k_e of the copper matrix is 0.872 W/m·K, an increase of 4.8x over the 0.15 W/m·K thermal conductivity of the liquid PCM. Table 6 shows the calculations of effective thermal conductivity of the copper enhanced PCMHX.

Table 6: Effective Thermal Conductivity Calculation of Copper Matrix Enhancement

Parameter	Symbol	Value	Units
Mass of copper enhancement	m_e	0.473	kg
Copper density	ρ	8,960	kg/m ³
Enhancement volume	V	0.0102	m ³
Foam porosity	ϵ_f	0.9948	-
Derived ligament parameter	λ	0.0256	-
Effective thermal conductivity	k_e	0.872	W/m·K

2.3.6.3.1 Four-tube PCMHX

The tube design of the copper enhanced PCMHX was the same as the non-enhanced: four 6.35 mm OD copper tubes, each 1.2 m long and 9.53 mm OD headers. The weight of PCM used is the same: 8.6 kg. The only difference is the addition of a copper mesh, evenly distributed throughout the PCMHX. The complete copper-enhanced PCMHX is shown in Figure 17. The average weight of each copper mesh was 13 g, a total of 37 copper meshes were used. The PCMHX has 4 helical tubes, each with 8 coils. A single copper mesh was wrapped around each coil, maximizing the contact area between the copper coil and the mesh. The remaining five meshes were used to fill any gaps in the matrix. Small plastic zip-ties were used to affix each mesh to the coil. The 5.5% by weight number was selected to mimic the graphite-enhanced PCMHX, as provided by Oak Ridge National Labs (ORNL).



Figure 17: 4-coil copper-enhanced PCMHX

After the copper meshes were affixed to the copper coils, the copper-enhanced PCMHX (CuPCMHX) was placed in a container the same size as the non-enhanced PCMHX and filled with liquified PCM. The weight of the PCM in the copper-enhanced PCMHX is same as the non-enhanced PCMHX. This CuPCMHX was instrumented with two thermocouples: one 28.0 cm from the top of the container near the outlet tube, and one 12.7 cm from the top of the container near the inlet tube.

2.3.6.3.2 Eight-tube PCMHX

In addition to the four-tube copper-enhanced PCMHX, an eight-tube PCMHX was designed and constructed. The purpose of the eight-tube PCMHX was to allow for an increase in the amount of PCM in the thermal battery, thus increasing the cooling time from 2 hours to 4 hours. The design is similar to the 2-hour version: both have 6.35 mm OD copper tubes, each 1.2 m long and 9.53 mm OD headers. The eight-tube PCMHX was instrumented with 46 type-T thermocouples: 30 directly attached to the copper tubes and 16 in the center of each helical coil, embedded in the PCM. The eight-tube copper-enhanced PCMHX is shown in Figure 18.



(a) PCMHEX with thermocouples



(b) PCMHEX with copper mesh

Figure 18: Eight-tube PCMHEX

2.3.6.4 Graphite-enhanced PCMHEX

Two graphite-enhanced condensers were tested, both designed by ORNL. One was designed for two hours of cooling operation, and the other was designed for four hours of cooling operation. Using graphite as a PCM enhancement will reduce the latent heat capacity of the PCM, but it increases the heat transfer between the copper refrigerant tubes and the PCM [47, 53]. The graphite was expanded under vacuum to a bulk-density of 100 kg/m^3 . Parametric studies on the bulk density of the graphite blocks, PCM and resulting thermal conductivity were done by Mallow et al. [32]. A graphite foam bulk density of 100 kg/m^3 was found to be the best balance between latent heat capacity and thermal conductivity. The blocks were then saturated with PCM and tested experimentally to confirm the simulated thermal conductivity of $11.3 \text{ W/m}\cdot\text{K}$. This is 7,433.3% higher than the liquid PCM thermal conductivity and 1,195.9% higher than the copper enhanced PCM.

2.3.6.4.1 2-hour graphite-enhanced PCMXH

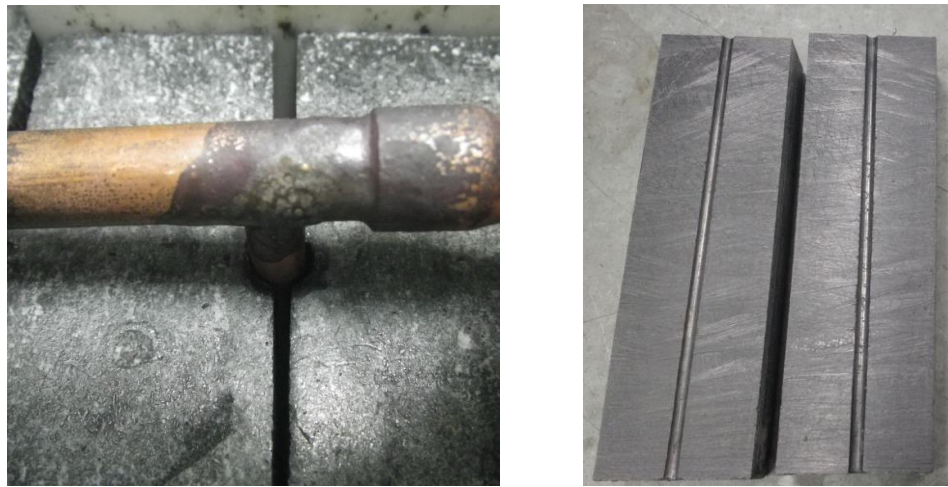
The two-hour graphite-enhanced PCMXH (GrPCMXH) tested in this experiment was designed by Mallow at ORNL. The tubes used in the 2-hour GrPCMXH are shown in Figure 19. Note that this design is radically different from the previous condensers: the tubes are straight and significantly shorter: 0.3 m rather than 1.2 m. The tubes are also vertical rather than helical.



Figure 19: Graphite-enhanced PCMXH

The GrPCMXH was designed from the ground up to be a 2-hour heat storage device with no safety factor. The copper tube design was also changed to accommodate the expected improvement in heat transfer enabled by the graphite enhancement. The GrPCMXH has 6.35 mm OD tubes with 9.53 mm OD headers, the same as the copper-enhanced PCMXH. The tube shape is straight rather than helical, and each tube is only 0.3 m long rather than 1.2 m long. The increased thermal conductivity of the graphite foam enhancement allows

for the smaller heat transfer area. Also note that the GrPCMHX was designed before the experimental condenser capacity values were available, and instead of 185 W of heat transfer in the condenser, 160 W was used in the calculation to determine the weight of PCM needed. Using Equation 1 and a safety factor of 0, the weight of the PCM in the blocks delivered from ORNL was 5.5 kg. The blocks were then post-processed by shaving material off the sides of each block to get them to fit in the 3D printed PCM container, 6.35 mm holes were drilled down the center of each block to allow for the tubes to pass through the blocks and then the blocks were cut in half lengthwise to allow for assembly.



a) Gap around the tube b) Full cross-section of GrPCM block

Figure 20: Post-processed graphite block, a) gap around tube, b) full cross-section

After all the post processing, the total weight of the PCM in the four blocks was 4.7 kg. Once the completed graphite-enhanced PCMHX was placed in the condenser container, the container was filled with 0.64 kg of PCM to fill any remaining gaps in the container. The total amount of PCM was 5.38 kg. Using the experimental condenser capacity of 185 W, this should be sufficient for a total cooling time of 1.7 hrs. The filled and completed graphite-enhanced PCMHX is shown in Figure 21.



Figure 21: Graphite-enhanced PCMXX with PCM

2.3.6.4.2 4-hour graphite-enhanced PCMXX

The 4-hour GrPCMXX was also designed by ORNL. It was produced by saturating disks of expanded graphite foam with 530 g of PT37. The disks were 0.254 m in diameter and .0127 m thick. The expanded graphite had a bulk density of 100 kg/m^3 , the same as the smaller graphite condenser. 24 of these disks were used to create a GrPCMXX with 12.7 kg of PCM. This condenser can provide 4 hours of cooling when the condenser is operating at the experimentally confirmed average capacity of 185 W. Like the 2-hour graphite-enhanced condenser, straight 6.35 mm OD copper tubes and headers were used. The 4-hour condenser has eight tubes, each 0.33 m long. The copper-tube heat exchanger was assembled except for the top header and then the disks were fitted onto the tubes. Thermocouples were inserted between the graphite disks during the assembly process. The top header was brazed to the tubes after the last graphite disk was put in place. Care was taken to minimize burning of the top graphite disk during final assembly. The assembled and instrumented 4-hour graphite-enhanced condenser is shown in Figure 22. The

assembled graphite disks and copper heat exchanger was placed in an 18.9 L (5 gal.) bucket. After running three cycle tests, the bucket was back-filled with enough liquid PCM to cover all the disks, eliminating any air gaps between each disk and between the copper tubes and graphite disks. The final weight of PCM in the 4-hour GrPCMHX was 14.3 kg.



Single 25.4 cm dia. graphite-enhanced
PCM disk



Fully assembled graphite-enhanced
PCM with thermocouples

Figure 22: 4-hour graphite-enhanced PCMHX

Chapter 3: Instrumentation

To compare the effectiveness of each PCMHX listed in section 2.3.6 the breadboard system was fully instrumented. Figure 2 shows the locations of the measurement devices on the breadboard system. On the refrigerant side, temperatures and pressures were measured at several places. These measurements were used to calculate the enthalpy at different stages in the cycle. A mass-flow meter was also installed to ensure a proper flow rate and for capacity calculations. The power of the compressor and fan were also measured. Not shown in Figure 2 are the thermocouples embedded in the PCMHX which measure the PCMHX tube temperatures as well as the PCM temperatures during the cooling and recharge cycles. More details on the number of thermocouples and their placement can be found in section 3.2.2 below.

3.1 Mass-flow Meter

The mass-flow meter used was a Micro Motion coriolis flow meter with a Micro Motion Model 2700 transmitter. The mass-flow meter used has an accuracy of $\pm 0.10\%$ for liquid and can be programmed to accept different ranges of mass-flow. The target mass-flow for this system is 1 g/s, so the device was calibrated to a range of 0 – 3 g/s. The mass flow meter was placed after the condenser in cooling mode and on the uphill side of the cycle, allowing the refrigerant flow to be measured as a liquid. Practically speaking, the mass flow is helpful in establishing the proper amount refrigerant charge when filling the system with refrigerant: when the system does not have enough refrigerant, overall pressure is too low, and the refrigerant is not fully liquified when exiting the condenser. The mass flow meter will show large fluctuations when the refrigerant has a quality greater than 0. By filling the system with refrigerant very slowly (with vapor) and watching the mass flow

meter reading, it is possible to ensure that the system has the minimum amount of refrigerant needed to operate correctly. Note that the mass-flow meter has a large thermal mass compared to the size of the rest of the system and it is recommended to insulate the flow meter during normal operation to prevent excessive heat loss. The output of the transmitter is a 4-20 mA signal, sent to the LabView data acquisition system.



Figure 23: Micro Motion coriolis flow-meter and transmitter

3.2 Temperature

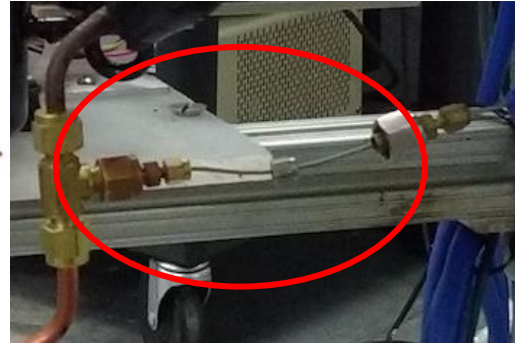
Temperature measurements were taken at various places in the cycle. Refrigerant, tube, and PCM temperatures were all recorded.

3.2.1 Refrigerant Temperature

The refrigerant temperature was measured in five places throughout the cycle using RTDs. Each RTD was a Class 1/10 DIN 4-wire sensor with a 3.175 mm ($1/8$ "") closed-end immersion probe. The model used was the ULTRA PRECISE RTD SENSORS P-M-1/10-1/8-6-0-P-3 8 which has an accuracy of ± 0.3 °C. The probes were fitted into the VCC system with 3.175 mm ($1/8$ "") Swagelok compression fittings as shown in Figure 24.



a) 4 wire 1/10DIN RTD



b) Installed RTD using Swagelok fitting

Figure 24: RTD sensor

The temperature sensors were placed to allow temperature readings of the of the refrigerant before and after the PCMHX, AHX, and the compressor. The RTD sensor locations are shown in Figure 25.

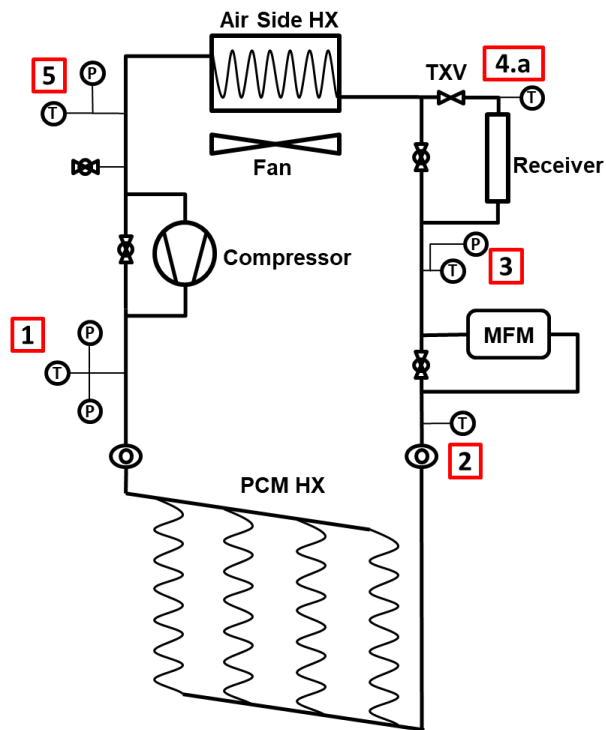


Figure 25: System schematic with sensor locations

When coupled with the readings from pressure sensors placed in the same locations and readings from the mass-flow meter, it was possible to make capacity calculations of the AHX and PCMHX, as shown in Table 7. Note that position 4.a in Figure 25 is before the TXV, and position 4.b (Figure 32) is after the TXV at the inlet to the AHX.

Table 7: Sensor Placement for Capacity of VCC Component

RTD Position	Change in Enthalpy of Component
1, 2	PCMHX
3, 5	AHX
5, 1	Compressor

3.2.2 PCMHX Temperature

To better understand the heat flow in the PCMHX, each was fitted with several Type T thermocouples. Type T thermocouples have an accuracy of ± 0.5 °C. In each PCMHX, thermocouples were placed to measure the temperature of each copper tube in the heat exchanger in multiple places, as well as the PCM temperature in multiple places. The thermocouple placement of the 2-hour GrPCMHX is shown in Figure 26. There are thermocouples placed on each of the tubes, and then three thermocouples evenly spaced between the tubes which measure the PCM temperature.

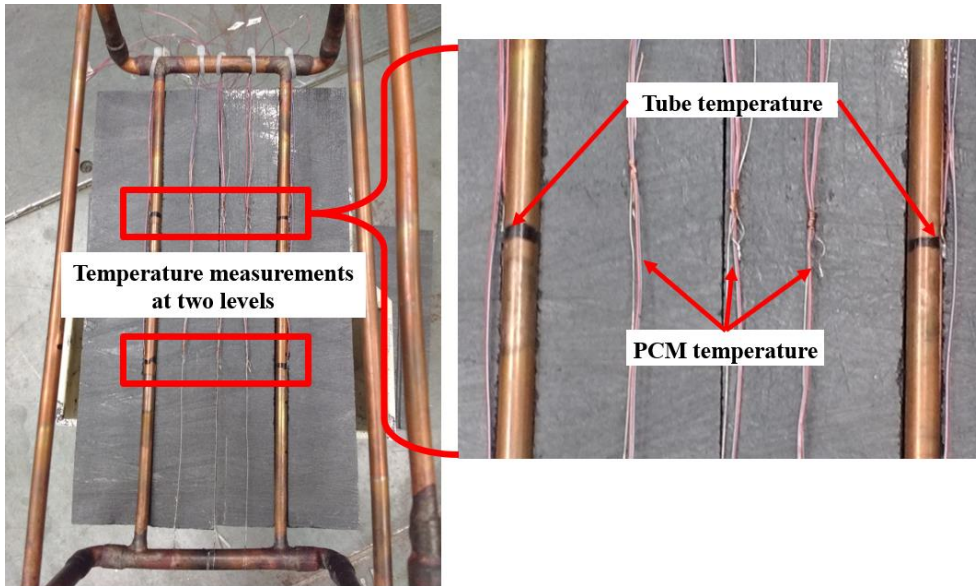


Figure 26: Typical thermocouple placement in PCMHX

Each thermocouple was calibrated in a temperature controlled bath at 10 °C increments from 10 °C - 60 °C. The R^2 value of each calibration was 6 nines or greater. Schematics of the thermocouple locations are shown for each of the PCMHX in Figure 27 - Figure 30.

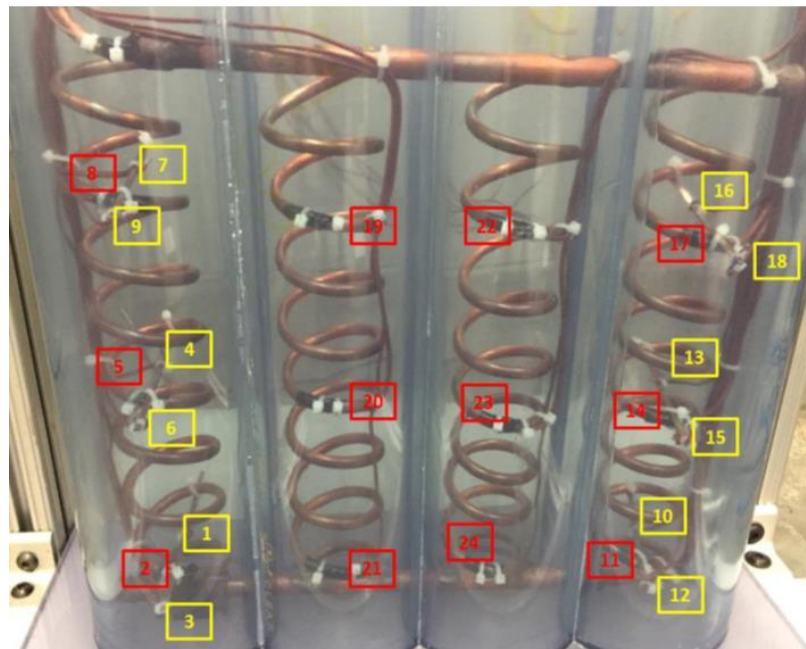


Figure 27: 2-hour non-enhanced PCMHX thermocouple placement

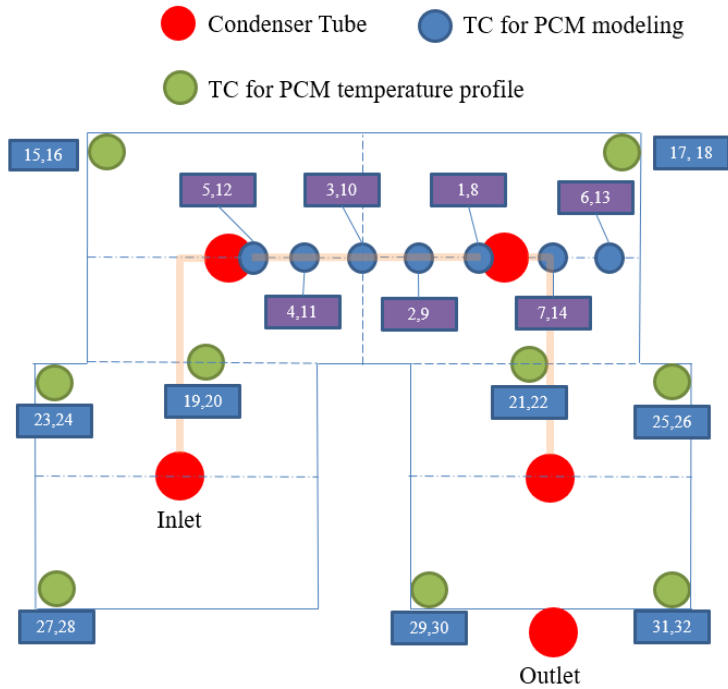


Figure 28: 2-hour GrPCMHX thermocouple placement

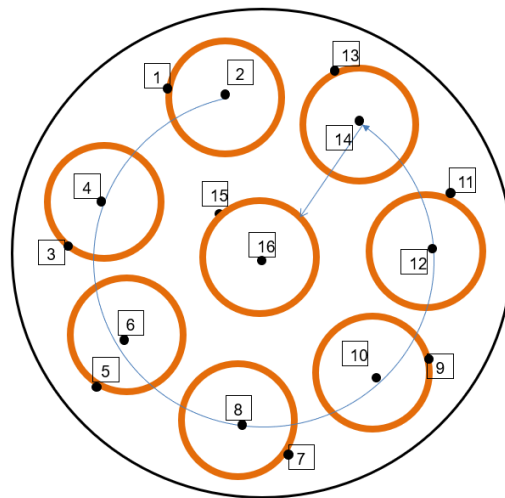


Figure 29: 4-hour CuPCMHX thermocouple placement

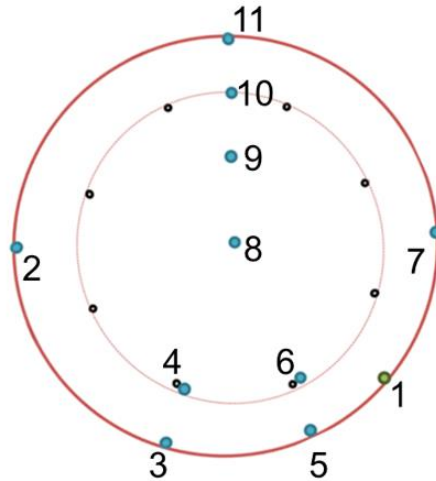
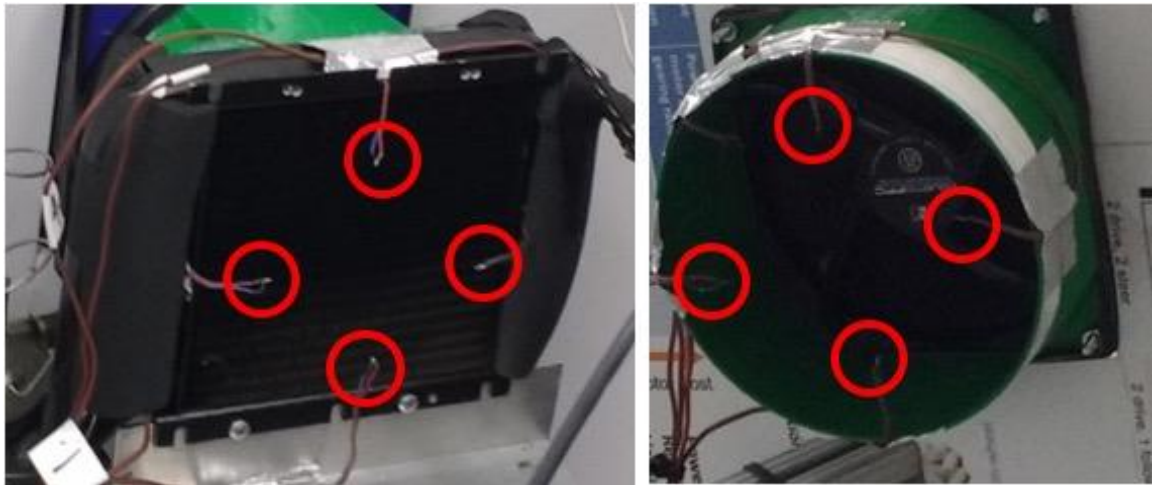


Figure 30: 4-hour GrPCMHX thermocouple placement

3.2.3 Air Temperature

T-type thermocouples were also used to measure the air temperature. The placement of the air-side thermocouples are shown in Figure 31.



a) Air-side HX inlet

b) Air-side HX outlet

Figure 31: Air temperature of AHX

Four thermocouples were used at the inlet and outlet to get an average temperature. This helps to reduce the sampling error of the T-type thermocouples. The average inlet temperature was also used to measure the ambient room temperature of the environmental

chamber. These thermocouples were calibrated using the same procedure as described in section 3.2.2 .

3.3 Pressure Transducers

The refrigerant pressure was measured at locations 1, 3 and 5 in Figure 25. Only two pressure readings were necessary because portions of the VCC system operates along lines of constant pressure, as shown in Figure 32. The pressure transducer at position 3 is redundant. It confirms the constant pressure assumption across the condenser and ensures that the pressure reading before the refrigerant enters the TXV is accurate. Experimental data confirmed that the constant pressure assumption across the condenser was valid.

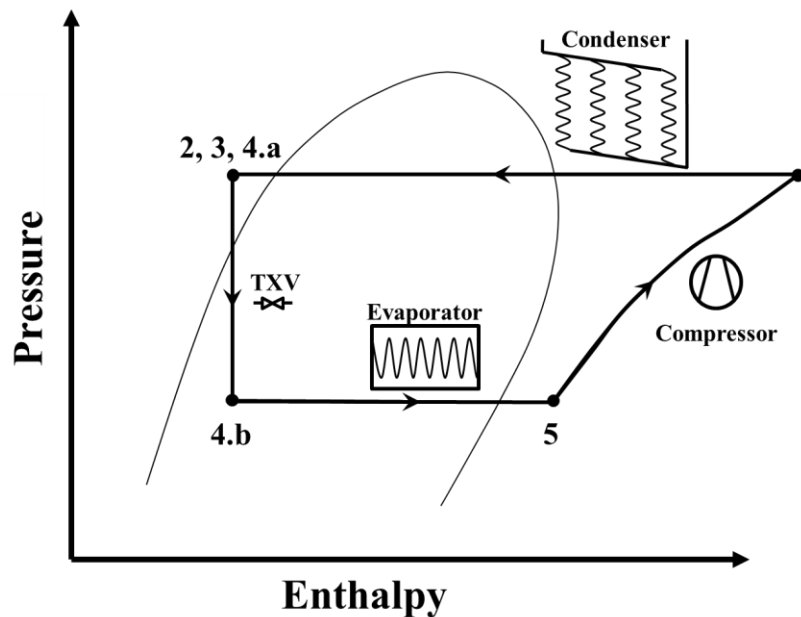


Figure 32: VCC pressure-enthalpy diagram

The pressure transducers used were Setra AccuSense™ Model ASM high accuracy pressure transducers. Each transducer has an accuracy of $\pm 0.05\%$. The pressure transducers used at positions 1 and 5 were absolute sensors with a range of 0 – 3,447 kPa and the transducer at position 3 measured gage pressure with a range of 101 – 3,548 kPa.

The output of the gage-pressure transducer was adjusted by one atmosphere (101.325 kPa) in the data acquisition program to give an absolute pressure reading. Also note that this transducer was not used for any calculations: it just confirmed the no-pressure drop assumption across the condenser.



Figure 33: Setra pressure transducer

The pressure transducers were each calibrated using the Omega PCL 5000 pressure calibrator. The calibrator has an accuracy of 0.05%. Each of the three pressure transducers was calibrated with a 6-point calibration from 101.3 kPa to 1,530.6 kPa, absolute pressure. The R^2 of each calibration was 7 nines or greater.



Figure 34: Pressure calibrator

3.4 Power/Current

To evaluate the performance of the VCC system, electrical power consumption of the system was compared with cooling capacity to get a coefficient of performance for the system, or COP. COP is traditionally defined as evaporator capacity in watts divided by the electrical power consumption of the compressor, as shown in Equation 8.

$$COP = \frac{\text{Cooling output}}{\text{Work input}} = \frac{Q_{cooling}}{W_{electrical}} \quad \text{Equation 8}$$

Voltage and current readings of the compressor were used to calculate the power consumption of the compressor. Power information of the fan was also gathered for RoCo run-time implications, but not included in COP calculations.

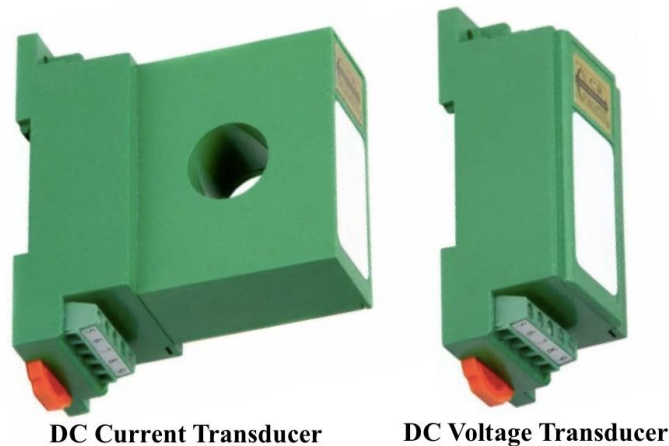


Figure 35: Current and voltage transducers

The current transducer is a CR Magnetics CR5211 DC Hall Effect Current Transducer with a range of 0 – 10 ADC \pm 1% and a 10 VDC output. The voltage transducer is a CR5310 DC Voltage Transducer with a 0 – 50 VDC input range and a 0 – 5 VDC output. The signals were sent to the LabView data acquisition software. All electrical components were powered with a 24 VDC power supply.

3.5 DAQ

The entire breadboard test system was controlled with a LabView data acquisition system (DAQ). The DAQ also read the sensors and transmitted the information to a computer. The thermocouples were read directly by dedicated thermocouple units, the NI-9214. The compressor, fan, and actuated ball valves were all controlled with a NI-9472 digital output unit. The NI-9472 unit has 8 output channels and each channel has a maximum voltage of 30 VDC and 0.75 A. All the transducer outputs were read by a NI-9207 unit which has 16 analog input channels: 8 current channels with a range of ± 20 mA and 8 voltage channels with a range of ± 10 VDC. The DAQ modules used are shown in Figure 36.



Figure 36: National Instruments DAQ modules

The DAQ was also used to automate system based on the temperature of the PCM. If the PCM temperature was a below the cooling setpoint, the DAQ closed all the ball valves and turned on the compressor for cooling mode. If the PCM temperature was above the cooling setpoint, the cycle switched to thermosiphon mode by turning off the compressor and opening the ball valves. The system was left to run continuously for a set number of cycles, typically at least three full cycles.

3.6 Safety Systems

Because the system was designed to run continuously, both mechanical and software safety systems were put in place. A pressure switch was installed directly after the compressor and set at a maximum pressure of 1,800 kPa. The maximum expected operating pressure of the VCC was 1,700 kPa. A high temperature switch was also installed on the compressor which turns the compressor off if it gets too hot. In the LabView DAQ, a software maximum operating pressure was set just below the mechanical pressure switch set-point at 1,790 kPa.

3.7 Uncertainty Analysis

Uncertainty analysis was conducted on all values that were gathered or calculated from measured data. Examples of measure data in this thesis includes temperature, pressure, mass-flow, power and current. Uncertainty of a measurement, or total uncertainty, (u_{total}) is the sum of random uncertainty (u_{rand}) and systematic uncertainty (u_{sys}). The systematic uncertainty of a measured variable is determined by the accuracy of the measurement device as shown in

Table 8: Instrument Specification and Systematic Uncertainty. Systematic uncertainty of a calculated variable can be found by using Equation 9. In Equation 9, u_n is the systematic uncertainty of the measured parameter and $\frac{\partial f}{\partial x_n}$ is the partial derivative of the calculated parameter, f , relative to the measured parameter, x_n . Random uncertainty is the standard deviation of the actual measurements collected over a certain time interval, as shown in Equation 10. The entire process studied here is dynamic and transient, therefore only systematic uncertainty was considered in this study, in accordance with the methodology adhered to by Du. Therefore, $u_{total} = u_{sys}$ as shown in Equation 11. Table 9 shows

example calculations of the systematic uncertainty in the system. The values in the 4th column are representative values taken from actual test data.

$$u_{sys} = \sqrt{\left(u_1 * \frac{\partial f}{\partial x_1}\right)^2 + \left(u_2 * \frac{\partial f}{\partial x_2}\right)^2 + \dots + \left(u_n * \frac{\partial f}{\partial x_n}\right)^2} \quad \text{Equation 9}$$

$$u_{rand} = \sqrt{\frac{\sum(x_j - \bar{x})^2}{N-1}} \quad \text{Equation 10}$$

$$u_{total} = u_{sys} + u_{rand} \quad \text{Equation 11}$$

Table 8: Instrument Specification and Systematic Uncertainty

Instrument	Type	Range	Unit	Accuracy
Pressure	Strain	0 – 3,447	kPa	±0.05%
Pressure	Strain	101 – 3,548	kPa	±0.05%
Temperature	T-type	-250 - 350	°C	± 0.5
Temperature	RTD 1/10 DIN	0 - 100	°C	± 0.3
Mass-flow	Coriolis	0 – 3	g/s	± 0.10 %
Current	Hall Effect	0 – 10	A	± 1 %
Voltage		0 - 50	V	± 1 %

Table 9: Uncertainty Analysis Sample Calculations

Measured or Calculated	Parameter (Figure 25)	Unit	Value	Systematic Uncertainty
Measured	P1	kPa	1,519.2	1.519
Measured	P3	kPa	1,533.9	1.534
Measured	P5	kPa	508.2	0.508
Measured	T1	°C	56.4	0.6
Measured	MFM	g/s	0.9964	0.0010
Measured	T _{PCM}	°C	45.9	2
Calculated	Fan Power	W	6.97	0.10
Calculated	Compressor Power	W	60.45	0.78
Calculated	Evap. Capacity	W	168.9	0.5
Calculated	Cond. Capacity	W	161.8	0.6
Calculated	Ave. Evap. Inlet (air)	°C	25.6	0.5
Calculated	Ave. Evap. Outlet (air)	°C	22.0	0.5
Calculated	COP	-	2.79	0.04

Chapter 4: Testing Procedures

RoCo was originally designed to deliver 150 W of cooling when used inside a building where the ambient room temperature was 26.0 °C. The original baseline BV1 tests were run under these conditions, with a single cooling and recharge cycle. Sufficient time was given at the end of the stand-alone test to allow the PCM temperature to reach equilibrium with the ambient room temperature. Additional use cases were added after the construction of the original device, and the BV2 system was tested under additional conditions. These conditions included different ambient room temperatures as well as repeated back-to-back cooling and recharge cycles. ASHRAE Standard 116, Section 8 specifies the test conditions under which air conditioners and heat pumps are to be tested [25]. These specifications were used to guide the conditions under which the RoCo breadboard system was tested. The critical difference between RoCo and a traditional VCC air conditioning system is that in a traditional system, the indoor and outdoor units operate in different temperatures. The indoor unit operates inside where the air is cooler, and the outdoor unit operates outside where the air temperature is much higher. In the RoCo system, both heat exchangers are inside the conditioned space. Therefore, the exact testing procedures in ASHRAE Standard 116, Section 8 were only used to guide the RoCo test conditions. Table 10 shows the conditions under which RoCo was tested.

Table 10: Ambient Air Test Conditions

Test Specification	RoCo Test Condition °C (°F)
Baseline (all PCMHX)	26.0 (80.1)
Cu PCMHX only	30.0 (86.0)
Cu PCMHX only	35.0 (95.0)

The baseline tests were performed in an environmental chamber set at 26.0 ± 0.5 °C. The humidity was not measured or controlled. Each of the five condensers were tested under this condition. This temperature was selected based on the original design parameters of the RoCo device: to deliver 150 W of cooling in a room at 26.0 °C. The CuPCMHX was tested under two additional ambient air conditions: 30.0 °C and 35.0 °C.

When each test was run, the environmental chamber was held at the specified test condition temperature. The compressor and evaporator fan were turned on and the cooling cycle began to run. The PCM temperature was monitored on the DAQ system and when the PCM was fully liquified, the compressor was turned off and the ball valves were opened. The system then ran in thermosiphon mode until the PCM temperature indicated that the PCM had fully solidified and was ready for another cooling cycle. For the single-cycle tests, this was the end of the test. For the cycle test, the procedure was repeated at least three times.

Chapter 5: Test Results

5.1 Single Cycle Tests at Room Temperature

5.1.1 8.6 kg Baseline Non-enhanced PCM Test

The results in this section are based on the results from Du's previous work.

For the baseline test, the RoCo breadboard system was run ambient air temperature of 26.0 ± 0.5 °C. The entire system was allowed to rest at room temperature until the PCM reached equilibrium with the air temperature at 26.0 °C. The cooling cycle was then initiated and run until most of the PCM was at least 37.0 °C. Once the minimum temperature was reached, all the ball-valves were manually opened, and the compressor was turned off, allowing the system to operate in thermosiphon mode. The system was allowed to run in thermosiphon mode until the PCM temperature once again reached equilibrium with the ambient room temperature. The temperature of the PCM for the baseline test is shown in Figure 37. Note that the lowest two temperatures, TC-3 and TC-12 correspond with the thermocouples at the very bottom and outside of the PCMHX, closest to the wall of the PCM container. The refrigerant has undergone full phase change at this point, and has very little heat to transfer to the PCM. The entire cycle took 549 minutes, or 9 hours and 9 minutes.

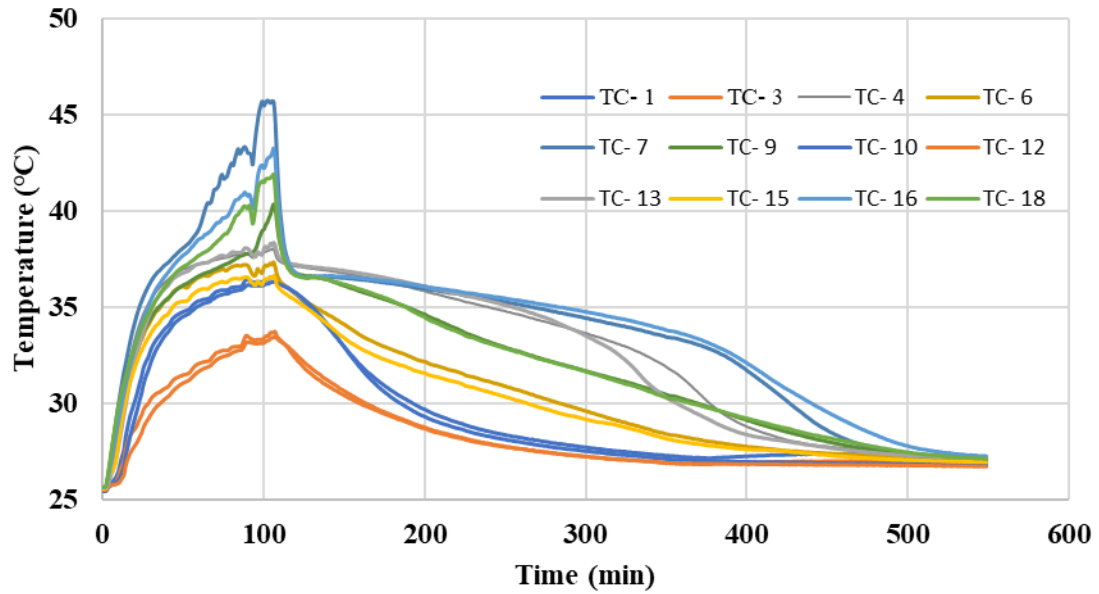


Figure 37: 8.6 kg baseline non-enhanced PCMHX PCM temperature

Figure 38 shows the tube temperature of the PCMHX. Note that the tube temperatures vary greatly with location. The tubes in Figure 38 are labeled according to Figure 27. Generally speaking, the tube temperatures are higher in the upper portion of the PCMHX, and now decrease in temperature towards the outlet at the bottom right of the PCMHX. This is a trend that is repeated throughout all the PCMHX that were tested.

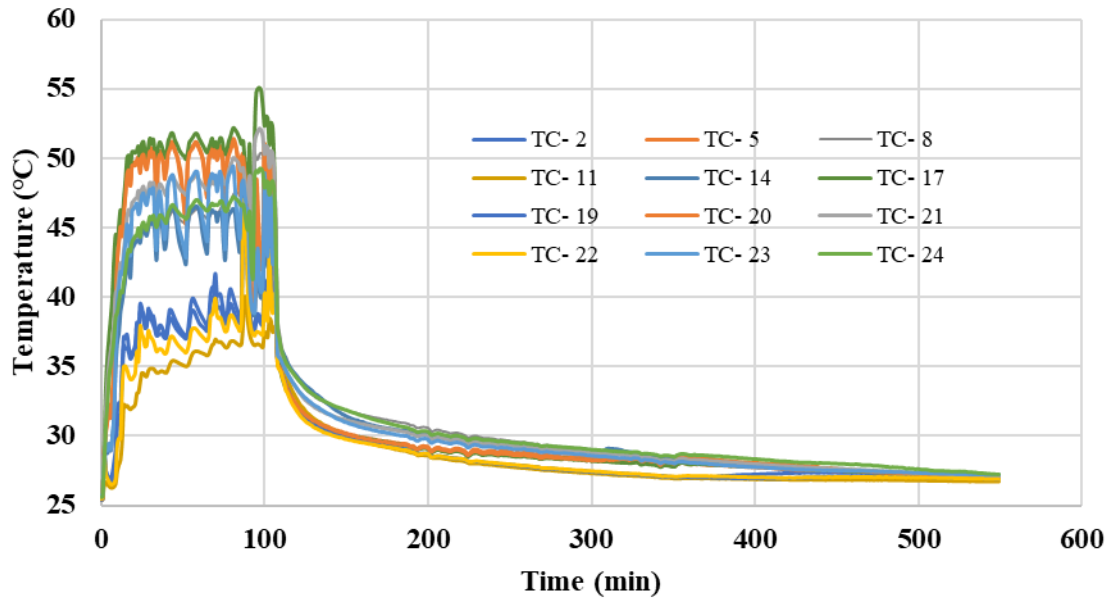


Figure 38: 8.6 kg baseline non-enhanced PCMHX tube temperature

Analysis of the initial breadboard test showed that the phase change is not complete at 37 °C. As shown in Figure 1, the PCM is fully melted after the temperature has inflected upwards. TC1 shows such an inflection point, and in future test the cycle was not switched from cooling to recharge until after this inflection point was reached at all points in the PCM. This temperature measurement is highly dependent on the location of the thermocouple within the PCM and should be carefully considered when determining where to place the thermocouples.

The COP of the non-enhanced cycle is shown in Figure 39. The large variation in COP is a result of the manually adjusted expansion valve used in BV1. The average COP was 2.41, but future baseline tests should be done with a TXV to stabilize the compressor pressure and overall performance of the system. The fluctuations in the pressure is shown in Figure 40.

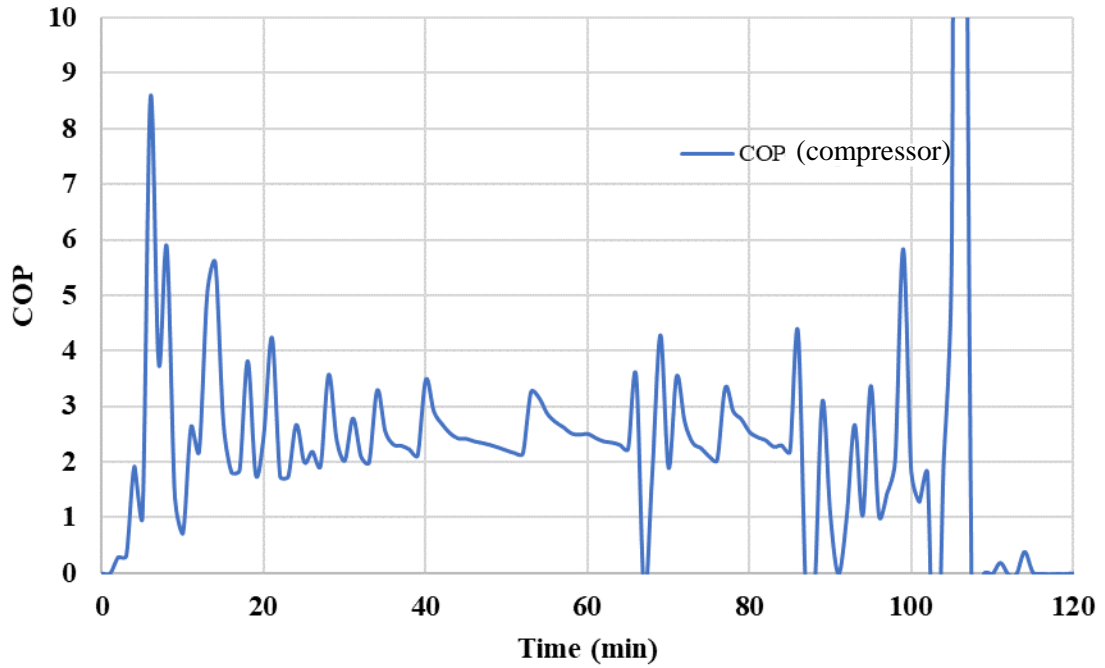


Figure 39: 8.6 kg baseline non-enhanced COP

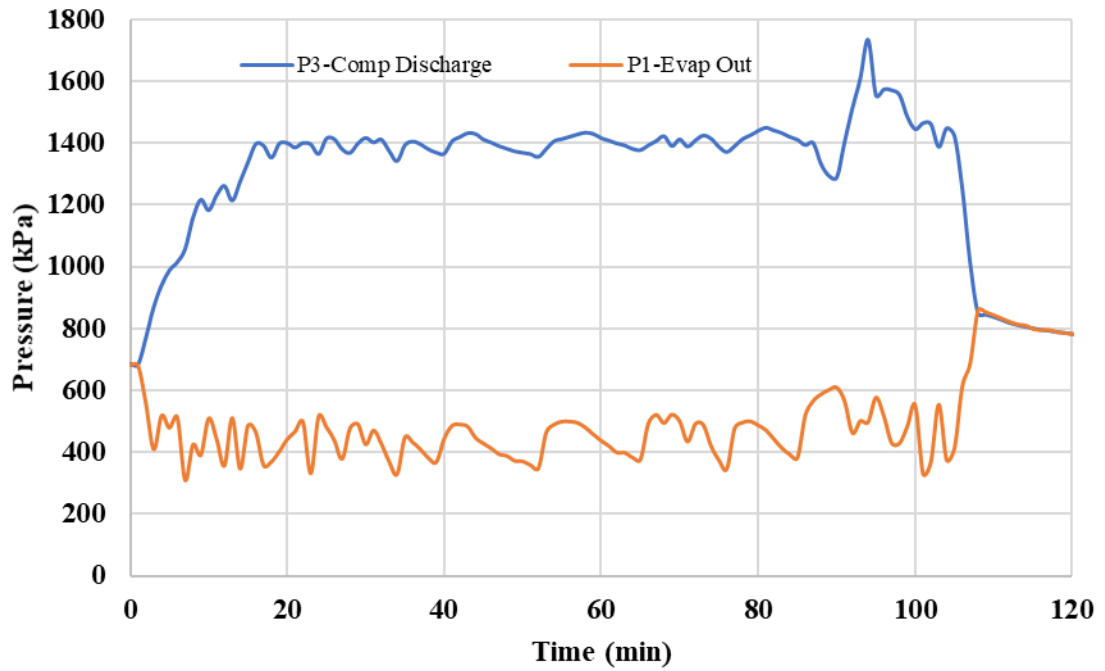


Figure 40: 8.6 kg baseline non-enhanced pressure

Figure 41 shows the average air temperature inlet and outlet for the AHX. The AHX had an average room temperature of 25.7 °C and an average delta T of -1.78 °C. during the cooling cycle.

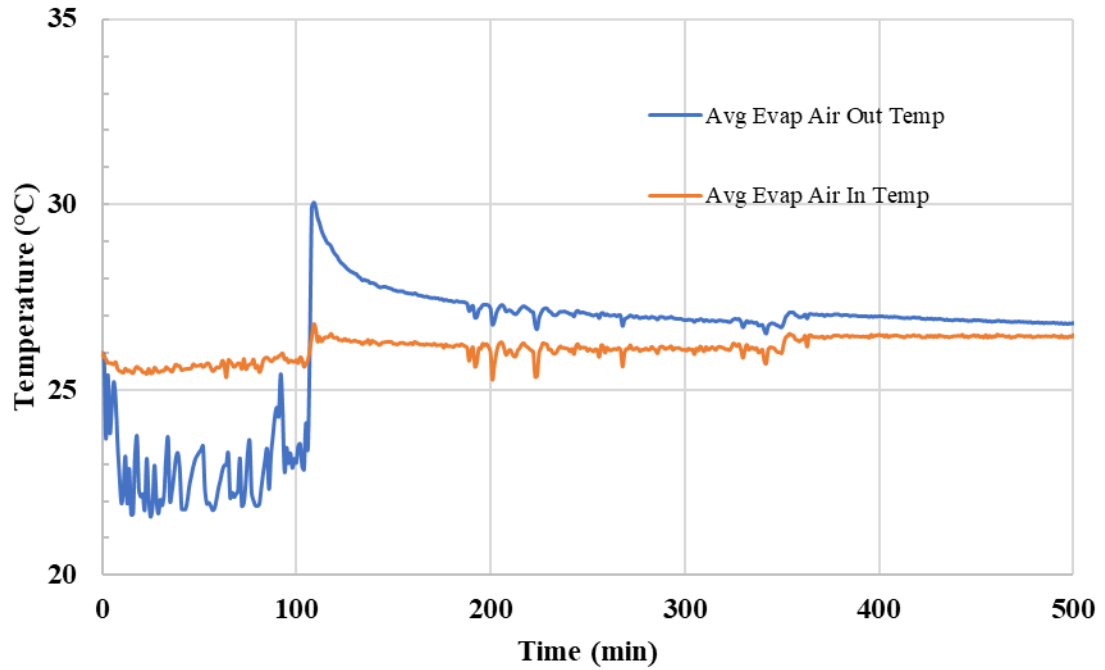


Figure 41: 8.6 kg baseline average air temperature in and out of AHX

Figure 42 shows the capacity of the evaporator and condenser throughout the cooling cycle.

The average condenser capacity was 169.1 W and the average evaporator capacity was

149.1 W

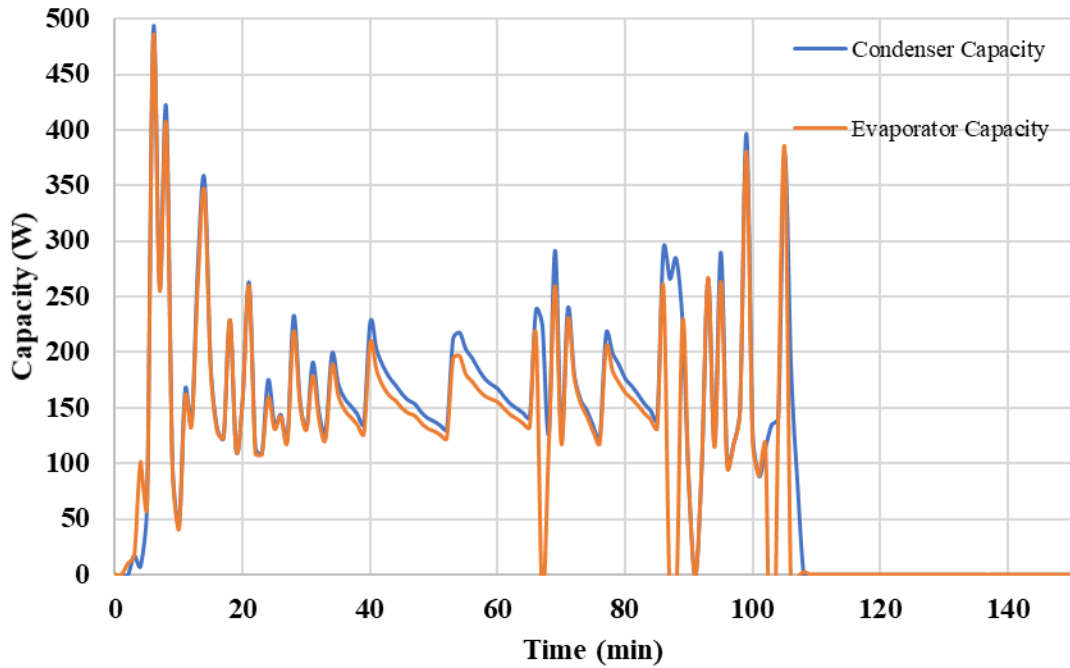


Figure 42: 8.6 kg baseline capacity of evaporator and condenser

Figure 43 shows the mass-flow rate of the refrigerant during the baseline test. The average mass-flow rate was 0.00092 kg/s.

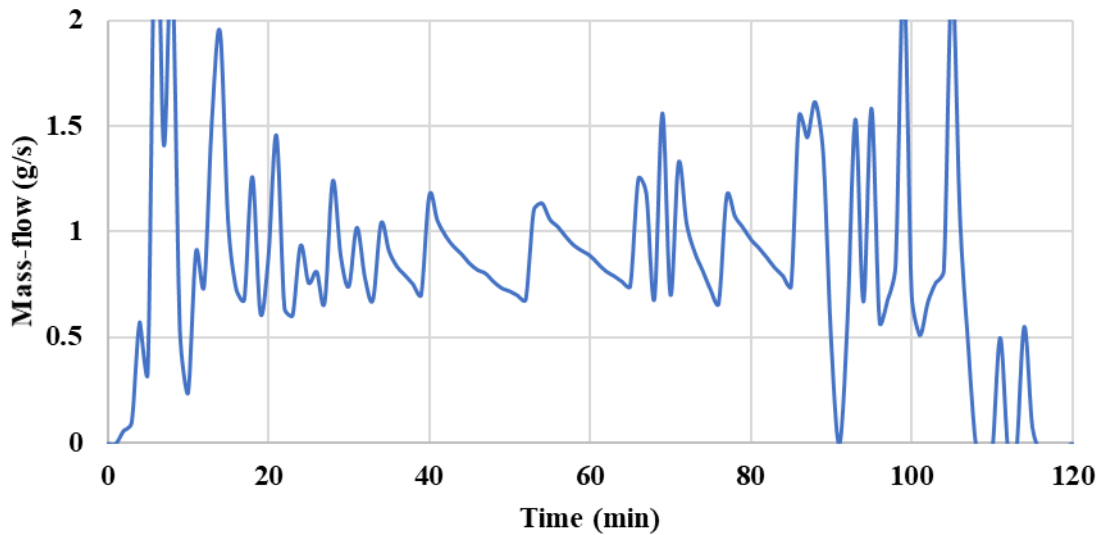


Figure 43: 8.6 kg baseline refrigerant mass-flow rate

5.1.2 8.6 kg Copper-enhanced PCM Test

After the non-enhanced PCM_{HX} was tested, the condenser was replaced with CuPCM_{HX} as described in 2.3.6.3.1 This condenser had 8.6 kg of PCM and 5.5% by weight of copper enhancement distributed throughout the volume of the condenser. The two condenser designs are otherwise the same. To determine when the PCM was fully melted or solidified, two thermocouples were placed in the PCM as described in section 3.2.2 The temperature profile of a typical cooling and recharge cycle is shown in Figure 44. TC-7 was placed 27.9 cm from the top of the container and as close to the wall of the container as possible. The lack of inflection point in the orange line shows that the thermocouple was too close to the wall of the container and was most likely measuring the wall temperature and not the PCM temperature. This thermocouple was inserted into the PCM after construction of the CuPCM_{HX} and its exact location with respect to the copper coils, copper mesh and container wall is not known. As noted previously, determining the state of the PCM by temperature is highly dependent on the location of the thermocouple.

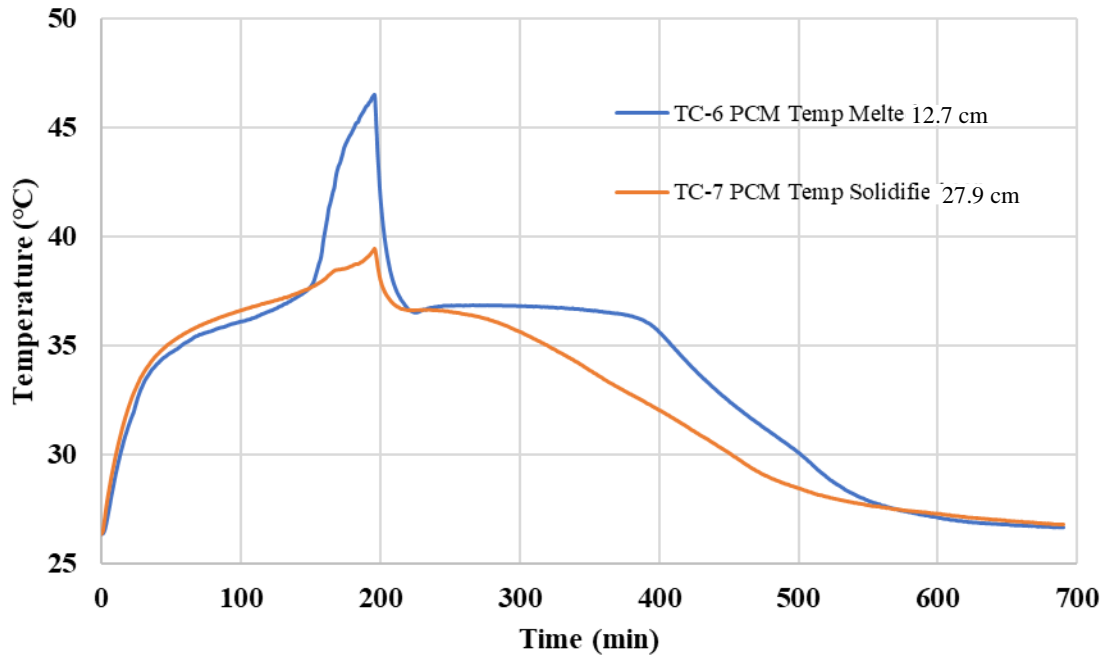


Figure 44: 8.6 kg copper-enhanced PCMHX PCM temperature

The COP of the first CuPCMHX test is shown in Figure 45. The COP trends downward over the course of the cycle, but the average value is significantly higher than the non-enhanced PCMHX. The compressor inlet and outlet pressures are shown in Figure 46. The increase in pressure just after the 100th minute coincides with the inflection point in the TC-6 thermocouple. As the temperature of the PCM changes from solid to liquid and the PCM becomes superheated, the condenser becomes less efficient and condensing pressure increases. This phenomenon will be observed to varying degrees for all the other PCMHX.

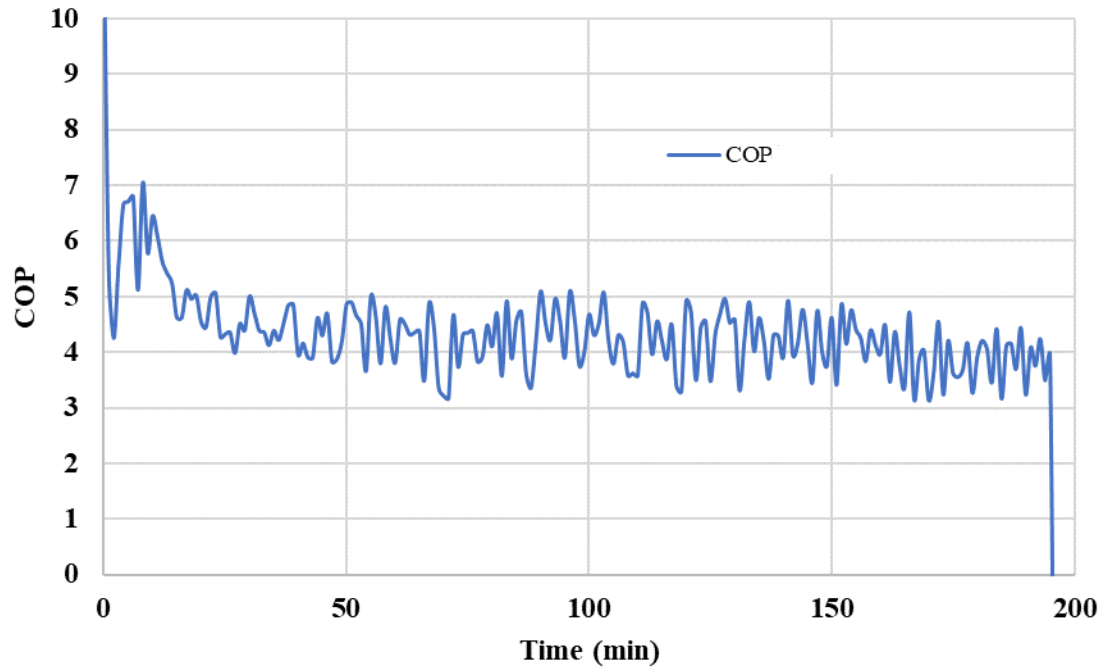


Figure 45: 8.6 kg copper-enhanced COP

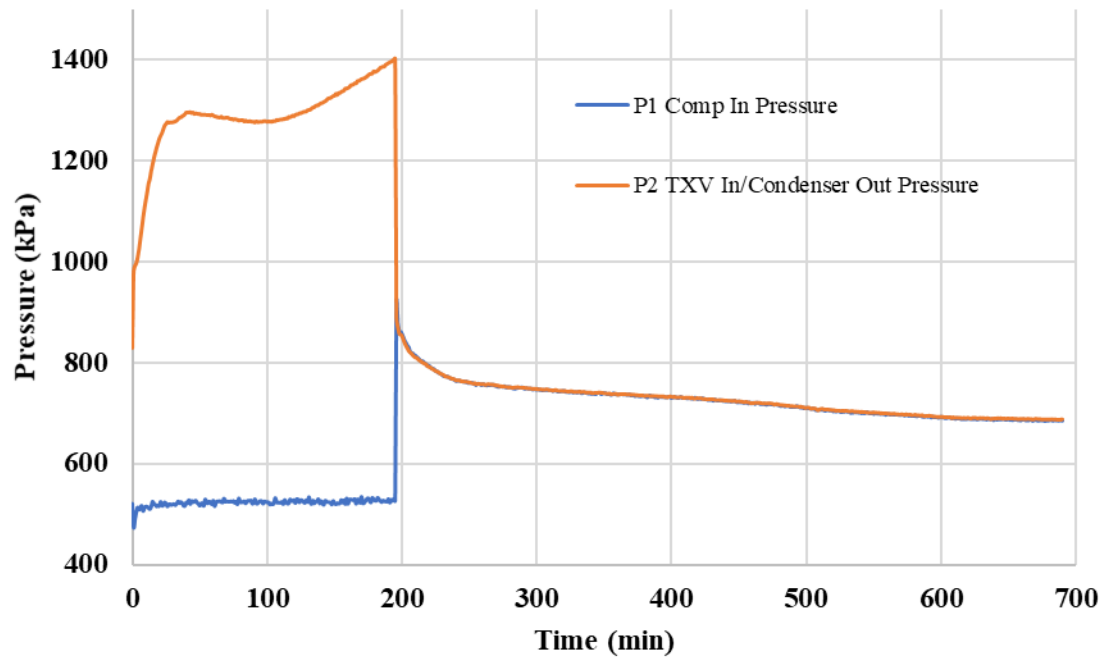


Figure 46: 8.6 kg copper-enhanced pressure

Figure 47 shows the average air temperature inlet and outlet for the AHX. The AHX had an average room temperature of 26.0 °C and an average delta T of -2.99 °C. during the cooling cycle.

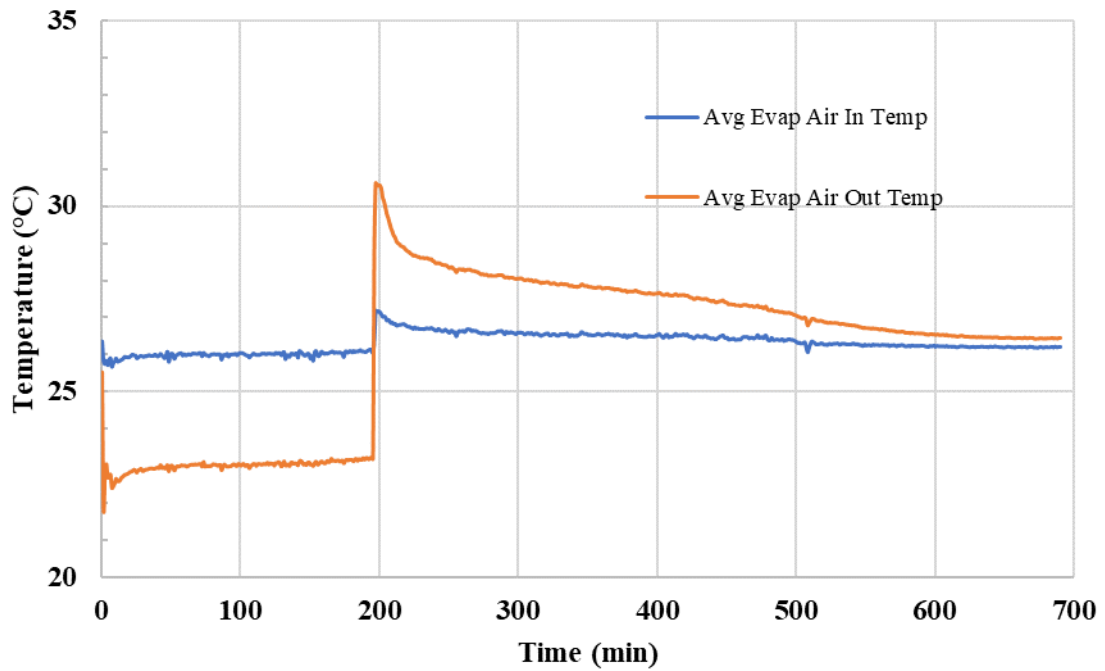


Figure 47: 8.6 kg copper-enhanced air temperature of AHX

Figure 48 shows the capacity of the evaporator and condenser throughout the cooling cycle. The average condenser capacity was 194.1 W and the average evaporator capacity was 192.3. The average condensing and evaporating values are so close because the system was not insulated between the condenser outlet and evaporator inlet.

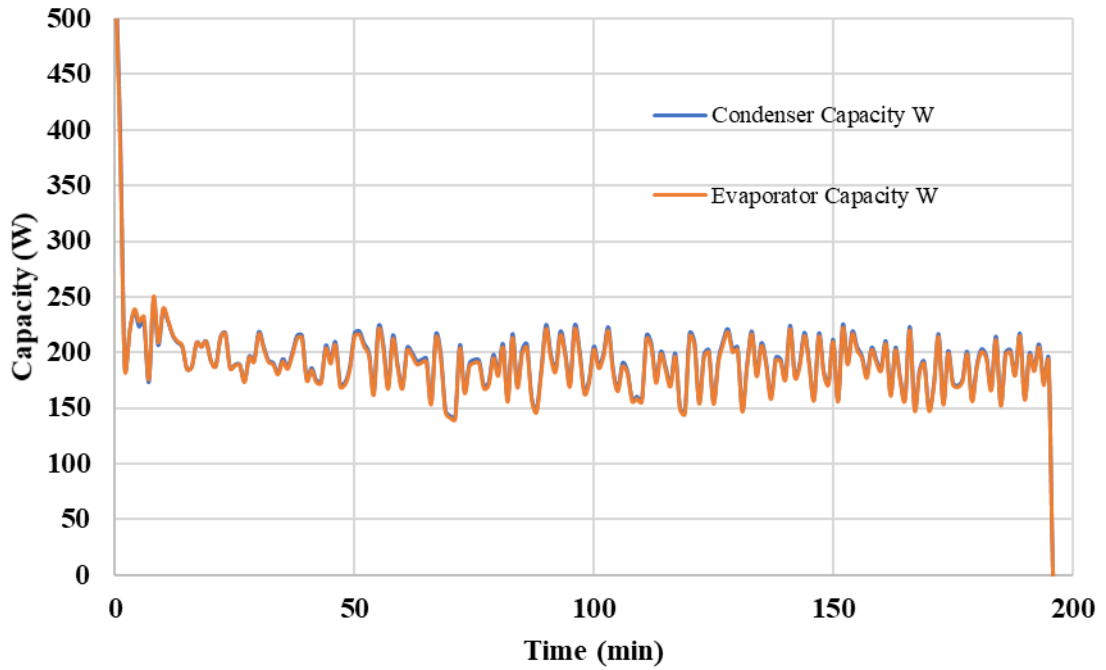


Figure 48: 8.6 kg copper-enhanced capacity of evaporator and condenser

Figure 49 shows the refrigerant mass-flow rate during the graphite-enhanced cooling cycle.

The average mass-flow rate was 0.00116 kg/s.

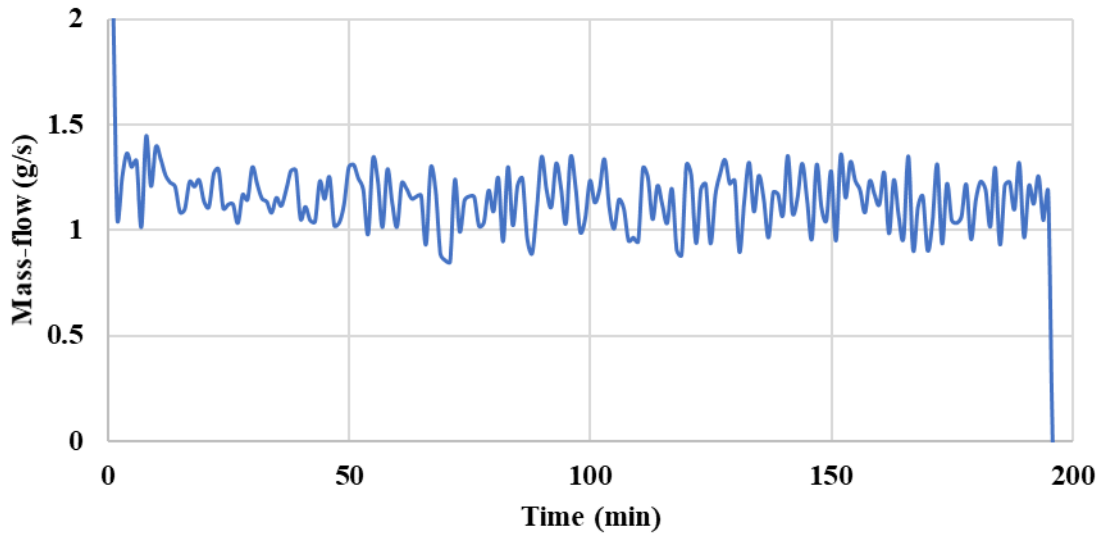


Figure 49: 8.6 kg copper-enhanced refrigerant mass-flow rate

5.1.3 5.4 kg Graphite-enhanced PCM Test

The 2-hour GrPCM_{HX} was tested next. The cooling cycle ran until the minimum PCM temperature was 36.0 °C. The group of thermocouples that do not show an inflection point are the thermocouples placed closest to the wall of the container. The heat map shown in Figure 50 shows the location of the cooler spots along the edge of the container. Again, this emphasizes the need to locate the thermocouples properly.

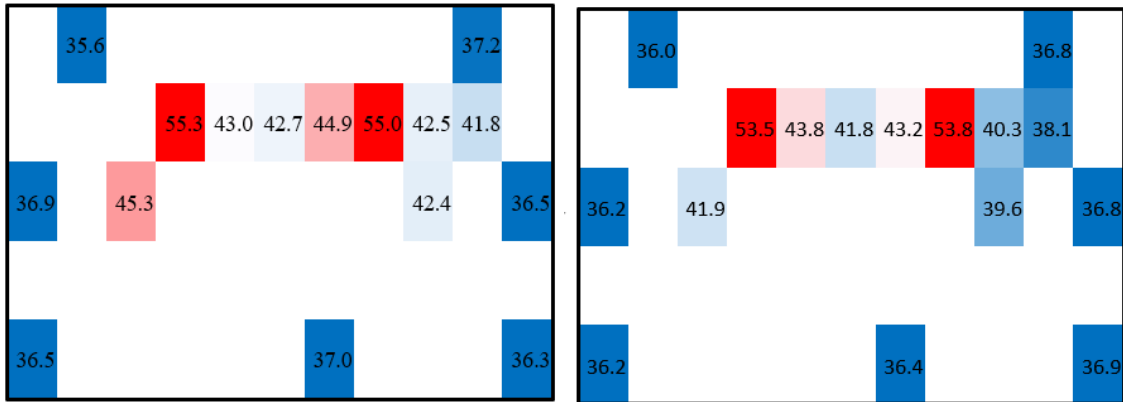


Figure 50: 2-hour GrPCM_{HX} heat map at 2.7 hours into the cooling cycle

The temperature profile of a typical cooling cycle of the 2-hour GrPCM_{HX} is shown in Figure 51. The PCM increases temperature in its sensible range until it begins to change phase at about 35 °C. The band of temperatures between the inflection points at 35 °C and 39 °C indicate the phase-change region of the PCM. Once the phase change is complete and the PCM is fully melted at around 140 minutes, the temperature of the PCM increases more rapidly as the heat from the condenser continues to transfer into the PCM. Figure 51 also shows that the full cooling cycle was 164 minutes.

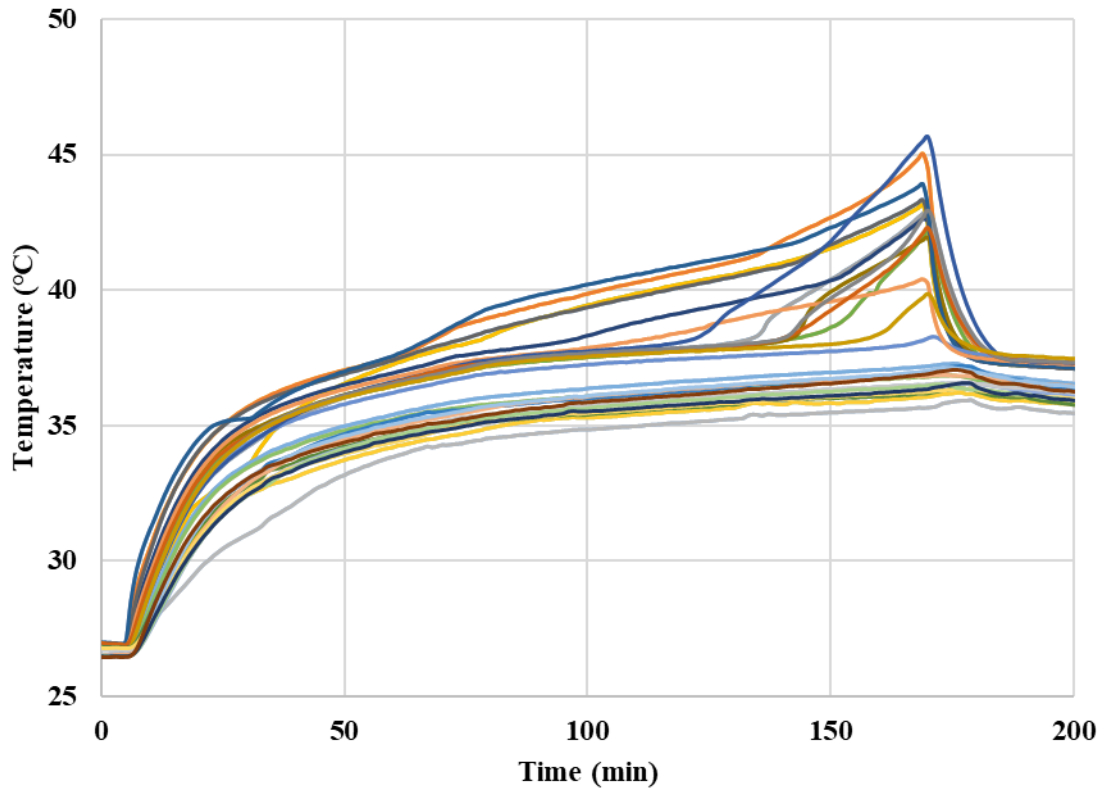


Figure 51: 5.4 kg graphite-enhanced PCMHX PCM temperature

Figure 52 shows the tube temperature of the 2-hour GrPCMHX. TC-12 and TC-5 show some fluctuation at the beginning of the cycle. During the post processing of the graphite blocks, the blocks were cut in half lengthwise and allowed to rest at room temperature for several days. Upon assembly of the GrPCMHX, two of the graphite blocks were warped, as shown in Figure 53. The temperature fluctuations are observed in the same block that was warped upon assembly. It is postulated that as the cooling cycle proceeded, the blocks

returned to their original shape and good contact between the tube and the block was finally achieved around minute 30.

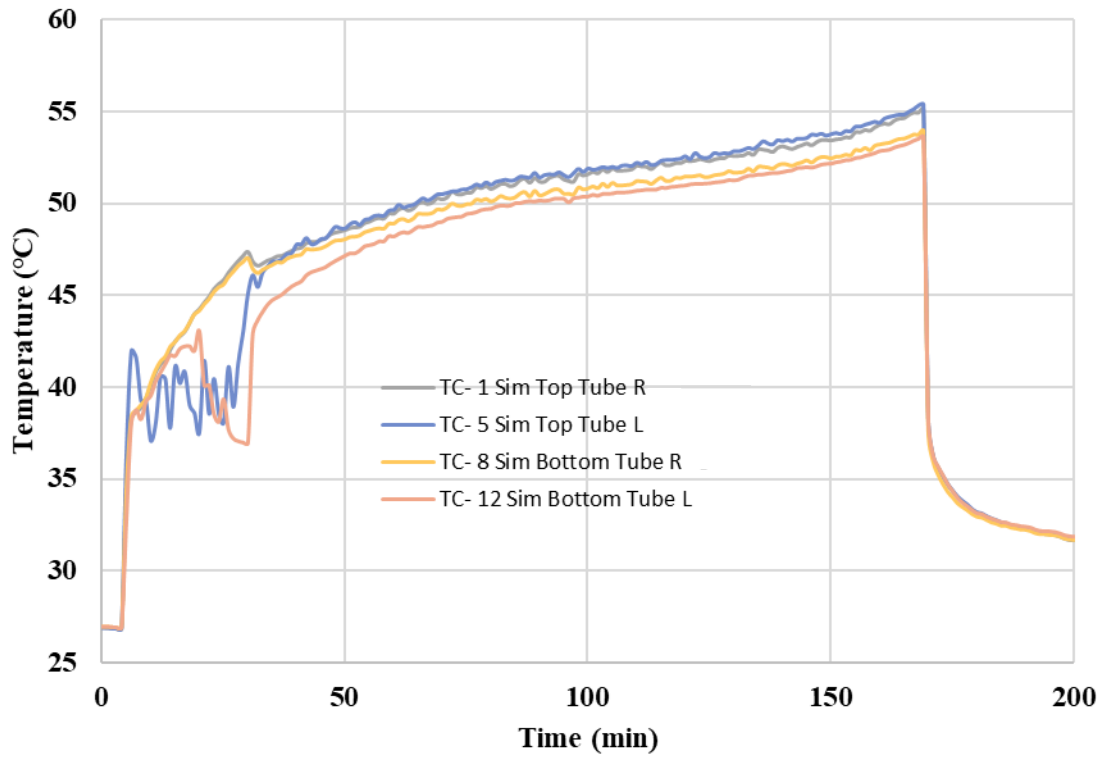


Figure 52: 5.4 kg graphite-enhanced PCMHX tube temperature



Figure 53: Warpage in the graphite blocks after post-processing

The COP of the cycle is shown in Figure 54. The general COP trend is downward and the average values are much lower than the 2-hour CuPCMHX. The pressure is shown in Figure 55 and shows a steadily increasing pressure. In the 2-hour CuPCMHX the pressure had an initial increase and then had over an hour of steadily decreasing pressure. No such trend is observed here.

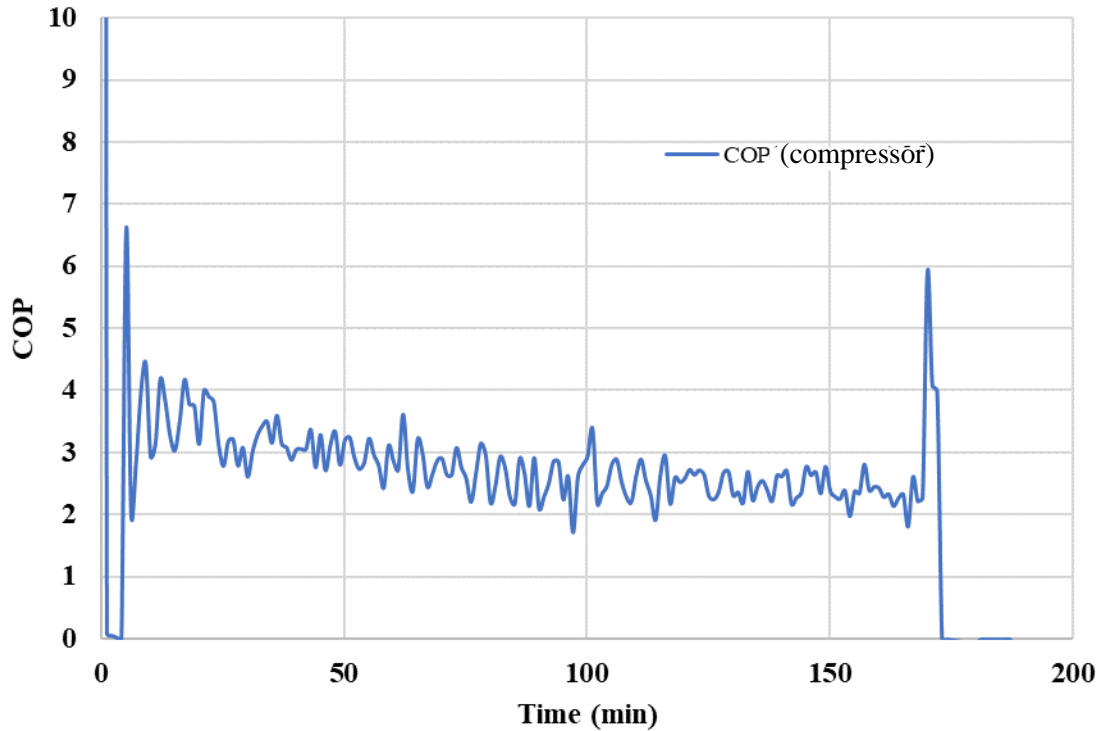


Figure 54: 5.4 kg graphite-enhanced COP

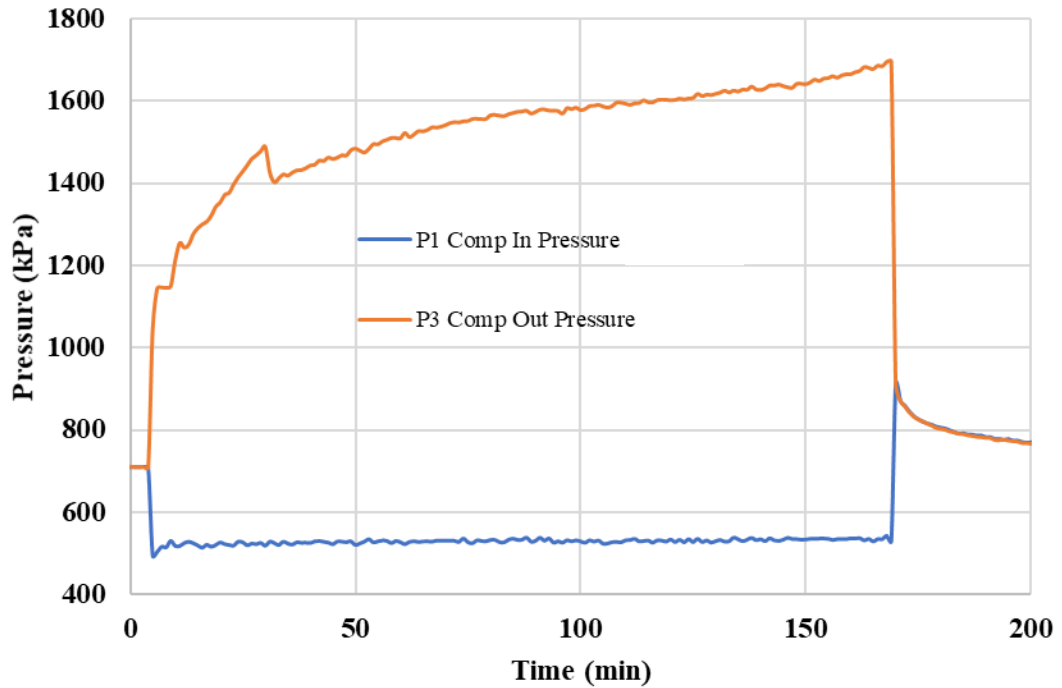


Figure 55: 5.4 kg graphite-enhanced pressure

Figure 56 shows the average air temperature inlet and outlet for the AHX. The AHX had an average room temperature of 25.7 °C and an average delta T of -2.70 °C. during the cooling cycle.

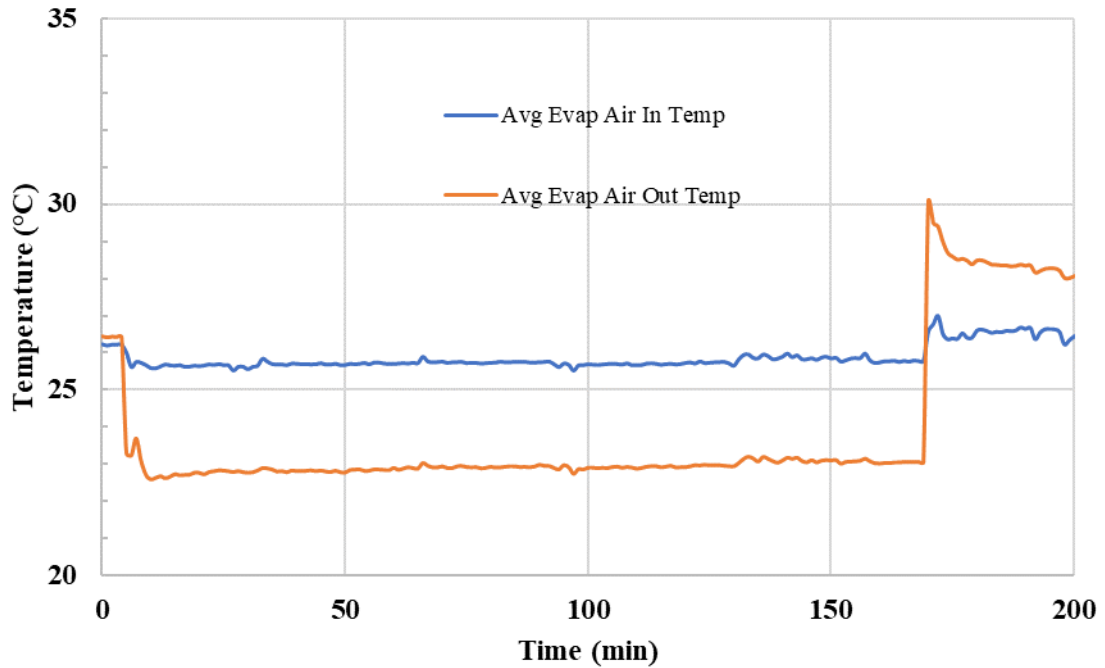


Figure 56: 5.4 kg graphite-enhanced air temperature of AHX

Figure 57 shows the capacity of the evaporator and condenser throughout the cooling cycle. The average condenser capacity was 144.78 W and the average evaporator capacity was 151.2. The evaporating capacity was higher than the condensing capacity because the system was not insulated between the condenser outlet and evaporator inlet.

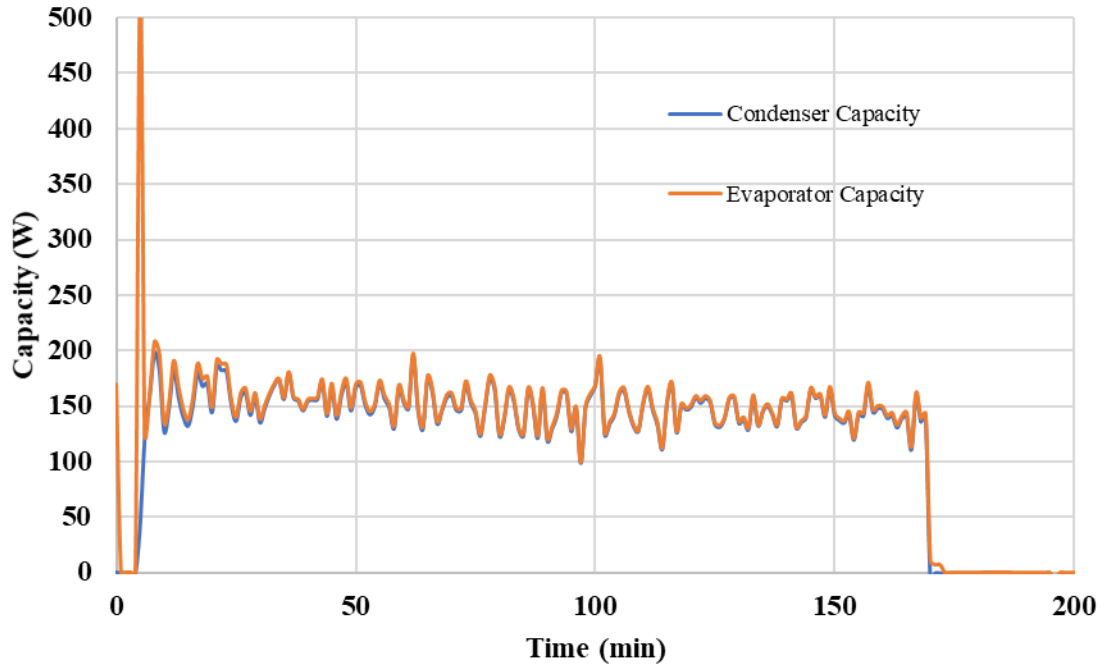


Figure 57: 5.4 kg graphite-enhanced capacity of evaporator and condenser

Figure 58 shows the refrigerant mass-flow rate during the graphite-enhanced cooling cycle.

The average mass-flow rate was 0.00093 kg/s.

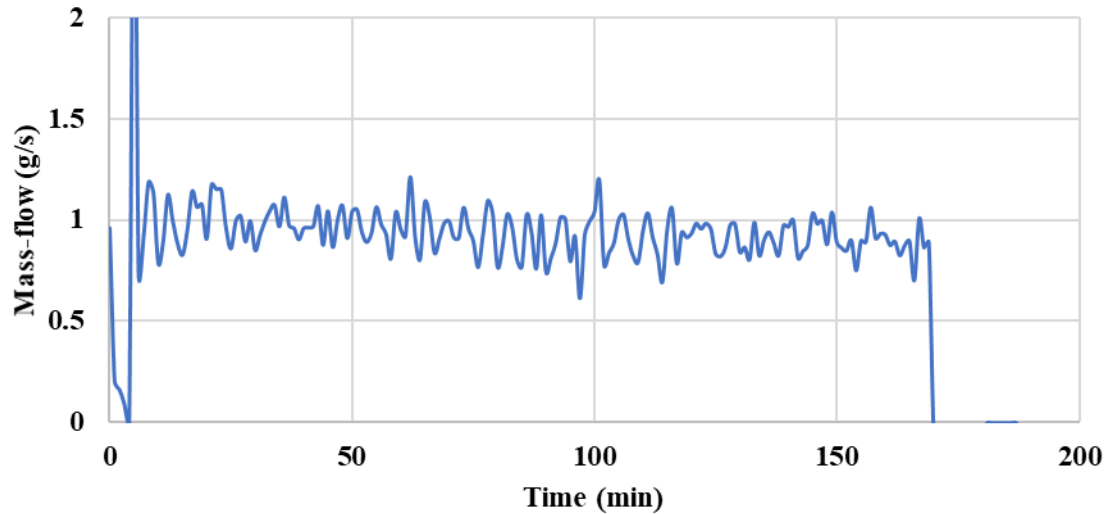
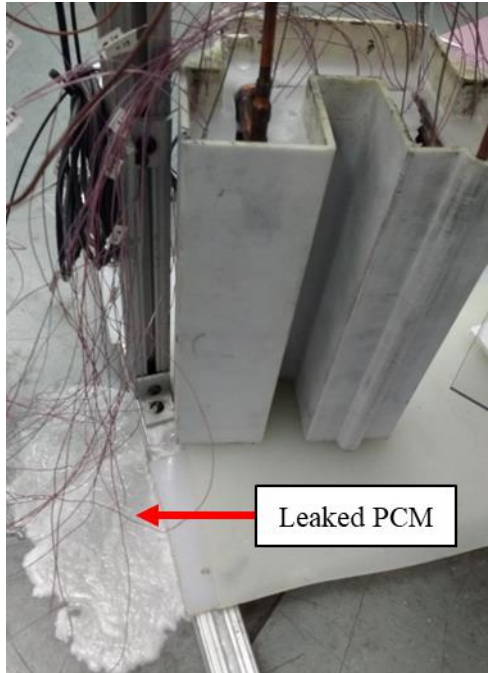
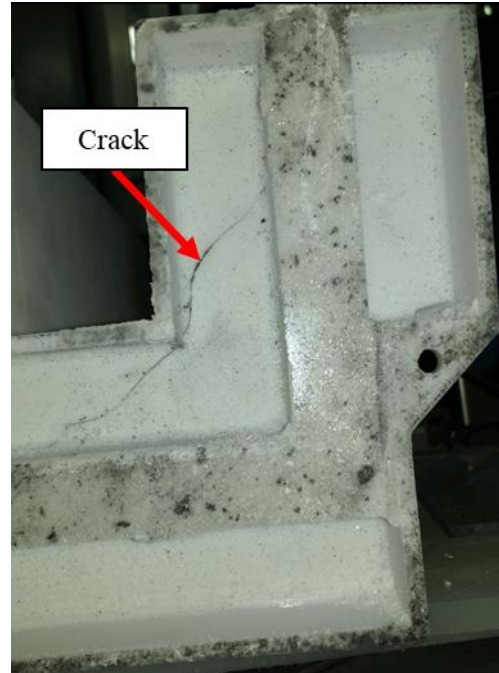


Figure 58: 5.4 kg graphite-enhanced refrigerant mass-flow rate



2-hour graphite-enhanced PCMHX leak



2-hour graphite-enhanced PCMHX
container crack

Figure 59: 2-hour graphite-enhanced PCMHX container crack

The container for the GrPCMHX cracked during the cooling operation (Figure 59) and liquified PCM leaked out. Therefore, a full recharge cycle was not recorded.

5.2 15.1 kg Copper-enhanced PCM Cycle Tests

After the single-cycle tests were run for the non-enhanced, graphite-enhanced and copper-enhanced PCMHX, the cooling and recharge cycles were automated for cycle testing. Based on results from previous tests, the cooling setpoint was set at 38.0 °C and the recharge setpoint was set at 35.0 °C. The cooling setpoint is the temperature at which the cycle switches from cooling to recharge mode, and the recharge setpoint is the temperature at which the cycle switches from recharge to cooling mode. Cycle tests were run with condensers designed for four hours of cooling operation. For the 4-hour CuPCMHX

system, the cycle test was conducted at ambient room temperatures of 26.0 °C, 30.0 °C and 35.0 °C, as described in Table 10.

5.2.1 Cycle Test: 26.3 °C

Results from the 4-hour CuPCMHX test are shown below in Figures Figure 60 - Figure 63. Lessons learned from previous tests informed placement of the thermocouples. The result is a very clean temperature profile. The system shows a high degree of repeatability from one cycle to the next for tube temperatures, PCM temperatures, COP and refrigerant pressures. The shapes of each graph are similar to what was recorded for the 2-hour CuPCMHX, showing that the design is scalable.

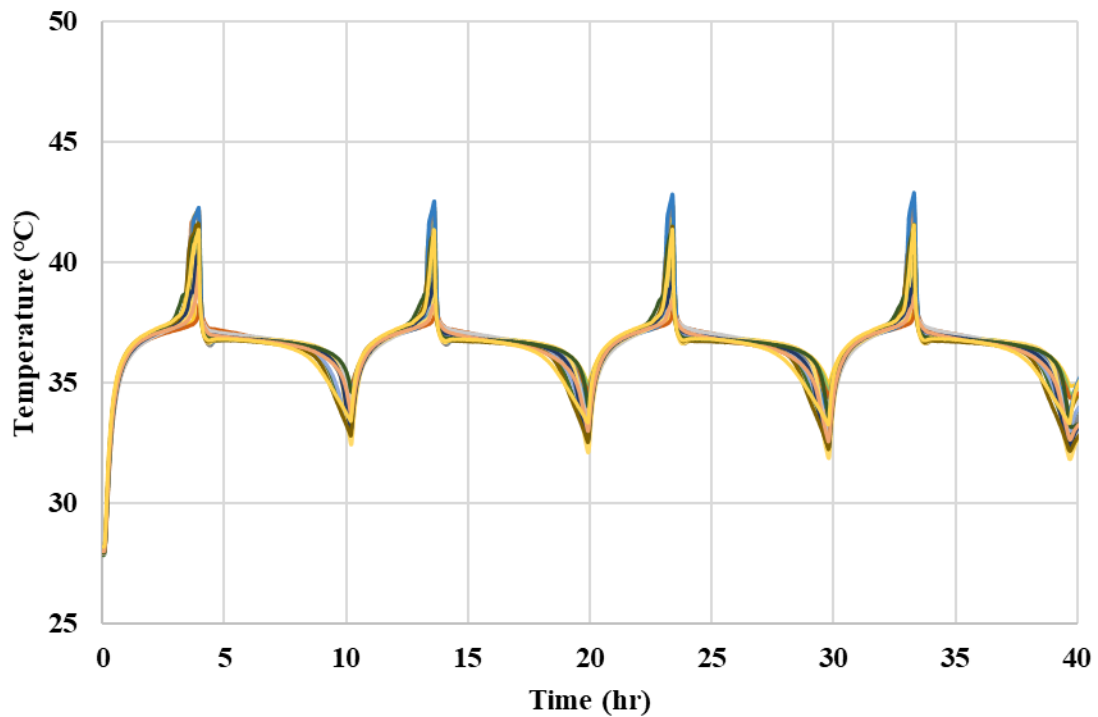


Figure 60: 15.1 kg copper-enhanced PCMHX PCM temperature cycle test

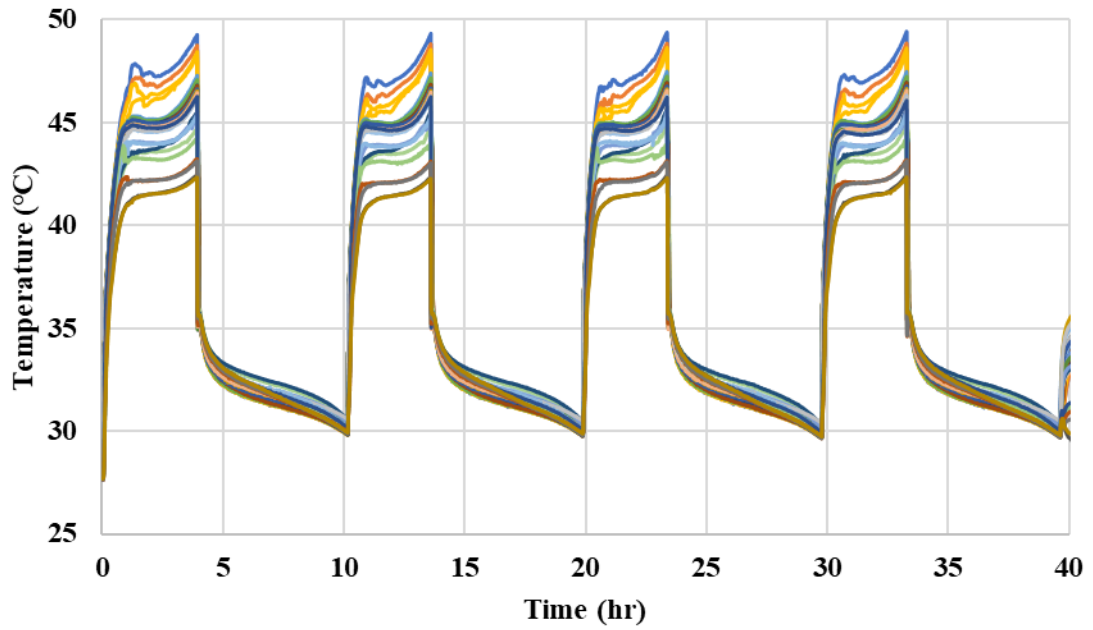


Figure 61: 15.1 kg copper-enhanced PCMHX tube temperature cycle test

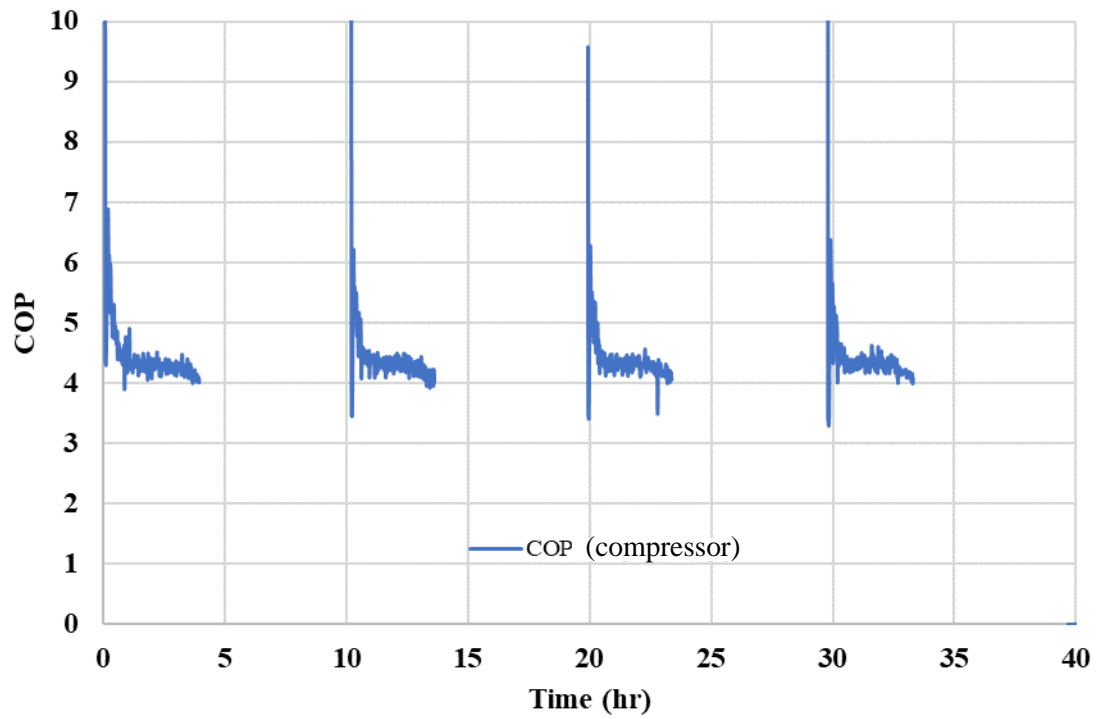


Figure 62: 15.1 kg copper-enhanced COP cycle test

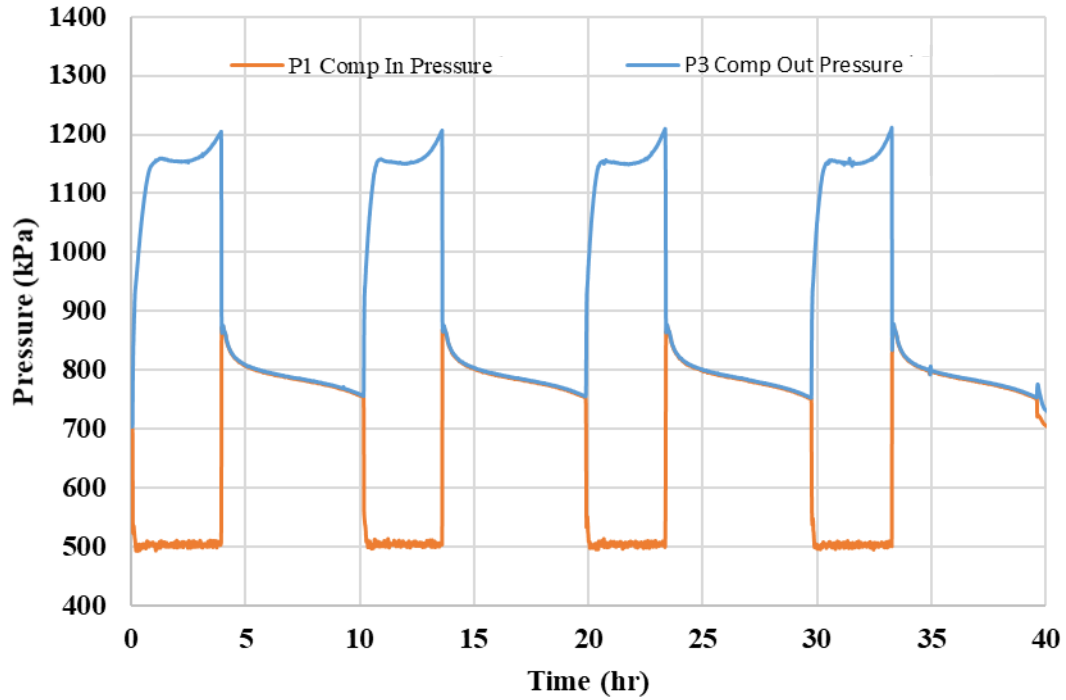


Figure 63: 15.1 kg copper-enhanced pressure cycle test

Figure 64 shows the average air temperature inlet and outlet for the AHX. The AHX had an average room temperature of 26.3 °C and an average delta T of -3.80 °C. during the cooling cycle.

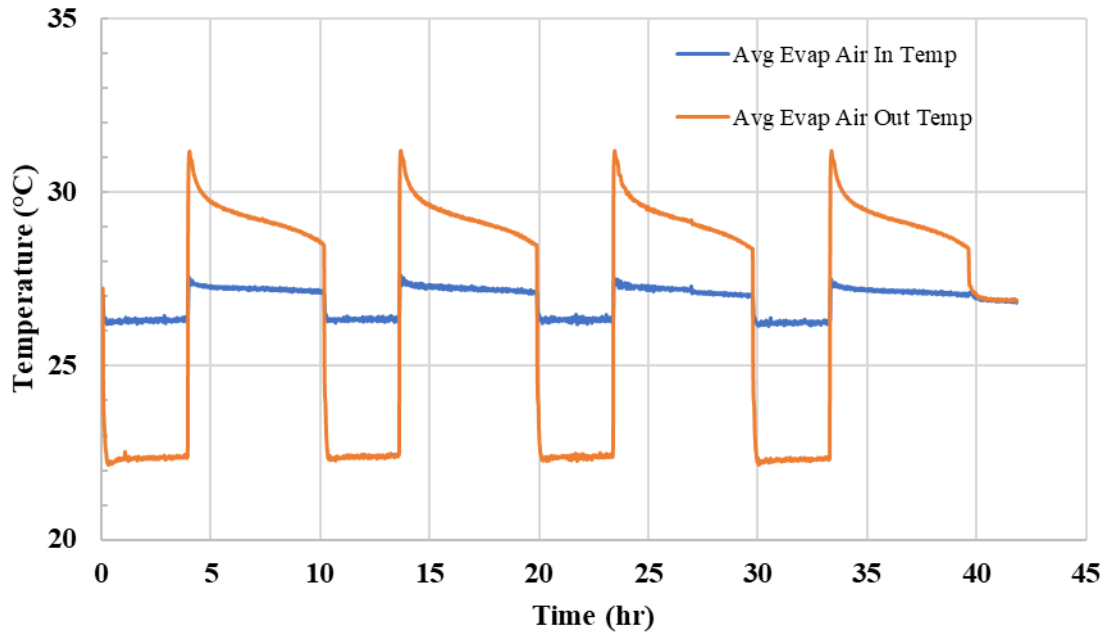


Figure 64: 15.1 kg copper-enhanced air temperatures of AHX for cycle test

Figure 65 shows the capacity of the evaporator and condenser throughout the cooling cycle. The average condenser capacity was 182.9 W and the average evaporator capacity was 185.8 W. The evaporating capacity was higher than the condensing capacity because the system was not insulated between the condenser outlet and evaporator inlet.

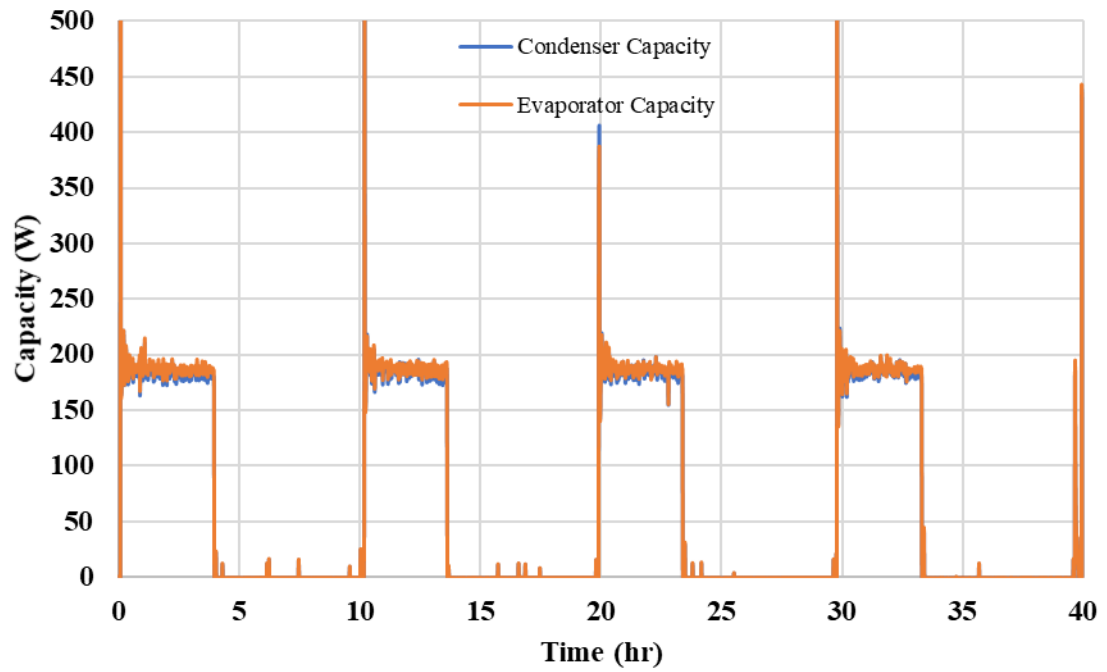


Figure 65: 15.1 kg copper-enhanced capacity of evaporator and condenser for cycle test

Figure 66 shows the mass-flow rate of the refrigerant during the copper-enhanced 15.1 kg cycle test. The average mass-flow is 0.00108 kg/s.

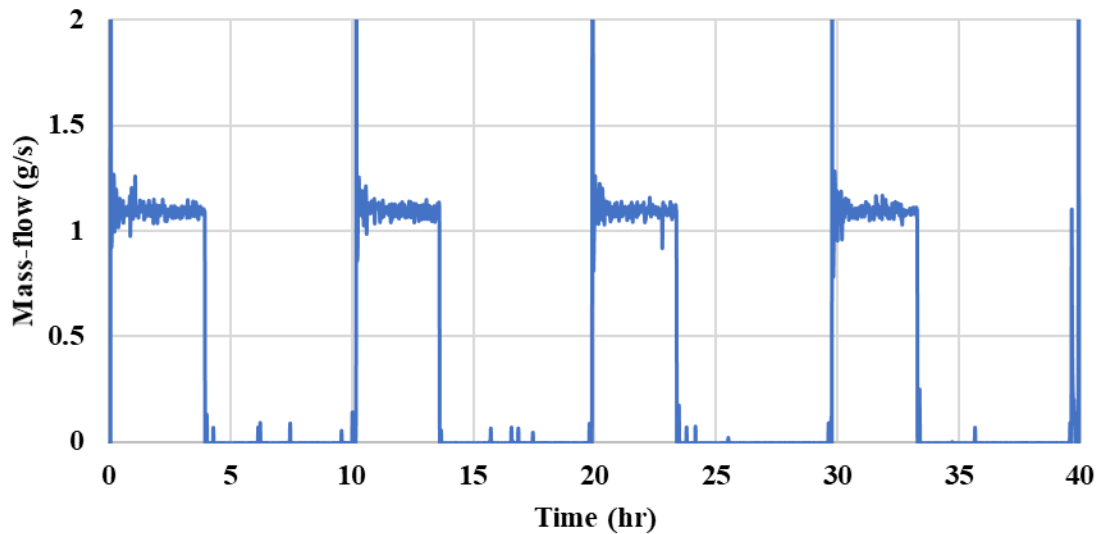


Figure 66: 15.1 kg copper-enhanced mass-flow for cycle test

5.2.2 Cycle Test: 30.0 °C

The same 4-hour CuPCMHX cycle test was completed with an ambient room temperature of 30.0 °C. The PCM temperature, tube temperature, system pressure and cycle COP are shown in Figures Figure 67Figure 70. The cooling cycle showed very similar performance to the 26.7 °C system, but with longer recharge times and better cooling COP due to the smaller difference between condensing and evaporating temperatures.

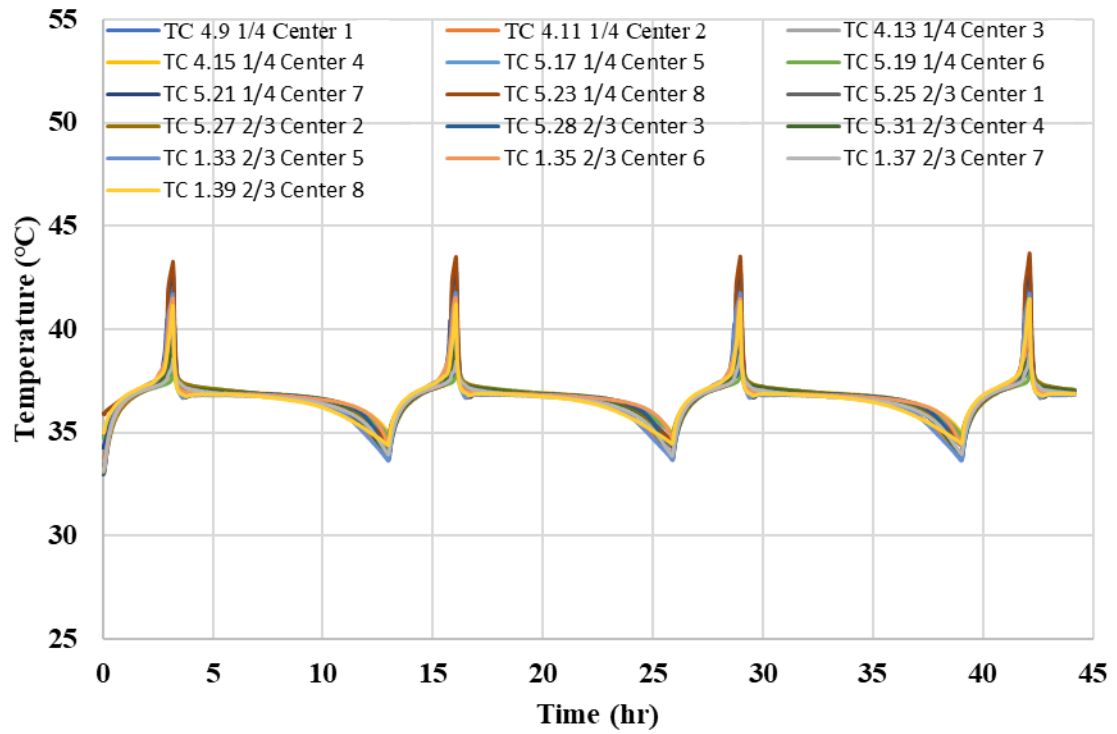


Figure 67: Copper-enhanced PCMHX PCM temperature cycle test with ambient air at 30.0 °C

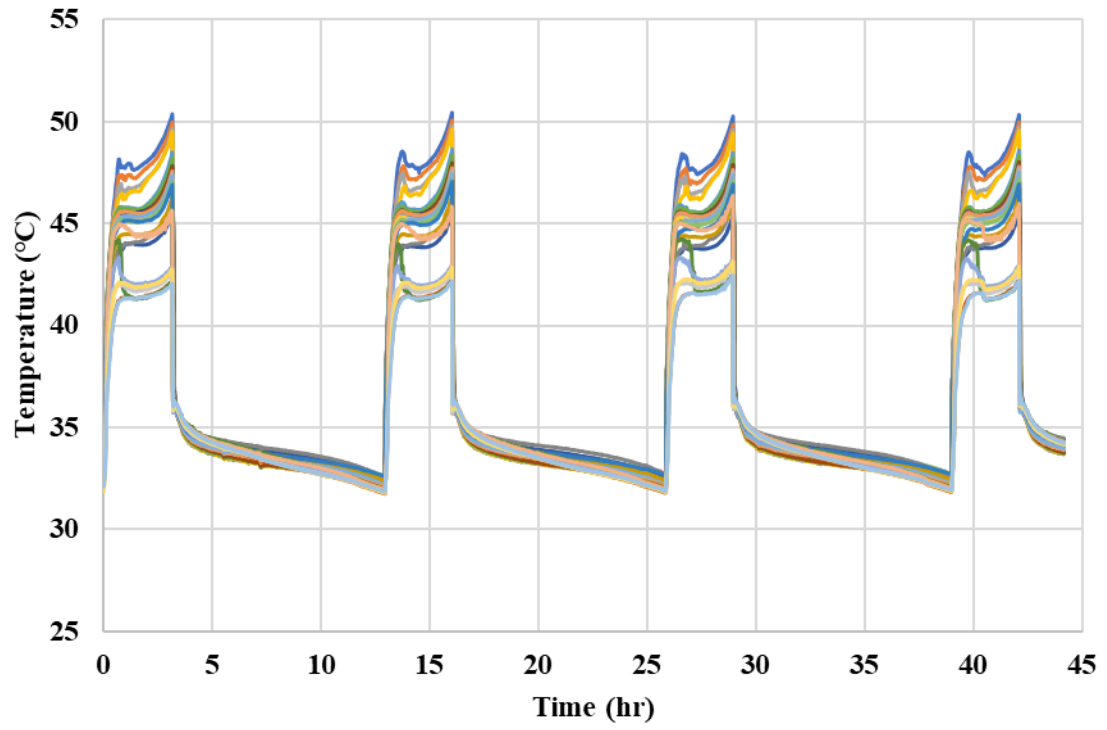


Figure 68: Copper-enhanced PCMHX tube temperature cycle test with ambient air at 30.0 °C

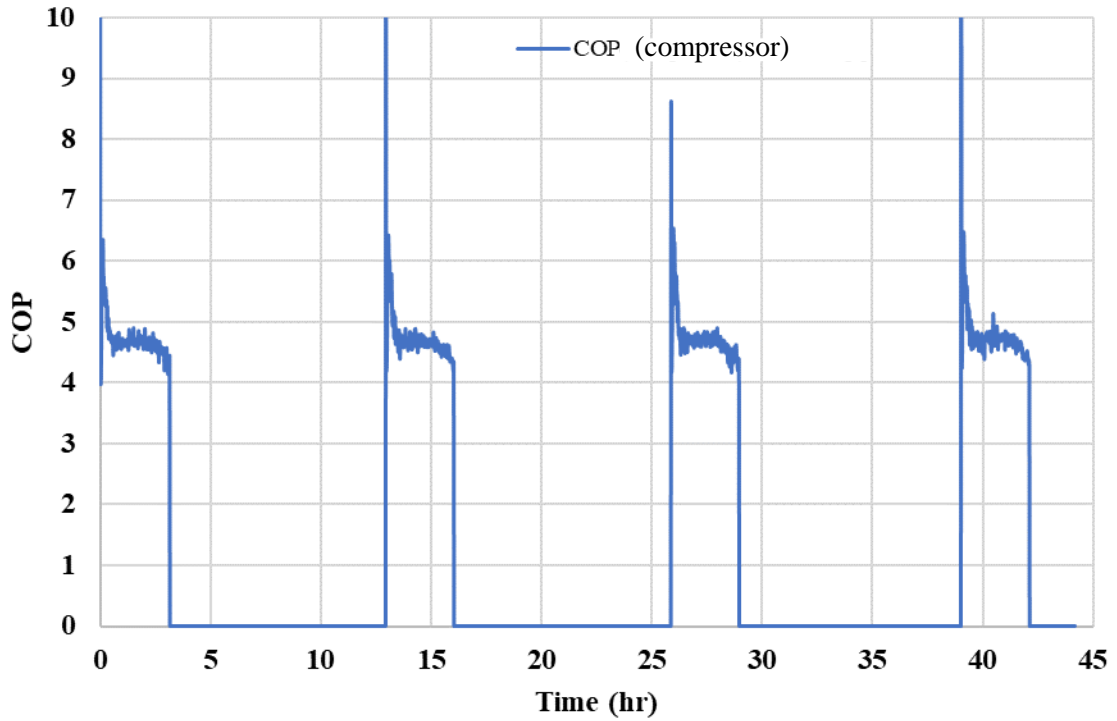


Figure 69: Copper-enhanced COP cycle test with ambient air at 30.0 °C

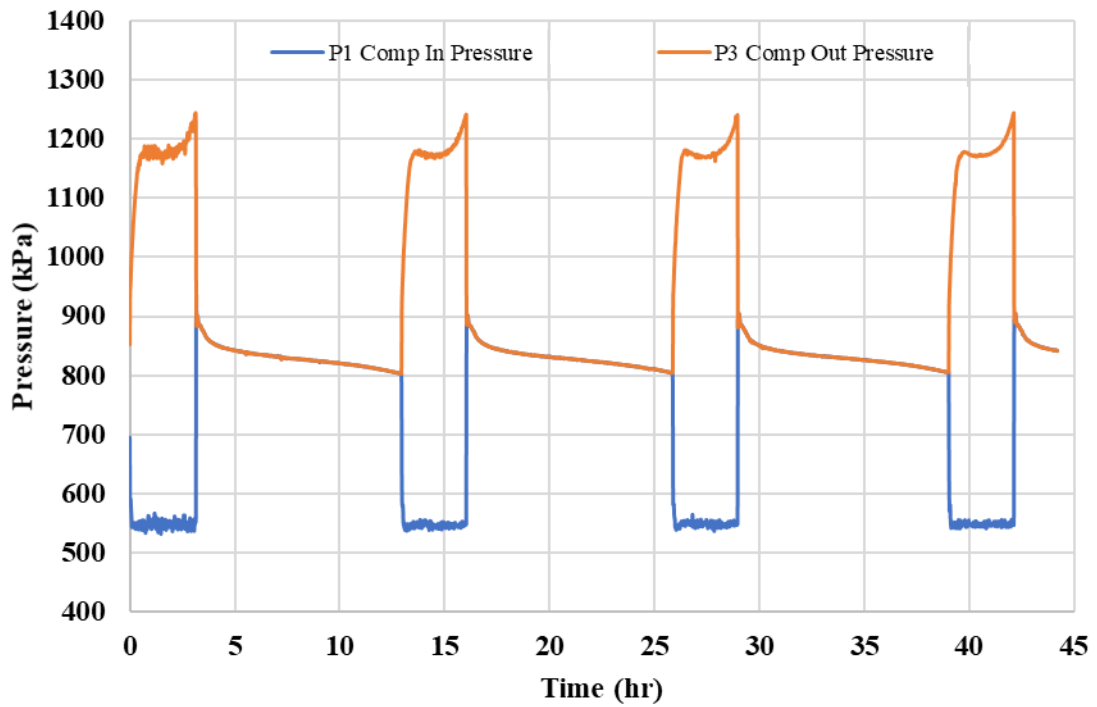


Figure 70: Copper-enhanced pressure cycle test with ambient air at 30.0 °C

5.2.3 Cycle Test: 35.0 °C

Only a single cooling cycle was run at an ambient room temperature of 35.0 °C. The results were close to the 30.0 °C, and the test was cut short. The PCM temperature, tube temperature, system pressure and cycle COP are shown in Figures Figure 71Figure 74.

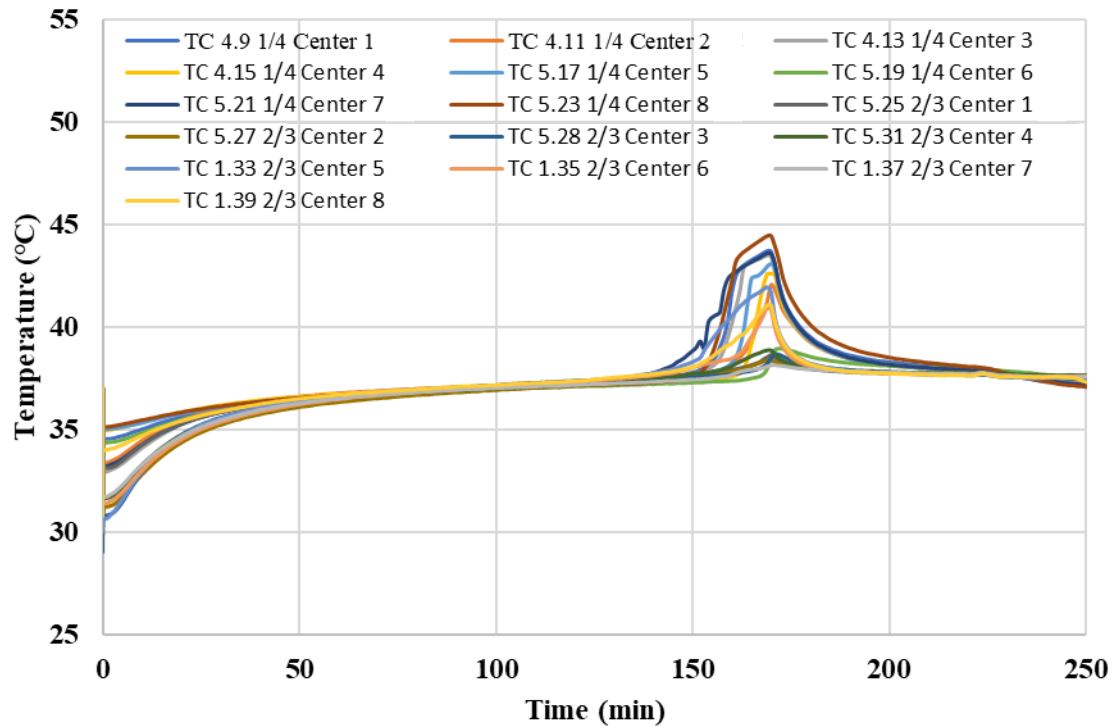


Figure 71: Copper-enhanced PCMHX PCM temperature, ambient air at 35.0 °C

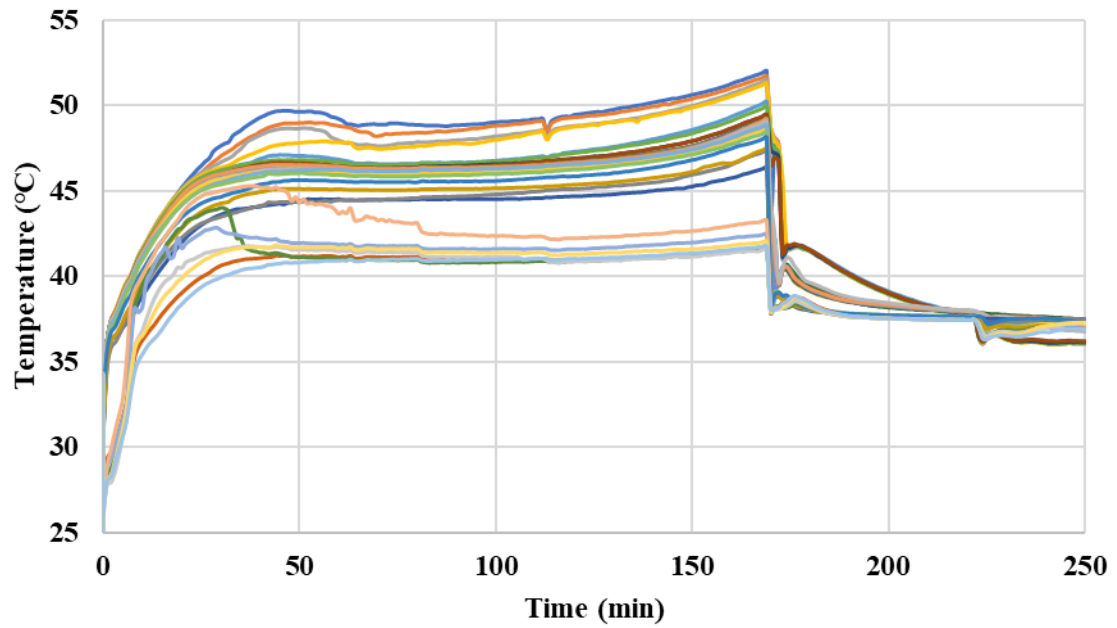


Figure 72: Copper-enhanced PCMHX tube temperature with ambient air at 35.0 °C

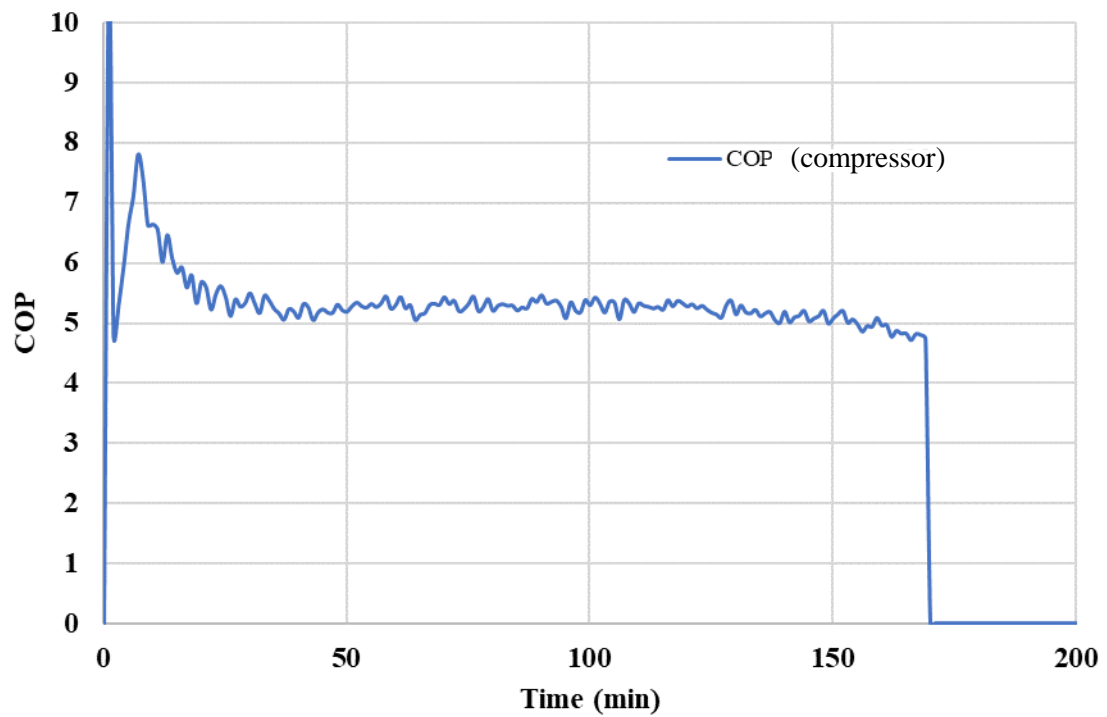


Figure 73: Copper-enhanced COP with ambient air at 35.0 °C

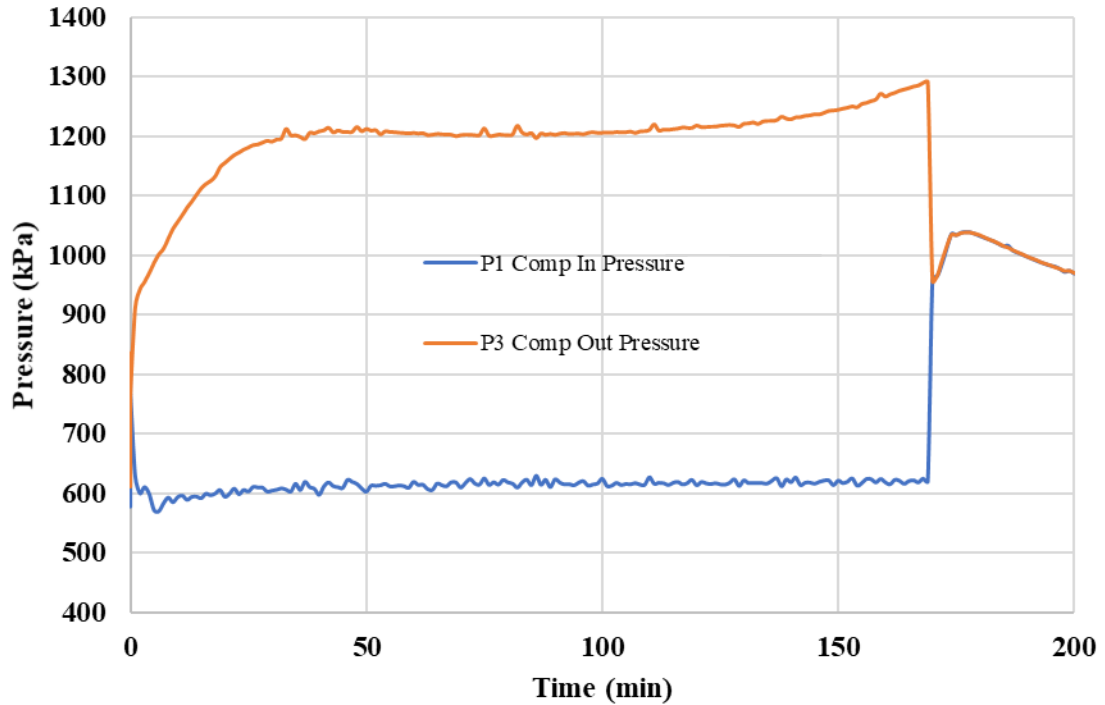


Figure 74: Copper-enhanced pressure with ambient air at 35.0 °C

5.3 12.7 kg Graphite-enhanced PCM Cycle Test

Although the initial results from the 2-hour GrPCMHX did not match the design capacity, lessons learned were incorporated in the design in of the next iteration of GrPCMHX. Additional tubes were added and the rectangular blocks, which required significant post processing, were replaced with disks. The disks did not need any post-processing and were symmetrical to resist any warpage. The PCM temperature show in Figure 75 followed the predictable profile seen in previous test.

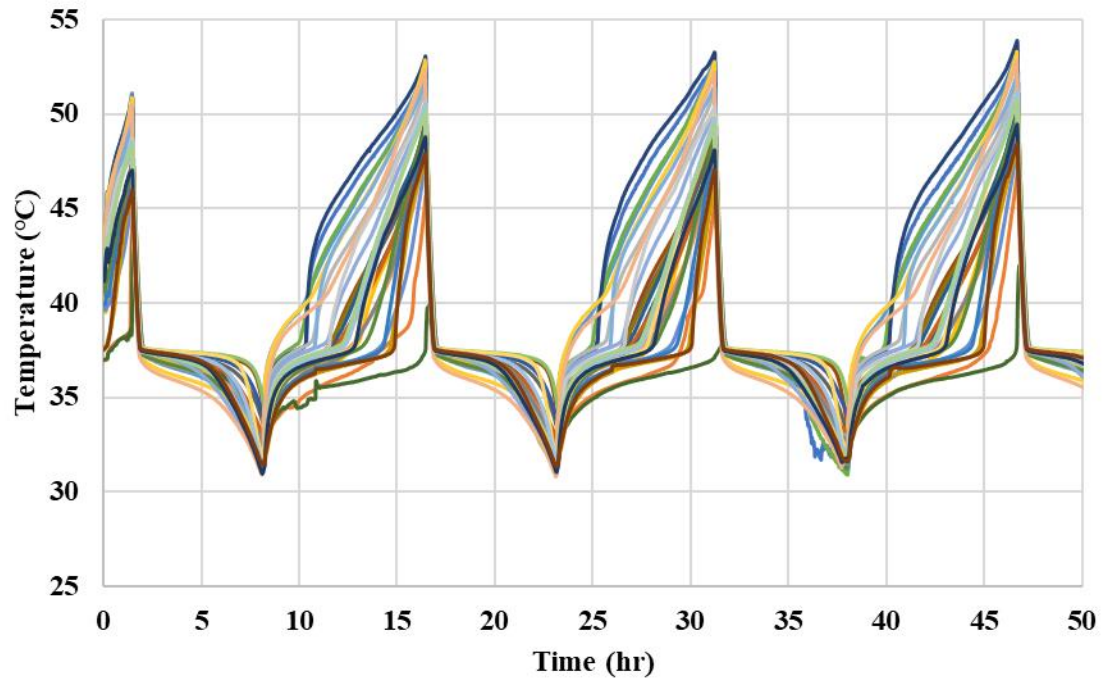


Figure 75: 12.7 kg graphite-enhanced PCMHX PCM temperature cycle

The COP (Figure 76) of the 4-hour GrPCMHX was again significantly lower than its copper-enhanced counterpart. The compressor outlet pressure (Figure 77) also increases steadily from the start of the cycle.

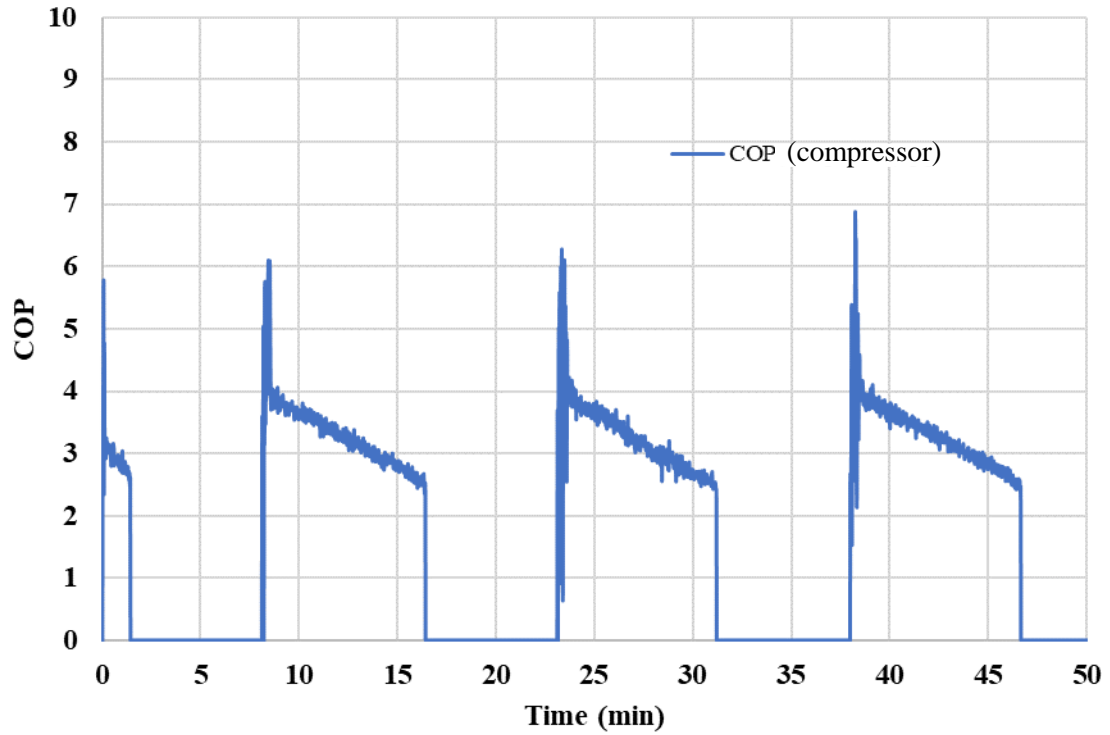


Figure 76: 12.7 kg graphite-enhanced cycle COP

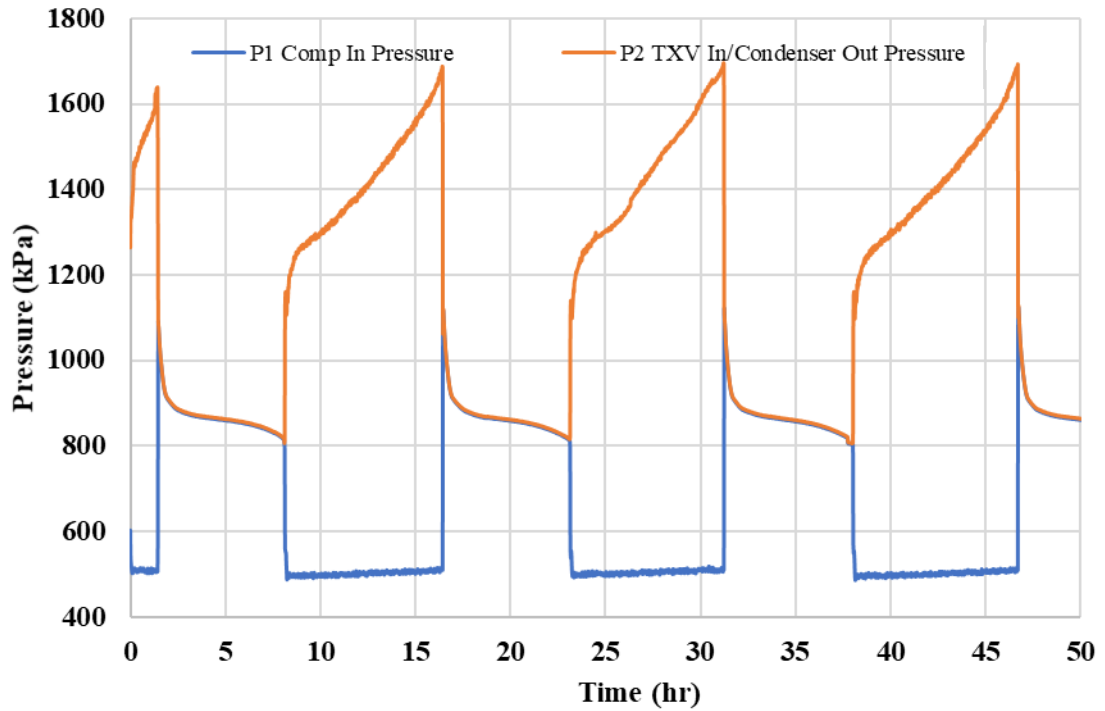


Figure 77: 12.7 kg graphite-enhanced cycle pressure

Figure 78 shows the average air temperature inlet and outlet for the AHX. The AHX had an average room temperature of 25.6 °C and an average delta T of -3.62 °C. during the cooling cycle.

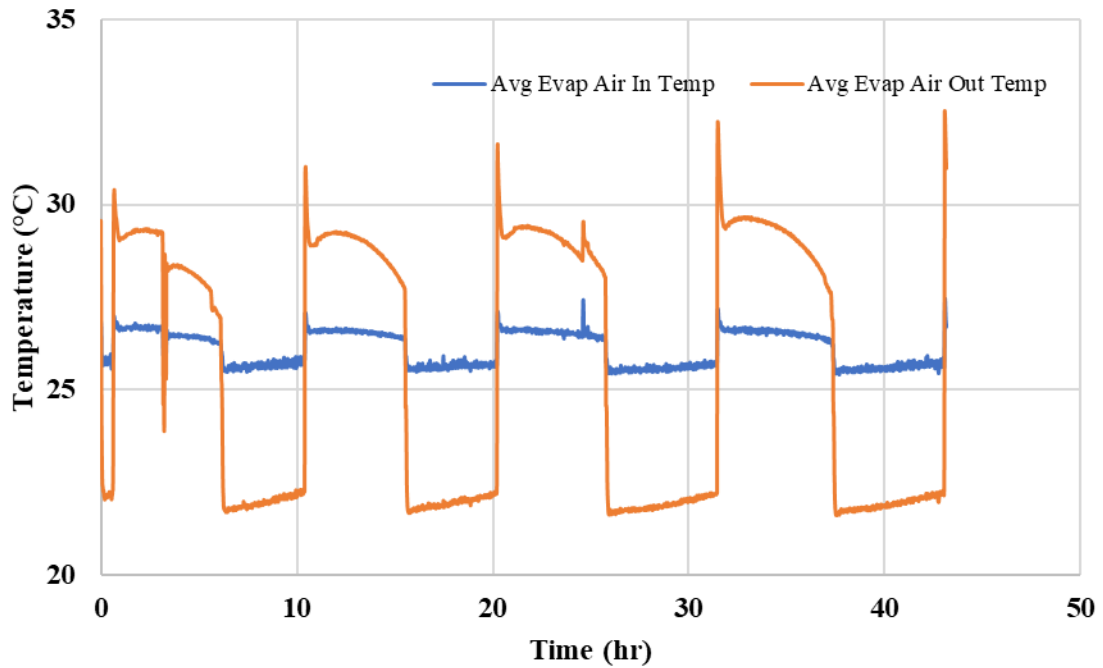


Figure 78: 12.7 kg graphite-enhanced air temperature of AHX for cycle test

Figure 79 shows the capacity of the evaporator and condenser throughout the cooling cycle. The average condenser capacity was 172.2 W and the average evaporator capacity was 177.3 W. The evaporating capacity was higher than the condensing capacity because the system was not insulated between the condenser outlet and evaporator inlet.

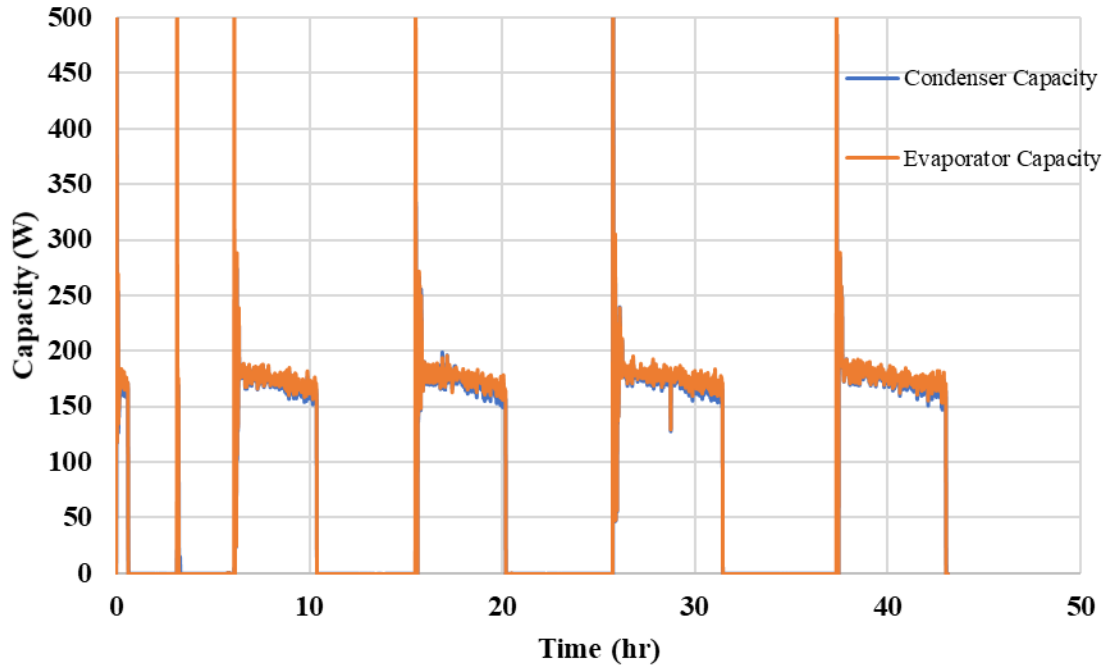


Figure 79: 12.7 kg graphite-enhanced capacity of evaporator and condenser for cycle test

Figure 80 shows the mass-flow rate of the refrigerant during the copper-enhanced 12.7 kg graphite-enhanced cycle test. The average mass-flow is 0.00105 kg/s.

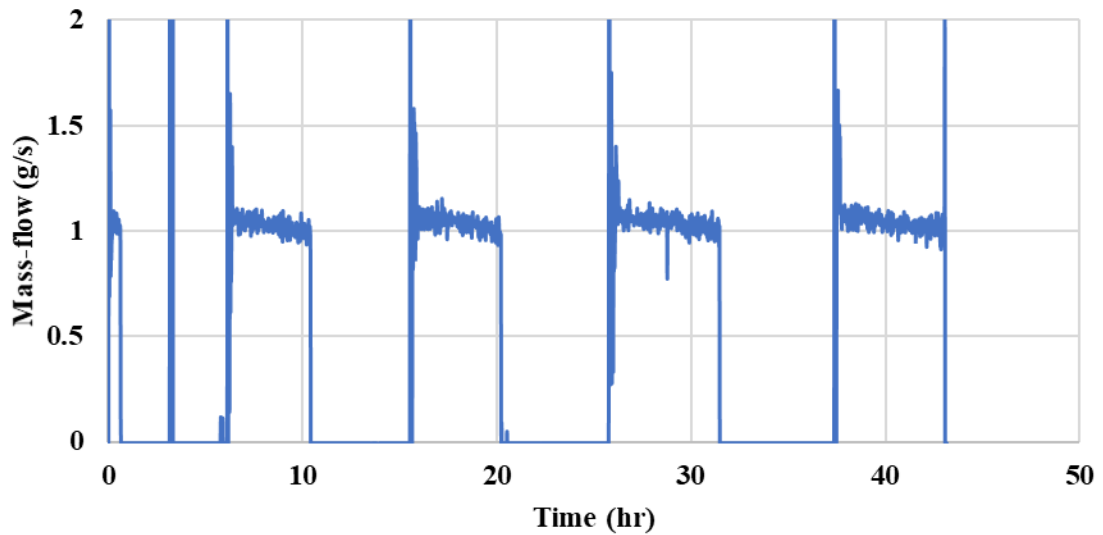
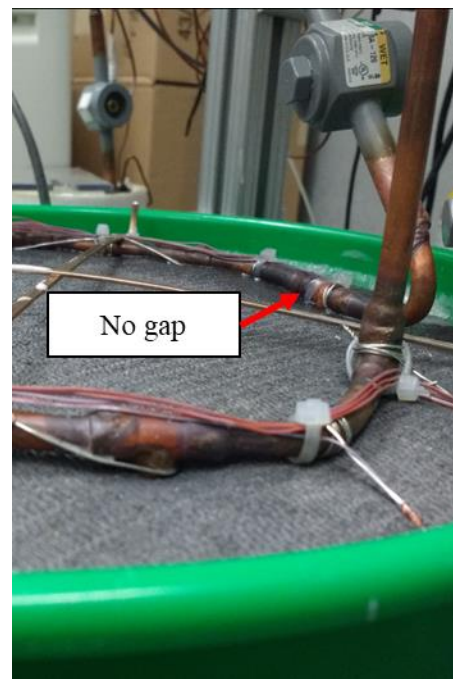


Figure 80: 12.7 kg graphite-enhanced mass-flow for cycle test

One result not observed in the 2-hour GrPCM_{HX} test was the swelling of the graphite disks after backfilling the condenser with liquified PCM. As shown in Figure 81, the graphite condenser had a gap of about 2.5 cm between the top of the disks and the copper header. The 18.9 L bucket was back-filled with liquified PCM and run for several cycles. During that time, the disks absorbed the PCM and swelled, like a dry sponge swelling when exposed to water. In theory, this is an advantageous result because the swelling should eliminate any air gaps between disk and copper tubes, reducing the thermal resistance in the system and increasing condensing performance. The results do not reflect this advantage.



Gap before PCM backfill and cycle test



Gap after PCM backfill and cycle test

Figure 81: Graphite disk swelling after PCM backfill and cycle test

Chapter 6: Data Analysis

When the original BV1 tests were run, it was unclear how to define the end of the cooling and recharge cycles. Initial tests were run until it appeared the PCM had undergone phase change, and then the thermosiphon recharge cycle ran until the PCM reached equilibrium with the ambient room temperature. The BV1 tests defined the PCM as “recharged” once the PCM was the same temperature as the ambient room temperature. Given the fact that the PCM is intended to be used as a latent heat storage device, this definition needs reworking. The cooling cycle should be considered finished after the PCM has fully liquified and the temperature of the PCM begins to rise more rapidly, as seen in Figure 1. Likewise, the recharge cycle should be considered finished and ready for another cooling cycle when the PCM has fully solidified and the temperature of the PCM begins to fall more rapidly. By measuring the temperature of the PCM in several places and using the PT37 DSC curve as a guide [29] these critical setpoints can be accurately defined. Experimentally derived cooling and recharge data can also be used to determine setpoint temperatures. Visual inspection of all the PCM temperature curves in Chapter 5: show that the PCM temperature consistently has an inflection point at 38.0 °C during the cooling mode, and an inflection point at 36.0 °C during the thermosiphon mode, regardless of the PCM enhancement type. Assuming that the PCM thermocouples are not placed in the coolest and warmest locations of the condenser, ± 1 degree is added to operating temperature band. Therefore, for all results included below, the cooling cycle is said to be complete when the lowest measured PCM temperature is 39.0 °C, and the thermosiphon recharge cycle is said to be complete when the warmest PCM temperature is 35.0 °C. All Cooling Times, Recharge Times, and COP are reported from values within these ranges,

regardless of the setpoint and times at which the test was run. This helps to normalize the data across different testing conditions. A new metric is also introduced here: Recharge Time per kg. Many of the tests were run with different amounts of PCM and different PCMHX tube configurations, and this new metric attempts to find a meaningful comparison between the different PCMHX performances during the recharge cycle. A lower Recharge Time per kg is better. Based on the results shown in Table 11, the three top performers for this metric are the non-enhanced PCMHX and the two CuPCMHX. No data is available for the 2-hour GrPCMHX because of the crack in the container.

Table 11: Cooling and Recharge Times with Different PCM Enhancement

PCM Enhancement	Air Temperature (°C)	PCM Weight (kg)	Cooling (min)	Recharge (min)	Recharge Rate (min/kg)
None	25.7	8.6	103	178	20.7
Copper mesh	26.0	8.6	195	212	24.7
Graphite foam	25.7	5.4	164	-	-
Graphite foam	25.6	12.7	500.0	403.3	31.7
Copper mesh	26.3	15.1	213.8	379.8	25.2
Copper mesh	30.0	15.1	186.5	593.4	39.3
Copper mesh	35.0	15.1	169	-	-

Two values to take note of in Table 11 are the 12.7 kg graphite foam cooling time (500 min) and the non-enhanced baseline recharge rate (20.7 min). The cooling time for the 12.7

kg graphite enhanced PCMHX is higher than it should because it was not properly insulated during operation. All the other PCMHX were insulated during operation. With 12.7 kg of PCM, the graphite enhanced PCMHX should be able to store enough heat at a condenser capacity of 185 W for 4.0 hours (the original design specification for the 12.7 kg PCMHX). For 500 minutes of cooling operation at an average condensing capacity of 185 W, a total PCM mass of 26.4 kg is needed. Therefore, the 500-minute cooling time is not a meaningful value, and emphasizes the need to insulate the PCMHX in future designs.

Similarly, the 20.7 min/kg recharge rate for the non-enhanced PCMHX is not a meaningful value. The baseline test was not run in cooling mode until all the PCM was fully melted. Visual inspection of Figure 37 shows that some of the PCM had not undergone phase-change when the device was switched into recharge mode. Therefore, the 20.7 min/kg recharge rate does not represent a full recharge cycle, as all the other values do. For this reason, the best recharge rate are the two copper-mesh enhanced PCMHX at 24.7 min/kg and 25.2 min/kg for the 8.6 kg and 15.1 kg PCMHX, respectively.

The COP of each test is reported in Table 12. The COP values for tests run within the specified ambient room temperature range (26.0 ± 0.05 °C) are open for direct comparison. The two top performers within this range are the two CuPCMHX versions.

Table 12: COP Results with Different PCM Enhancements

PCM Enhancement	Air Temperature (°C)	PCM Weight (kg)	COP
None	25.7	8.6	2.41
Copper mesh	26.0	8.6	4.37
Graphite foam	25.7	5.4	2.80
Graphite foam	25.6	12.7	3.25
Copper mesh	26.3	15.1	4.43
Copper mesh	30.0	15.1	4.78
Copper mesh	35.0	15.1	5.36

A note about the condenser capacities reported in Chapter 5: the tubing, receiver, mass-flow meter and TXV were not insulated between the PCMHX outlet and AHX inlet. Therefore, the condenser capacities are the same or lower than the reported evaporator capacities. The goal of this study is to characterize the PCMHX and the AHX, and so the heat loss between the condenser outlet and TXV inlet is not considered. As an example, Table 13 shows typical operating conditions from the copper-enhanced 15.1 kg condenser. Referring to Figure 25 for the sensor positions, Δ_{h1-2} shows the change in enthalpy through the condenser. The last column, $\Delta_{h1-4.a}$, shows the change in enthalpy from the condenser outlet all the way to the TXV inlet. In this case, an additional 14.5 W are accounted for, and the overall condensing capacity is higher than the evaporator capacity, as expected. All

PCMHX capacity calculations focus only on the condenser (position 1 to position 2 in Figure 25) and do not take into account the additional heat loss between position 2 and 4.a.

Table 13: Additional Heat Loss Between Condenser Outlet and Evaporator Inlet

T₁ (K)	T₂ (K)	T_{4.a} (K)	P₁ (kPa)	h₁ (kJ/kg)	h₂ (kJ/kg)	h_{4.a} (kJ/kg)	Δ_{h1-2} (kJ/kg)	Δ_{h1-4.a} (kJ/kg)
47.35	40.47	30.64	1160	276.1	108.9	94.49	167.2	181.7

Chapter 7: Results and Discussion

The objective of this thesis is to evaluate PCM enhancements for a mobile cooling system. The PCM is used as a heat storage container for waste heat from the VCC air-conditioning system. The two most important factors that are impacted by the PCM are the COP of the system during cooling operation, and the time it takes to re-solidify, or “recharge” the PCM after the cooling cycle has completed and the PCM has been fully liquified. Both of these factors are positively impacted by an increase in thermal conductivity of the PCM. The PCM used was a commercially available product called PT37. The length of time of the cooling operation is a function of the heat storage capacity of the PCM and the total mass of the material used. The COP of the cooling operation is a function of the cooling capacity of the evaporator and the work done by the compressor. The rate of flow of refrigerant into the evaporator and thus its capacity is controlled by the TXV, and the compressor work is a function of the pressure differential between the inlet and outlet of the compressor. As the condenser capacity decreased, the compressor must deliver refrigerant at a higher pressure to the condenser to allow for adequate condensation of the refrigerant. In a traditional HVAC system, high condensing temperature is associated with an ineffective condenser [33]. In the test system, the condensing capacity of the system is dependent on the heat transfer between the condenser tubes and the PCM. By increasing the thermal conductivity of the PCM, the heat transfer rate will remain high and system performance will be improved. The thermal conductivity of the PT37 is 0.25 W/m·K in the solid form, and 0.15 W/m·K in the liquid form. During the cooling process, the PCM closest to the copper tubes in the condenser melts first, and so the effective thermal conductivity of the bulk material is the liquid value: 0.15 W/m·K.

7.1 Setpoint Thermocouple Placement

In order to improve the thermal conductivity of the PCM, it must be enhanced with some material that has a higher thermal conductivity. The enhancement material should be able to be distributed evenly throughout the PCM, it should be able to withstand repeated (thousands) of phase changes and the associated change in density of the PCM (840 kg/m³ liquid and 920 kg/m³ solid, a + 9.5% change), and it should resist stratification and settling when the PCM is in the liquid phase. It should also resist corrosion when in contact with the PCM. The two materials chosen as enhancements for testing were copper sponge, and expanded graphite foam.

As shown above in Table 11, the 12.7 kg graphite-enhanced PCMHX has a total cooling time of 500.0 minutes (8.3 hours), more than double the next closes which is the 15.1 kg copper-enhanced PCMHX. Unfortunately, these results are not as promising as they seem. 12.7 kg of PT37 is only capable of a theoretical maximum of 4.3 hours of operation with a condensing capacity of 185 W. During testing, the graphite-enhanced PCMHX was not insulated as shown in Figure 82 (left). The lack of insulation on the graphite-enhanced PCMHX resulted in heat loss to the room through natural convection and thus increased the overall cooling time.



Figure 82: Different level of insulation on the graphite-enhanced PCMHX (left) and the copper-enhanced PCMHX (right)

On the other hand, the cooling time of the 15.1 kg copper-enhanced PCMHX was only 213.7 minutes (3.6 hours). 15.1 kg of PT37 should be able to operate for 4.8 hours with a condensing capacity of 185 W. The thermocouples in the copper-enhanced PCMHX were placed in the center of each copper helical tubes (Figure 83): with one layer $\frac{1}{4}$ from the top of the container and one layer $\frac{1}{4}$ from the bottom of the container (Figure 84). There were no thermocouples placed near the edge of the PCMHX, or in the space between the coils. Therefore, it is likely that not all the PCM in the PCMHX underwent phase change, and cooling time was sacrificed.

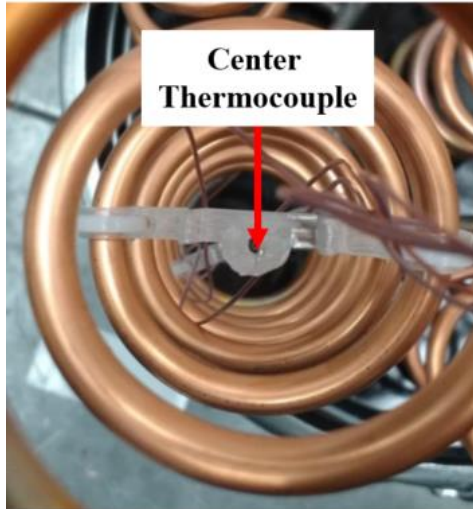


Figure 83: Copper-enhanced PCMHX thermocouple placement

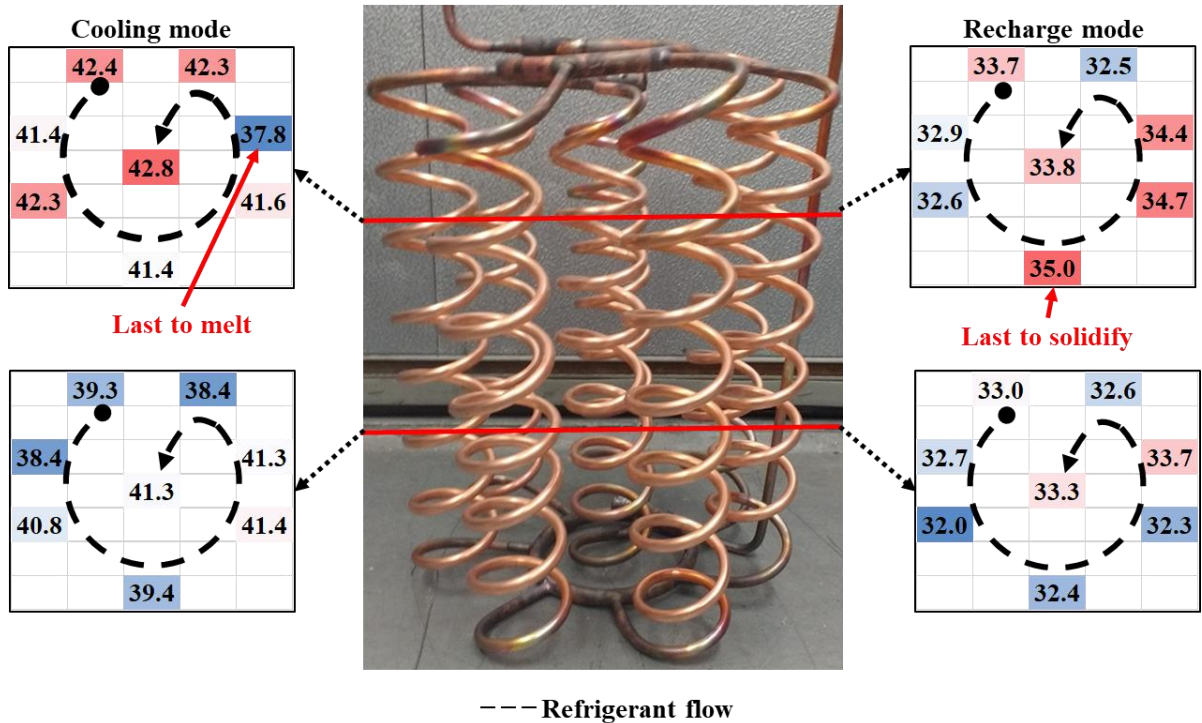


Figure 84: Copper-enhanced PCMHX cooling and recharge heat map

From the heat maps shown in Figure 84 for the copper-enhanced PCMHX, good locations for the setpoint thermocouples can be identified. In cooling mode, the last point to melt was in the upper layer of the thermocouples in the 6th helical coil. Therefore, the cooling

setpoint thermocouple should be placed near this thermocouple, but outside of the helical coil. For the recharge setpoint, the last point to solidify was the upper portion of the 4th coil. Because the placement of the thermocouples inside the helical coils are measuring the warmest part of the PCMHX, this is the ideal location for the recharge setpoint thermocouple.

Both the copper-enhanced PCMHX and the graphite-enhanced PCMHX reach the end of the recharge cycle at around the same time: 403.3 minutes for the graphite-enhanced PCMHX and 379.8 minutes for the copper-enhanced PCMHX. For the graphite-enhanced PCMHX, the last point in the sample to reach the setpoint temperature of 35.0 °C was in the very middle of the sample, as shown on the right side in Figure 85. This makes sense because there is no tube in the middle of the sample. Therefore, for a disk-shaped graphite-enhanced PCMHX with multiple layers, the thermocouple which determines when the sample is fully solidified should be placed at the very center of the sample. In cooling mode, the last portion of the PCMHX to melt is the outside of the middle disk. Therefore, the thermocouple that determines when the cooling mode operation is complete and the PCM is fully melted should be placed in the middle layer, on the outside, near the second-to-last tube in the heat exchanger.

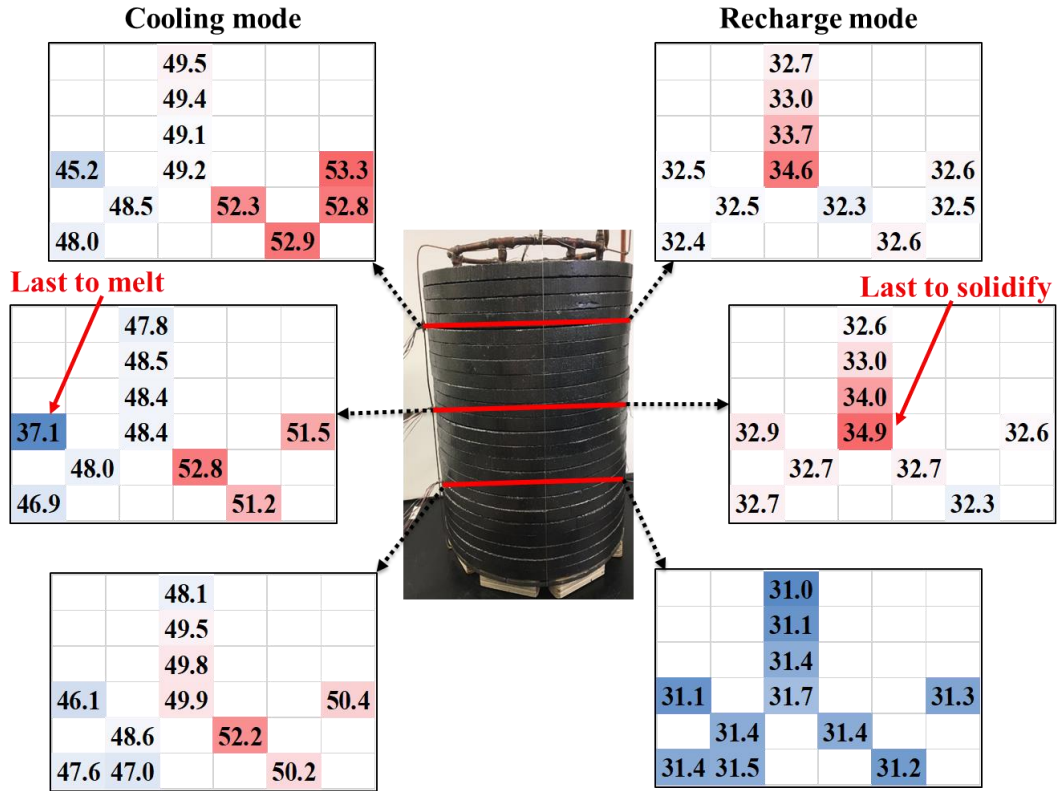


Figure 85: Graphite-enhanced PCMHX cooling and recharge heat map

7.2 System Performance

7.2.1 COP

The COP of the different systems are shown in Figure 86. The last two bars on the chart were run at higher ambient room temperatures: they were run at 30.0 °C and 35.0 °C, respectively. The goal of these tests was to compare the cooling and recharge times to the baseline cycle test at 26.0 ± 0.5 °C, not to compare the COP. The higher COP makes sense because the temperature difference between the hot and cold reservoirs is smaller when the ambient room temperature is higher: similar to the way your residential AC is more efficient on moderate days than it is on very hot days.

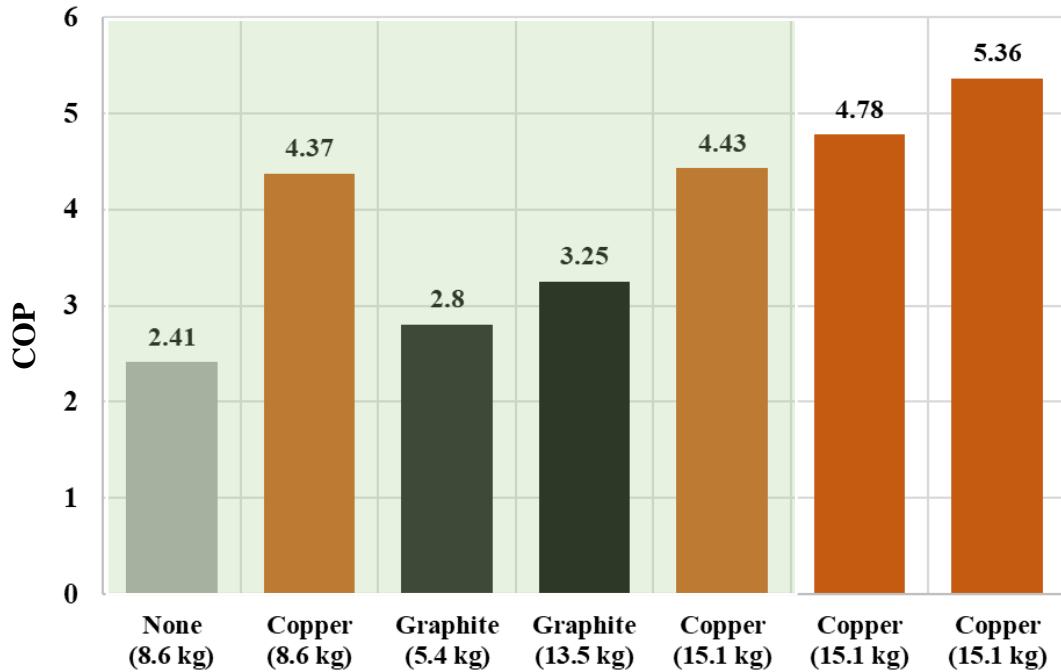


Figure 86: COP by weight of PCM and enhancement type

The more instructive values are the first 5 COP values. The non-enhanced PCM has the lowest COP, and both copper-enhanced systems have the highest COP. A direct comparison cannot be made, though, especially between the graphite and copper-enhanced systems. The graphite-enhanced system has significantly shorter tube lengths, and therefore less heat transfer area. When comparing the 12.7 kg graphite system to the 15.1 kg copper system, the copper system has a total of 9.6 m of tube length, and the graphite-enhanced system has 2.4 m of tubes, a 75% decrease in heat transfer area. Although the increase in thermal conductivity of the graphite-enhanced PCM should theoretically be able to compensate for the reduced heat transfer area, the results do not support that theory. Potential problems with the implementation of the graphite-enhanced PCMHX have been suggested: thermal resistance related issues and header related issues. The thermal resistance theory is based on poor contact between the graphite disks and the copper tube

and exacerbated by the use of layered disks. This was tested by back-filling the GrPCMHX with liquified PCM. This backfilling process was repeated after two cooling and recharge cycles because the graphite disks absorbed most of the added liquified PCM. Backfilling with liquified PCM ensured that any air gaps and associated thermal resistance between the tubes and the graphite disks as well as between each graphite disk was eliminated, and any voids in the graphite matrix were filled. After running tests in this configuration, the COP was 3.27: effectively the same. This suggests that the 2.4 m of 6.35 mm OD copper tube is insufficient for effective condensation of the refrigerant.

The other possibility for poor GrPCMHX system performance was an insufficient top header diameter. The non-enhanced PCMHX and copper enhanced PCMHX both used 9.525 mm OD copper tubes for the top header and bottom headers. The 4-hour graphite enhanced condenser on the other hand used a 6.35 mm OD copper tube for the top and bottom headers. Future work is recommended to test at GrPCMHX with a larger top header diameter, at least 8.0 mm ID. A larger bottom header diameter is not needed because the refrigerant is always liquid in the bottom of the condenser, regardless of the operating cycle.

Another potential issue with the GrPCMHX design is the orientation of the tubes. Both graphite versions have straight, vertical tubes. The copper versions all have helical tubes. According to Incropera, heat transfer can be enhanced for internal flow by coiling the tube. The centrifugal forces within the fluid induce secondary flow and heat transfer is enhanced, especially in laminar flow situations [34]. While the graphite enhancement increases the thermal conductivity of the PCM, the tube orientation decreases the heat transfer on the inside of the tube.

When comparing the copper-enhanced PCMHX with the non-enhanced baseline, the results are very encouraging. For the 8.6 kg versions, the COP increased from 2.41 to 4.37, an increase of 81.3%. The results were shown to be scalable to the 15.1 kg version, which had a COP of 4.43. The condenser enhancement types, PCM mass, PCM bulk density, condenser tube surface area, COP and Recharge Time per kg are listed in Table 14.

Table 14: PCM Heat Exchanger Performance and Characteristics

Enhancement Type	PCM mass (kg)	Bulk Density (kg/m³)	Tube Area (m²)	COP	Recharge time (min/kg)
None	8.6	-	0.096	2.41	20.7
Graphite	12.7	100.0	0.049	3.25	31.7
Copper	15.1	46.2	0.192	4.43	25.2

7.2.2 Overall Heat Transfer Coefficient

To compare the effectiveness of each condenser and PCM enhancement, an overall heat transfer coefficient analysis was conducted. The system was analyzed using a thermal resistance analysis. The circuit is shown in Figure 87. T_{sat} is calculated from the experimentally measured value P_i . Single-phase heat transfer of the R134a liquid was found to be less than 10% by Du [23], and was therefore neglected. The refrigerant enters the condenser at a quality greater than 0, so no single-phase vapor heat transfer is considered. The values for T_{PCM} were calculated as average values when \dot{Q} is 180 W, as close to the half way point of the cooling cycle. By keeping \dot{Q} constant, the heat transfer into the PCM is constant and UA values can be directly compared. The tube wall radii are as specified in the Copper Development Handbook [26] such that $r_i = 0.002794$ m and $r_o = 0.003175$ m. In R_2 , the thermal conductivity of copper used was 401 W/m·K.

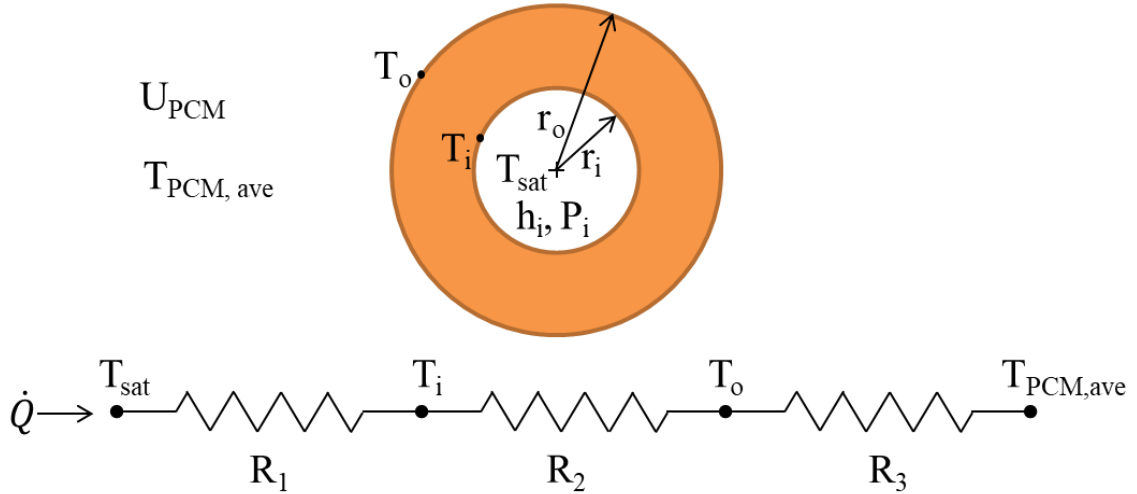


Figure 87: Thermal resistance analysis of PCM condenser

The general overall heat transfer coefficient equation is defined in Equation 12. Note that $UA = U_i A_i = U_{PCM} A_o$, so U_{PCM} can be found from Equation 12. The thermal resistances of each part of the circuit are shown in Equations (13 – 15). Equations (13, 15) are thermal resistances for convective heat transfer, and R_2 is for thermal resistance of radial conduction in a cylindrical wall. Equation 15 represents the heat transfer outside of the condenser tube to the PCM. The PCM temperature is calculated as a simple average of all the PCM temperatures when \dot{Q} is 180 W, close to the half-way point of the cooling cycle.

$$\dot{Q} = UA\Delta T = \frac{\Delta T}{\sum R} \quad \text{Equation 12}$$

$$R_1 = \frac{1}{h_i 2\pi r_i L} \quad \text{Equation 13}$$

$$R_2 = \frac{\ln\left(\frac{r_o}{r_i}\right)}{k_{Cu} 2\pi L} \quad \text{Equation 14}$$

$$R_3 = \frac{1}{U_{PCM} A_o} \quad \text{Equation 15}$$

Table 15 shows the measured and calculated values of the UA analysis. In Table 15, \dot{Q} is the condenser capacity. The COP values are included in Table 15 for reference.

Table 15: UA Calculations

Condenser Type	\dot{Q} (W)	P_i (kPa)	T_{sat} (°C)	T_{PCM} (°C)	Area (m²)	UA (W/K)	U_{PCM} (W/m²·K)	COP
Baseline	180.8	1409.7	52.7	37.2	0.096	11.7	122.3	2.41
Cu (8.6)	180.3	1303.4	49.5	37.1	0.096	14.5	151.8	4.37
Gr (5.4)	179.6	1560.2	56.8	37.8	0.024	9.4	394.5	2.80
Gr (12.7)	180.0	1344.3	50.8	38.3	0.053	14.5	274.6	3.25
Cu (15.1)	181.0	1154.4	54.3	36.7	0.192	21.0	109.5	4.43

To evaluate the overall performance of the heat exchanger design and the PCM enhancement, comparison of the UA value is appropriate. The highest UA value is 21.0 from the 15.1 kg copper-enhanced PCMHX. It also has the highest COP and is helped by the largest heat transfer surface area. At the other end of the spectrum is the 5.4 kg graphite enhanced PCMHX with a UA value of 9.4. It also has the lowest COP other than the baseline at 2.80, but it also has by far the least heat transfer area, with 75% less heat transfer area when compared to the baseline PCMHX. The most useful comparison is the baseline vs the 8.6 kg copper-enhanced PCMHX. The UA value increases 24%, even though the heat transfer area was the same. The COP is also 81% higher. The UA value offers some insight as to how the enhanced PCM impacts the system without considering the copper tube circuitry, but the information that can be gained is limited. With \dot{Q} held constant, the UA value is sensitive to the temperature difference between the saturation temperature of the refrigerant and the temperature of the PCM. The PCM temperature only varies by 1.6

K, but the saturation temperature varies by 7.3 K. The graphite-enhanced PCMHX has the highest saturation temperature and the lowest COP. To make up for the small heat transfer surface area in the 5.4 kg graphite enhanced PCMHX, a large temperature gradient is needed between the refrigerant and the PCM. To achieve this, system pressure increases, and compressor power likewise increases. Evaporator capacity stays the same, and COP goes down. Inspection of the U_{PCM} values reveal that the graphite enhanced condensers work well, but are limited by short tube lengths and reduced heat transfer area. Adding additional tubes to increase the heat transfer area for the graphite enhanced condensers is recommended. Also, when selecting a PCMHX design, consider the COP first and the UA value second.

Chapter 8: Conclusion and Future Work

The field of personal thermal comfort is growing. The push to reduce energy usage while maintaining adequate thermal comfort in indoor spaces is leading to novel approaches to space cooling. A prototype battery powered personal air conditioner was built and tested by Yilin Du in CEEE at the University of Maryland. The device used a PCM to store the waste heat from the air conditioner on-board the system. Because the system is designed to be mobile and battery powered, any improvement in efficiency not only saves energy, but also increases run time and cooling ability. PCMs are often limited in their effectiveness by their thermal conductivity, which is often less than 1 [35]. A known approach to improve the effectiveness of a phase change material as an energy storage container is to enhance the material with another material of higher thermal conductivity. In this thesis, both expanded graphite foam PCMHX and copper matrix enhanced PCMHX were tested.

The most meaningful measurements of how well the PCMHX is working are (1) the COP for the cooling cycle and (2) the minutes/kg for the recharge cycle. Theoretically, the graphite-enhanced PCMHX should have the best overall heat transfer and therefore have the best system COP. The high U_{PCM} values of the two graphite foam enhanced PCMHX confirm this, but the low COP results from insufficient tube length. The manufacturing limitations of the graphite-enhanced blocks means that the tubes must be straight and vertical, which reduces overall heat transfer area of the condenser and eliminates the possibility for a helical coil and its associated improvement in heat transfer. The copper-enhanced PCMHX on the other hand had sufficiently long tubes and helical coils to allow for better performance of the system. For future work it is recommended that more tubes be used for the graphite-enhanced PCMHX, increasing the overall heat transfer area.

The evaporator heat exchangers were also analyzed cooling ability in this work. The Thermatron 2-row evaporator heat exchanger was used on the baseline system and was shown to deliver more than the minimum required cooling of 150 W. For this work, Coil Designer simulations were done on the Thermatron 2-row, Thermatron 1-row and Sanhua Microchannel heat exchangers. Based on the Coil Designer simulations, the Thermatron 2-row and Sanhua Microchannel condensers provide sufficient cooling, but the Thermatron 1-row does not. The Sanhua Microchannel is not compatible with the thermosiphon recharge cycle currently in use on the device, but if in future designs the recharge cycle is compressor drive, then the Sanhua Microchannel should be installed and tested.

It must also be reiterated that there is an insufficient baseline test for this body of work. The original PCMHX was tested with limited knowledge of the capabilities of the system and the test apparatus used a manually adjusted expansion valve instead of a TXV. This resulted in a less efficient system requiring constant supervision and manual expansion valve adjustments throughout the test. No cycle testing was done with the non-enhanced PCMHX, and the cooling cycle was only allowed to run for two hours.

The RoCo device is a promising personal thermal comfort technology. Improved condenser performance will lead to more efficient operation and decreased PCM recharge time. As the desire for improved thermal comfort and energy efficiency continues, novel cooling devices such as RoCo will lead the way.

Bibliography

- [1] "World's population increasingly urban with more than half living in urban areas | UN DESA | United Nations Department of Economic and Social Affairs," [Online]. Available: <http://www.un.org/en/development/desa/news/population/world-urbanization-prospects-2014.html>.
- [2] R. Forgiarini Rupp, N. G. Vásquez and R. Lamberts, "A review of human thermal comfort in the built environment," *Energy & Buildings*, vol. 105, pp. 178-205, 2015.
- [3] "ROE Home | Report on the Environment (ROE) | US EPA," [Online]. Available: <https://cfpub.epa.gov/roe/chapter/air/indoorair.cfm>.
- [4] L. Pérez-Lombard, J. Ortiz and C. Pout, "A review on buildings energy consumption information".
- [5] M. Veselý and W. Zeiler, "Personalized conditioning and its impact on thermal comfort and energy performance – A review," *Renewable and Sustainable Energy Reviews*, vol. 34, pp. 401-408, 2014.
- [6] L. Nelson and J. MacArthur, "Energy savings through thermostat setback," *ASHRAE J.; (United States)*, vol. 84:2, 1 1 1978.
- [7] A. C. Roussac, J. Steinfeld and R. de Dear, "A preliminary evaluation of two strategies for raising indoor air temperature setpoints in office buildings," *Architectural Science Review*, vol. 54, no. 2, pp. 148-156, 31 5 2011.
- [8] J. W. Moon, "Thermostat strategies impact on energy consumption in residential buildings," *Energy and Buildings*, vol. 43, no. 2, pp. 338-346, 2011.
- [9] T. Hoyt, E. Arens and H. Zhang, "Extending air temperature setpoints: Simulated energy savings and design considerations for new and retrofit buildings," *Building and Environment*, vol. 88, pp. 89-96, 2015.
- [10] G. Brager, H. Zhang and E. Arens, "Evolving opportunities for providing thermal comfort," *Building Research & Information*, vol. 43, no. 3, pp. 274-287, 4 5 2015.
- [11] ASHRAE, "ASHRA Std 55-2010 Thermal Environmental Conditions for Human Occupancy," 2010.
- [12] E. Arens, M. A. Humphreys, R. De Dear and H. Zhang, "Are 'class A' temperature requirements realistic or desirable?," *Building and Environment*, vol. 45, pp. 4-10.
- [13] P. M. B. Marco A. Ortiz *, Stanley R. Kurvers, "A review of comfort, health, and energy use: Understanding daily energy use and wellbeing for the development of a new approach to study comfort," *Energy and Buildings*, vol. 152, pp. 323-335, 2017.
- [14] J. Nicol and M. Humphreys, "Adaptive thermal comfort and sustainable thermal standards for buildings," *Energy and Buildings*, vol. 34, no. 6, pp. 563-572, 1 7 2002.

- [15] Advanced Research Projects Agency-Energy, "ARPAE | DELTA," 16 12 2014. [Online]. Available: <https://arpa-e.energy.gov/?q=arpa-e-programs/delta>. [Accessed 30 11 2017].
- [16] A. K. Melikov, "Personalized ventilation," *Indoor Air*, vol. 14, no. s7, pp. 157-167, 1 8 2004.
- [17] M. Heidarinejad, D. A. Dalgo, N. W. Mattise and J. Srebric, "Personalized cooling as an energy efficiency technology for city energy footprint reduction," 2018.
- [18] L. Kirkeide, "Effects of Three-Hour On-Peak Time-of-Use Plan on Residential Demand during Hot Phoenix Summers".
- [19] Y. Qiu, L. Kirkeide and Y. D. Wang, "Effects of Voluntary Time-of-Use Pricing on Summer Electricity Usage of Business Customers," *Environmental and Resource Economics*, pp. 1-24, 10 11 2016.
- [20] Y. Yau and B. Rismanchi, "A review on cool thermal storage technologies and operating strategies," *Renewable and Sustainable Energy Reviews*, vol. 16, no. 1, pp. 787-797, 1 1 2012.
- [21] Y. Sun, S. Wang, F. Xiao and D. Gao, "Peak load shifting control using different cold thermal energy storage facilities in commercial buildings: A review," *Energy Conversion and Management*, vol. 71, pp. 101-114, 1 7 2013.
- [22] H. Hoag, *How cities can beat the heat*, 2015.
- [23] Y. Du, "BATTERY POWERED PORTABLE VAPOR COMPRESSION CYCLE SYSTEM WITH PCM CONDENSER," 2016.
- [24] A. M. Mallow, "STABLE PARAFFIN COMPOSITES FOR LATENT HEAT THERMAL STORAGE SYSTEMS," 2015.
- [25] *Methods of Testing and Rating Seasonal Efficiency of Unitary Air Conditioners and Heat Pumps*, Atlanta: ASHRAE, 1995, p. 46.
- [26] Copper Development Association Inc. Copper Alliance, *CDA Publication A4015-14/17: Copper Tube Handbook*, New York, New York: Copper Alliance, 2017, p. 96.
- [27] R. Khodabandeh and R. Furberg, "Instability, heat transfer and flow regime in a two-phase flow thermosiphon loop at different diameter evaporator channel," *Applied Thermal Engineering*, 2010.
- [28] R. Dhumane, Y. Du, J. Ling, V. Aute and R. Radermacher, "Transient Modeling of a Thermosiphon based Air Conditioner with Compact Thermal Storage: Modeling and Validation," in *International Refrigeration and Air Conditioning Conference*, 2016.
- [29] T. Ahmed, M. Bhouri, D. Groulx, M. A. White and S. Kahwaji, "Experimental Investigation of Thermal Management of Table Computers using Phase Change materials (PCMs)," in *Proceedings of the ASME 2016 Summer Heat Transfer Conference*, Washington, DC, 2016.
- [30] W. Wu, X. Yang, G. Zhang, X. Ke, Z. Wang, W. Situ, X. Li and J. Zhang, "An experimental study of thermal management system using copper mesh-enhanced composite phase change materials for power battery pack," *Energy*, vol. 113, pp. 909-916, 15 10 2016.

- [31] Y. Yao, H. Wu and Z. Liu, "A new prediction model for the effective thermal conductivity of high porosity open-cell metal foams," *International Journal of Thermal Sciences*, vol. 97, pp. 56-67, 11 2015.
- [32] A. Mallow, O. Abdelaziz and S. Graham, "Thermal charging study of compressed expanded natural graphite/phase change material composites," *Carbon*, vol. 109, pp. 495-504, 2016.
- [33] John Tomczyk, "What Causes High Compressor Discharge Temperature?," 2006. [Online]. Available: <https://www.achrnews.com/articles/97890-what-causes-high-compressor-discharge-temperature>.
- [34] F. Incropera, D. Dewitt, B. Theodore and A. Lavine, *Principles of Heat and Mass Transfer*, Wiley, 2014.
- [35] M. Martinelli, F. Bentivoglio, A. Caron-Soupart, R. Couturier, J. F. Fourmigue and P. Marty, "Experimental study of a phase change thermal energy storage with copper foam," *Applied Thermal Engineering*, vol. 101, pp. 247-261, 2016.
- [36] O. Seppanen, W. J. Fisk and D. Faulkner, "Control of Temperature for Health and Productivity in Offices," 2004.
- [37] R. Kosonen and F. Tan, "Assessment of productivity loss in air-conditioned buildings using PMV index".
- [38] A. Hedge, W. Sakr and A. Agarwal, "THERMAL EFFECTS ON OFFICE PRODUCTIVITY".
- [39] X. Chen, Q. Wang and J. Srebric, "Occupant feedback based model predictive control for thermal comfort and energy optimization: A chamber experimental evaluation," 2016.
- [40] J. Huang and K. R. Gurney, "The variation of climate change impact on building energy consumption to building type and spatiotemporal scale," 2016.
- [41] *. Fan Zhang a, Shamila Haddad a, Bahareh Nakisa b, Mohammad Naim Rastgoo b, Christhina Candido a, Dian Tjondronegoro b and Richard de Dear a, "The effects of higher temperature setpoints during summer on office workers' cognitive load and thermal comfort," *Building and Environment*, vol. 123, pp. 176-188, 2017.
- [42] M. Luo, B. Cao, W. Ji, Q. Ouyang, B. Lin and Y. Zhu, "The underlying linkage between personal control and thermal comfort: Psychological or physical effects?," *Energy and Buildings*, vol. 111, pp. 56-63, 2016.
- [43] M. Luo, B. Cao, X. Zhou, M. Li, J. Zhang, Q. Ouyang and Y. Zhu, "Can personal control influence human thermal comfort? A field study in residential buildings in China in winter," *Energy & Buildings*, vol. 72, pp. 411-418, 2014.
- [44] P. Shen, "Impacts of climate change on U.S. building energy use by using downscaled hourly future weather data," *Energy and Buildings*, vol. 134, pp. 61-70, 1 1 2017.
- [45] Y. Zhang and R. Zhao, "Effect of local exposure on human responses," *Building and Environment*, vol. 42, no. 7, pp. 2737-2745, 1 7 2007.
- [46] H. Zhang, "Human thermal sensation and comfort in transient and non-uniform thermal environments," 2003.

- [47] W. Turner, I. Walker and J. Roux, "Peak load reductions: Electric load shifting with mechanical pre-cooling of residential buildings with low thermal mass," *Energy*, vol. 82, pp. 1057-1067, 15 3 2015.
- [48] K. Herter, P. McAuliffe and A. Rosenfeld, "An exploratory analysis of California residential customer response to critical peak pricing of electricity," *Energy*, vol. 32, no. 1, pp. 25-34, 1 1 2007.
- [49] U. Stritih and V. Butala, "Experimental investigation of energy saving in buildings with PCM cold storage," *International Journal of Refrigeration*, vol. 33, no. 8, pp. 1676-1683, 1 12 2010.
- [50] F. Kuznik and J. Virgone, "Experimental assessment of a phase change material for wall building use," *Applied Energy*, vol. 86, no. 10, pp. 2038-2046, 1 10 2009.
- [51] B. M. Diaconu, "Thermal energy savings in buildings with PCM-enhanced envelope: Influence of occupancy pattern and ventilation," *Energy and Buildings*, vol. 43, no. 1, pp. 101-107, 1 1 2011.
- [52] B. M. Diaconu and M. Cruceru, "Novel concept of composite phase change material wall system for year-round thermal energy savings," *Energy and Buildings*, vol. 42, no. 10, pp. 1759-1772, 1 10 2010.
- [53] V. Butala and U. Stritih, "Experimental investigation of PCM cold storage," *Energy and Buildings*, vol. 41, no. 3, pp. 354-359, 1 3 2009.
- [54] C. Voelker, O. Kornadt and M. Ostry, "Temperature reduction due to the application of phase change materials," *Energy and Buildings*, vol. 40, no. 5, pp. 937-944, 1 1 2008.
- [55] A. Mallow, K. Gluesenkamp, O. Abdelaziz and S. Graham, "Optimization of Graphite Composite Latent Heat Storage Systems," in *ASME 2017 International Technical Conference and Exhibition on Packaging and Integration of Electronic and Photonic Microsystems*, 2017.
- [56] Z. Liu, Y. Yao and H. Wu, "Numerical modeling for solid–liquid phase change phenomena in porous media: Shell-and-tube type latent heat thermal energy storage," *Applied Energy*, vol. 112, pp. 1222-1232, 1 12 2013.
- [57] K. Lafdi, O. Mesalhy and S. Shaikh, "Experimental study on the influence of foam porosity and pore size on the melting of phase change materials," *Journal of Applied Physics*, vol. 102, no. 8, p. 083549, 15 10 2007.